

Copyright is owned by the Author of the thesis. Permission is given for a copy to be downloaded by an individual for the purpose of research and private study only. The thesis may not be reproduced elsewhere without the permission of the Author.

**Synthesis and Characterisation of Pyrazine-  
Based Ligands for the Analysis of Metal-Metal  
Communication**

---

A thesis presented in partial fulfilment of the requirements for the degree of

**Master of Science**

**in**

**Chemistry**

at Massey University, Manawatū

New Zealand

---

Michael James Brown

2018



## Acknowledgements

I would like to acknowledge and thank everybody within the Plieger and Rowlands groups for their assistance in and out of the laboratory, as well as the “dank bantz”. Special mentions include Sidney Woodhouse for reading my thesis at least 23,796 times prior to submission; Rebecca (Becky) Severinsen for the guidance you have provided from day one; and Tyson Dais (my chemistry husband) for sharing his vast knowledge over wide range of chemistry. I would also like to acknowledge Jenna for her awesomeness (#jennaisawesome). Whilst you all had to endure my constant onslaught of puns, I considered it ‘pun’ishment for being too ‘pun’ctual with corrections to my ‘pun’ctuation.

To my co-supervisor Associate Professor Gareth Rowlands. Thank you for answering my barrage of questions and for not kicking me out of your office after the fifth visit within ten minutes. Thank you for your support and guidance throughout the course of this project.

To my Supervisor Associate Professor Paul Plieger. Thank you for the constant positive energy you bestow onto everyone around you. Most importantly, thank you for allowing me to undertake an MSc project under your supervision and providing me with the necessary tools to obtain various life skills. I will always be a Plieger Pal.

I am grateful to Dr Martyn Coles at Victoria University, Wellington, New Zealand for analysing the **L3** ligand crystals at Victoria University.

I would like to thank Dr Jason Price, who analysed the crystals of complexes **C3A** and **C3B** at the Australian Synchrotron, Victoria, Australia.

I would also like to thank Dr Joanne Harvey for allowing myself to use your ozonator near the beginning of this project. The success brought on from this inspired us to acquire an ozonator ourselves.

I would also like to thank François Laur for his efforts in assisting me in the synthesis of various Schiff base ligands. I would also like to thank Brodie Matheson for aiding me in the attempted synthesis of several compounds (in particular **A2** and **K1**).

I would like to thank my friends for supporting me throughout this project. I love you all with varying portions of my heart.

I would like to thank the Potangaroa family for all of their guidance and support throughout the ups and downs of this research. The kai is also amazing as well.

To my brother and sisters, thank you for the support you have given me throughout this time. We did it. Thank you to my cousin Simon who helped me take well-needed breaks during the writing process with gaming sessions. I will beat you someday. To my mum and dad, thank you for everything you have done for me throughout the course of this project. It goes without saying that I would not have come this far without your love and support.

To my partner Tiriana Potangaroa, aka Nani. Thank you for putting up with me these last couple of years; I know I was not easy to deal with. Thank you for being so understanding and supportive, especially within the closing months of this project. To quote Six60 “you’re so special to me, all that I want and need”.

To people such as Caren August, David Lun, all of my previous lecturers at Massey University and too many others to name, thank you for everything that you have done.

Pyrazine Pirate. Out.

## Abstract

Pyrazine is an attractive molecule that has been incorporated as a bridging ligand between two metal centres. These complexes have been shown to exhibit both magnetic and electrochemical exchange between the metal centres through the pyrazine unit. Addition of functionality onto the 2 and 5 position of pyrazine can reinforce the coordination of  $3d$  octahedral metal ions to the pyrazine ring.

The Schiff base condensation of **A1** with various primary amine reactants produced three unique ligand systems. The confirmed synthesis of these ligands was verified with a variety of characterisation techniques. A single crystal structure was generated for one ligand system (**L3**), which revealed both imine –  $\pi$  stacking interactions, as well as alkane hydrogen – pyridine interactions.

Several complexations were attempted with the three ligand systems synthesised. Manganese and cobalt complexes were successfully synthesised with **L3**, the single crystal structures generated showed cyclohelicate triangles, which were unique at the time. The electrochemical analysis of these complexes in MeCN showed similar redox processes as was seen in the electrochemical analysis of **L3**. Signs of possible metal-metal communication within the cyclohelicate triangles was also noticed, with oxidation (and reduction) processes present. Further analysis is necessary to verify these interpretations, including magnetic analysis. Complexations with identical metal salts and **L2** could not be characterised by SCXRD. Other techniques such as mass spectrometry and conductivity measurements indicated the likely formation of a polymorphic – potentially cyclohelical structure with this ligand. Complexations with **L1** incorporated the inclusion of a larger collection of metal salts. Unfortunately, due to time constraints, only three complexes were suitably characterised. From the various characterisation methods used,

it was deduced that all three complexes were likely simple  $M_2L_1$  systems, where the coordination of the 6-coordinate  $3d$  metal centres were accompanied by the coordination of either water, solvent, counterion or a combination of these.

## Contents

Acknowledgements.....	i
Abstract.....	iii
List of Figures and Schemes.....	viii
List of Tables.....	xiii
Abbreviations.....	xiv
Chemical.....	xiv
Equipment.....	xv
Units.....	xv
Compound codes.....	xv
Literature compound codes.....	xvi
Chapter 1 Introduction.....	1
1.1 Cyclohelicates.....	1
1.1.1 Cyclohelicate squares and triangles.....	1
1.2 Magnetism.....	4
1.2.1 Magnetic coupling.....	4
1.2.2 Superexchange.....	5
1.2.3 Characterisation of magnetism – SQUID.....	6
1.3 Electronic coupling – Metal-Metal communication.....	7
1.3.1 Robin and Day classification of mixed-valence complexes.....	8
1.3.2 Measuring electrochemical properties – Cyclic voltammetry.....	9
1.4 Creutz-Taube ion.....	11
1.5 Pyrazine.....	12
1.5.1 Pyrazine as a bridging ligand.....	13
1.6 Examples of cyclohelicate squares and triangles with pyrazine bridging ligands.....	14
1.6.1 Synthesis of cyclohelicate squares by Shen <i>et al.</i> .....	14
1.6.2 Synthesis of a cyclohelicate square by Hausmann <i>et al.</i> .....	17
1.6.3 Synthesis of cyclohelicate triangles by Hogue <i>et al.</i> .....	18
1.7 Summary.....	20
1.8 Research aims and hypothesis.....	20
1.9 Thesis outline.....	21
Chapter 2 Ligand Design.....	23
2.1 Schiff base.....	23
2.2 Schiff base with pyrazine.....	25
2.3 Summary.....	26
Chapter 3 Synthesis of Schiff Base Precursors.....	27



3.1	Introduction .....	27
3.2	Synthesis of pyrazine-2,5-dicarbaldehyde.....	27
3.2.1	Synthesis of pyrazine-2,5-dicarbaldehyde – Das method.....	28
3.2.2	Synthesis of pyrazine-2,5-dicarbaldehyde – Coufal method .....	31
3.2.3	Synthesis of pyrazine-2,5-dicarbaldehyde – Hogue <i>et al.</i> method .....	33
3.3	Future work .....	35
3.4	Summary.....	36
Chapter 4	Synthesis of Ligands.....	37
4.1	Introduction .....	37
4.2	General protocol for the synthesis of Schiff base ligands .....	37
4.3	Characterisation of Schiff base ligands .....	38
4.4	Synthesis and characterisation of H <sub>2</sub> L1, L2 and L3.....	40
4.5	Future work .....	44
4.6	Conclusions .....	44
Chapter 5	Synthesis of Complexes.....	45
5.1	Introduction .....	45
5.2	General protocol for the synthesis of complexes.....	45
5.3	Characterisation of complexes.....	46
5.3.1	Structural characterisation of complexes.....	46
5.3.2	Electrochemical analysis of complexes .....	48
5.4	Synthesis and characterisation of complexes with L3.....	50
5.4.1	Electrochemical analysis of C3A and C3B .....	56
5.5	Synthesis and characterisation of complexes with L2.....	59
5.6	Synthesis and characterisation of complexes with L1.....	63
5.7	Conclusion.....	68
6	Conclusion.....	70
Appendix 1	Synthesis of L4 – L7 .....	72
A1.1	Synthesis of H <sub>2</sub> L4 and H <sub>4</sub> L5 .....	73
A1.2	Conclusion.....	73
A1.3	Synthesis of L6 and L7 .....	74
A1.4	Conclusion.....	78
Appendix 2	Synthesis of Pyrazine-2,5-diacetaldehyde (A2) and 2,5-pyrazinyldiacetone (K1) .....	79
A2.1	Synthesis of pyrazine-2,5-diacetaldehyde (A2).....	80
A2.2	Synthesis of 2,5-pyrazinyldiacetone (K1).....	86
A2.3	Future work .....	88

A2.4	Summary .....	90
Appendix 3	General Experimental Section .....	91
A3.1	Experimental generic description.....	91
A3.1.1	Reagents and solvents .....	91
A3.1.2	Synthetic methods.....	91
A3.1.3	Characterisation methods.....	91
A3.2	X-Ray crystallography .....	95
Appendix 4	Synthetic Methods.....	97
A4.1	Synthesis of <b>A1</b> and precursors to <b>A1</b> .....	97
A4.1.1	2,5-dimethyl-1,4-dioxidopyrazine.....	98
A4.1.2	2,5-di(acetoxymethyl)pyrazine .....	100
A4.1.3	2,5-distyrylpyrazine .....	101
A4.1.4	Pyrazine-2,5-dicarbaldehyde ( <b>A1</b> ).....	103
A4.2	Synthesis of <b>H<sub>2</sub>L1</b> , <b>L2</b> and <b>L3</b> .....	105
A4.2.1	2,2'-[2,5-pyrazinediylbis(methylidynenitrilo)]bis(phenol) ( <b>H<sub>2</sub>L1</b> ).....	105
A4.2.2	<i>N,N'</i> -(2,5-pyrazinediyl dimethylidyne)bis(2-pyridinemethanamine) ( <b>L2</b> ).....	106
A4.2.3	<i>N,N'</i> -(3,6-pyrazinediyl dimethylidyne)bis(2-pyridineethanamine) ( <b>L3</b> ).....	107
A4.2.4	Crystallisation attempts of <b>H<sub>2</sub>L1</b> , <b>L2</b> and <b>L3</b> .....	108
A4.3	Synthesis of complexes.....	109
A4.3.1	Complexation with <b>L3</b> .....	110
A4.3.2	Complexation with <b>L2</b> .....	112
A4.3.3	Complexation with <b>L1</b> .....	113
A4.4	Synthesis of N-Boc protected 2-aminoethanol .....	116
A4.5	Synthesis of N-Boc protected 2-aminophenol .....	118
References.....		119
Additional Spectra .....		130

## List of Figures and Schemes

Figure 1.1. The cyclohelicate square (A) and triangle (B) complex.....	1
Figure 1.2. 2D Molecular library with various building units for creating supramolecular structures .....	3
Figure 1.3. Theoretical view of neighbouring electron spins in (a) paramagnetic, (b) ferromagnetic and (c) antiferromagnetic upon exposure to magnetic field, B .....	4
Figure 1.4. $\sigma$ -type ferromagnetic (a), $\sigma$ -type antiferromagnetic superexchange (b), and $\pi$ -type antiferromagnetic superexchange (c) .....	5
Figure 1.5. Magnetic susceptibility, $\chi$ vs temperature, T, showing typical ferro-, antiferro- and paramagnetic slopes .....	7
Figure 1.6. A three-electrode electrochemical cell. ....	9
Figure 1.7. The Creutz-Taube Ion, $[(\text{NH}_3)_5\text{Ru}]_2\text{pz}^{5+}$ where pz = pyrazine.....	11
Figure 1.8. Calculated $\beta$ -HOMO of the CT ion .....	12
Figure 1.9. The three structural isomers of the diazine: Pyridazine (a), Pyrimidine (b) and Pyrazine (c) .....	12
Figure 1.10. Framework of the ligand <b>FL</b> (left) and SCXRD structure of the cyclohelicate square, <b>FC<sup>H</sup></b> .....	15
Figure 1.11. Cyclic voltammogram of <b>FC<sup>H</sup></b> (top voltammogram, 1), <b>FC<sup>Me</sup></b> (middle voltammogram, 2) and <b>FC<sup>Br</sup></b> (bottom voltammogram, 3) .....	16
Figure 1.12. <b>JL</b> ligand structure (left) and SCXRD structure of the formed cyclohelicate square <b>JC·12.75MeCN</b> (right).....	17
Figure 1.13. <b>RL</b> ligand structure (left) and SCXRD structure of the cyclohelicate triangle (right). SCXRD structure shown is <b>RC2</b> .. .....	18
Figure 1.14. Directional-bonding approach for the synthesis of $[\text{M}_3\text{L}_3]$ triangles, exhibiting conformational strain similar to cyclohelicate triangles <b>RC1-2</b> .....	19
Figure 2.1. Pyrazine with 2 and 5 positions indicated .....	23

Scheme 2.1. Mechanism for Schiff base condensation.....	23
Figure 2.2. The expected coordination of a transition metal (M) to a pyrazine ligand (ligand <b>L3</b> is shown as an example).....	25
Figure 2.3. Pyrazine with 2 and 5 positions labelled with R substituents.....	26
Scheme 3.1. Synthetic scheme for the synthesis of pyrazine-2,5-dicarbaldehyde ( <b>A1</b> ).	27
Figure 3.1. <sup>1</sup> H NMR spectra of 2,5-dimethylpyrazine-1,4-dioxide (in D <sub>2</sub> O) obtained from the methods provided by Das et al. (top) and Klein et al. (bottom).....	28
Scheme 3.2. Proposed mechanism for the acetylation of 2,5-dimethylpyrazine-1,4-dioxide.....	29
Figure 3.2. <sup>1</sup> H NMR spectrum of 2,5-di(acetoxymethyl)pyrazine (CDCl <sub>3</sub> ). ....	30
Scheme 3.3. General Knoevenagel condensation .....	31
Scheme 3.4. Criegee mechanism for the ozonolysis of 2,5-E,E-distyrylpyrazine.....	33
Figure 3.3. <sup>1</sup> H NMR spectrum of pyrazine-2,5-dicarbaldehyde ( <b>A1</b> ) with assigned peaks (CDCl <sub>3</sub> ) .....	35
Scheme 3.5. The three-step reaction scheme reported by Hogue et al. to produce <b>A1</b> from 2,5-dimethylpyrazine .....	36
Scheme 4.1. The general reaction scheme of a Schiff base condensation between pyrazine-2,5-dicarbaldehyde ( <b>A1</b> ) and a primary amine .....	38
Figure 4.1. Assigned <sup>1</sup> H NMR spectrums (top <sup>1</sup> H NMR spectrum ( <b>H<sub>2</sub>L1</b> ): DMSO-d <sub>6</sub> , middle <sup>1</sup> H NMR spectrum ( <b>L2</b> ): CDCl <sub>3</sub> ; bottom <sup>1</sup> H NMR spectrum ( <b>L3</b> ): CDCl <sub>3</sub> ).....	41
Scheme 4.2. Tautomerism exhibited in <b>L2</b> .....	42
Figure 4.2. Molecular structure of <b>L3</b> .....	43
Figure 4.3. Packed structure of <b>L3</b> .....	43
Figure 5.1. A plot of the molar conductivity of coordination complexes in acetonitrile as a function of the number of counterions per complex present.....	48

Figure 5.2. SCXRD generated molecular structure of $[M_3L_3](ClO_4)_6$ .....	52
Figure 5.3. SCXRD generated molecular structure of two neighbouring $[M_3L_3](ClO_4)_6$ viewed from the side (left) and the front (right) .....	52
Figure 5.4. Packed structure of triangle complex (viewed down the c-axis).....	52
Figure 5.5. TGA plot of cobalt Triangle <b>C3A</b> .....	55
Figure 5.6. TGA plot of manganese triangle <b>C3B</b> .....	55
Figure 5.7. Cyclic voltammogram of <b>L3</b> .....	57
Figure 5.8. Cyclic voltammogram of <b>C3A</b> .....	58
Figure 5.9. Cyclic voltammogram of <b>C3B</b> .....	59
Figure 5.10. The unidentate ( <b>A</b> ), bidentate ( <b>B</b> ) and bridging ( <b>C</b> ) coordination fashion of acetate anions to a metal centre.....	66
Figure 5.11. The ligand $H_2L1$ with assigned hydrogens (bottom) and the comparison of the assigned $^1H$ NMR spectrum of <b>L1</b> (bottom spectrum) against the assigned $^1H$ NMR spectrum of the zinc acetate coordinated complex <b>C1C</b> (top spectrum) .....	67
Scheme A1.1. The general reaction scheme of a Schiff base condensation between pyrazine-2,5-dicarbaldehyde ( <b>A1</b> ) and a primary amine .....	72
Scheme A1.2. Reaction scheme for the synthesis of <b>L6</b> and <b>L7</b> .....	76
Figure A1.1. Assigned $^1H$ NMR spectra of N-Boc protection of 2-aminoethanol and 2-aminophenol.....	77
Scheme A2.1. Synthetic scheme for the synthesis of pyrazine-2,5-diacetaldehyde ( <b>A2</b> ) and ( <b>K1</b> ).....	79
Scheme A2.2. The keto, enol and enaminone tautomers of pyrazine-2,5-diacetaldehyde .....	80
Scheme A2.3. General Wittig reaction scheme .....	81
Figure A2.1. $^1H$ NMR spectrum of pyrazine dimethoxyvinyl ether crude product.....	82

Scheme A2.4. Reaction scheme for the lithiation and electrophilic substitution of an amide on 2,5-dimethylpyrazine.....	83
Figure A2.2. <sup>1</sup> H NMR spectrum of the crude product obtained from the lithiation with n-BuLi and electrophilic substitution with DMF .....	84
Scheme A2.5. General reaction scheme for the formation of a bisulfite adduct of an aldehyde, followed by the hydrolysis back into the desired aldehyde compound.....	85
Figure A2.3. <sup>1</sup> H NMR spectrum of the crude 2,5-pyrazinyldiacetone ( <b>K1</b> ) obtained from the procedure by Paine et al. with assigned peaks (CDCl <sub>3</sub> ).....	86
Scheme A2.6. Mechanism for the base-promoted condensation of 2,5-dimethylpyrazine with MeCN.....	87
Figure A2.4. <sup>1</sup> H NMR spectrum of 2,5-pyrazinyldiacetone from the base-promoted condensation of 2,5-dimethylpyrazine with MeCN, with assigned peaks (CDCl <sub>3</sub> ).....	88
Scheme A2.7. Mechanism for the formation of the stable tetrahedral intermediate and the desired carbonyl product brought on by the addition of an organolithium reagent to a Weinreb amide .....	89
Scheme A2.8. Clavulanic acid (top structure) and its degradation products .....	90
Scheme 3.1. Synthetic scheme for the synthesis of pyrazine-2,5-dicarbaldehyde ( <b>A1</b> ) .	97
Figure AS1. Assigned <sup>1</sup> H NMR spectrum of 2,5-E,E-distyrylpyrazine .....	131
Figure AS2. Assigned <sup>13</sup> C NMR spectrum of <b>L1</b> (DMSO – d <sub>6</sub> ).....	131
Figure AS3. HMQC spectrum of <b>L1</b> with solvent peak assigned (DMSO – d <sub>6</sub> ).....	131
Figure AS4. Assigned <sup>13</sup> C NMR spectrum of <b>L2</b> (CDCl <sub>3</sub> ).....	131
Figure AS5. HMQC spectrum of <b>L2</b> (CDCl <sub>3</sub> ).....	131
Figure AS6. Assigned <sup>13</sup> C NMR spectrum of <b>L3</b> (CDCl <sub>3</sub> ).....	131
Figure AS7. HMQC spectrum of <b>L3</b> (CDCl <sub>3</sub> ).....	131

Figure AS8. Mass spectrum of impure 2-[2-(tert-butoxycarbonylamino)ethoxy]acetic acid ethyl ester (step iii in Scheme A1.1) .....	131
Figure AS9. Assigned <sup>1</sup> H NMR spectrum of 2-[2-(tert-butoxycarbonylamino)ethoxy]acetic acid ethyl ester (step iii in Scheme A1.1) .....	131
Figure AS10. Mass spectrum of impure <b>A2</b> .....	131
Figure AS11. Permission to use Figures 1.2 and 1.14 in this thesis from Chakrabarty, R.; Mukherjee, P. S.; Stang, P. J. <i>Chemical Reviews</i> <b>2011</b> , 111, 6810.....	131
Figure AS12. Permission to use Figure 1.11 in this thesis from Shen, F.; Huang, W.; Wu, D.; Zheng, Z.; Huang, X.-C.; Sato, O. <i>Inorganic Chemistry</i> <b>2016</b> , 55, 902. ....	131

## List of Tables

Table 4.1. The synthesis and appearance of ligands <b>H<sub>2</sub>L1</b> , <b>L2</b> and <b>L3</b> with the selected characterisation data used to verify the successful formation of these ligands.....	40
Table 5.1. Comparison of selected bond angles (°) for compounds <b>C3A</b> , <b>C3B</b> , <b>RC1</b> and <b>RC2</b> .....	51
Table 5.2. CHN analysis data of <b>C3A</b> with expected molecular formulas for <b>[Co<sub>3</sub>L<sub>3</sub>](ClO<sub>4</sub>)<sub>6</sub></b> and <b>[Co<sub>3</sub>L<sub>3</sub>](ClO<sub>4</sub>)<sub>6</sub> · 5H<sub>2</sub>O</b> .....	54
Table 5.3. Assigned peaks observed in the ATR-IR spectra and IR with KBr pellets spectra of <b>L2</b> , <b>C2A</b> and <b>C2B</b> .....	60
Table 5.4. Possible structures of <b>C2A</b> and <b>C2B</b> and the respective calculated molar conductivity of <b>C2A</b> (0.0436 g) in MeCN (25 mL) and <b>C2B</b> (0.0456 g) in MeCN (25 mL).....	63
Table 5.5. Complexations with <b>L1</b> and various metal salts, with the respective solvent system used, the colour changes observed and the complexation code.....	64
Table 5.6. Assigned peaks observed in the ATR-IR spectra and IR with KBr pellets spectra of <b>H<sub>2</sub>L1</b> , <b>C1A</b> , <b>C1B</b> and <b>C1C</b> .....	65
Table A3.1. X-Ray data of crystals obtained for <b>L3</b> , <b>C3A</b> and <b>C3B</b> .....	96
Table A4.1. Crystallisation attempts of <b>H<sub>2</sub>L1</b> , <b>L2</b> and <b>L3</b> .....	108



## Abbreviations

---

### Chemical

A.R	Analytical reagent
Ac <sub>2</sub> O	Acetic anhydride
Boc	<i>Tert</i> -butyloxycarbonyl protecting group
(Boc) <sub>2</sub> O	Di- <i>tert</i> -butyl dicarbonate
CDCl <sub>3</sub>	Deuterated chloroform
ClO <sub>4</sub> <sup>-</sup>	Perchlorate
Co(CH <sub>3</sub> COO) <sub>2</sub> ·4H <sub>2</sub> O	Cobalt acetate tetrahydrate
Co(ClO <sub>4</sub> ) <sub>2</sub> ·6H <sub>2</sub> O	Cobalt perchlorate hexahydrate
CT	Creutz Taube
DME	Dimethoxyethane
DMF	Dimethylformamide
DMSO-d <sub>6</sub>	Deuterated dimethyl sulfoxide
Et <sub>2</sub> O	Diethyl ether
EtOAc	Ethyl acetate
Fc	Ferrocene
Fe(ClO <sub>4</sub> ) <sub>2</sub> ·6H <sub>2</sub> O	Iron perchlorate hexahydrate
HOMO	Highest occupied molecular orbital
HSAB	Hard-soft acid-base
IPA	Isopropyl alcohol
LDA	Lithium diisopropylamide
<i>m</i> -CPBA	<i>Meta</i> -chloroperoxybenzoic acid
MeOH-d <sub>4</sub>	Deuterated methanol
Mn(ClO <sub>4</sub> ) <sub>2</sub> ·6H <sub>2</sub> O	Manganese perchlorate hexahydrate
Mn(NO <sub>3</sub> ) <sub>2</sub> ·4H <sub>2</sub> O	Manganese nitrate tetrahydrate
Na <sub>2</sub> S <sub>2</sub> O <sub>5</sub>	Sodium metabisulfite
NBu <sub>4</sub> ClO <sub>4</sub>	Tetrabutyl ammonium perchlorate
O <sub>3</sub>	Ozone
OsO <sub>4</sub>	Osmium tetroxide
Ph <sub>3</sub> P=O	Triphenylphosphine oxide
(Ph <sub>3</sub> PCH <sub>2</sub> OCH <sub>3</sub> )Cl	Triphenylphosphine methoxymethyl ether

Pz	Pyrazine
S.M	Starting material
SeO <sub>2</sub>	Selenium dioxide
THF	Tetrahydrofuran
TLC	Thin layer chromatography

---

### Equipment

ATR-IR	Attenuated total reflectance – infrared spectroscopy
CE	Counter electrode
CV	Cyclic voltammetry
HMQC	Heteronuclear multiple quantum coherence
HPLC	High performance liquid chromatography
IR	Infrared spectroscopy
KBr	Potassium bromide
M.W	Microwave
NMR	Nuclear Magnetic Resonance
RE	Reference electrode
SCXRD	Single crystal X-ray diffraction
SQUID	Superconducting quantum interference device
TGA	Thermogravimetric analysis
WE	Working electrode

---

### Units

c	Concentration
$\mu_{\text{eff}}$	Effective magnetic moment
$\chi$	Magnetic susceptibility
$\kappa$	Measured conductivity of sample
$\kappa_s$	Measured conductivity of solvent
o/n	Overnight
rt	Room temperature

---

### Compound codes

<b>A#</b>	Aldehyde (# = number code)
<b>K#</b>	Ketone (# = number code)
<b>L#</b>	Ligand (# = number code)
<b>C#X</b>	Complex (# = number code, X = letter code)

---

Literature compound codes

<b>FL<sup>X</sup></b>	Ligands as published by Shen <i>et al.</i> ( <b>X</b> = letter code)
<b>FC<sup>X</sup></b>	Complexes as published by Shen <i>et al.</i> ( <b>X</b> = letter code)
<b>JL</b>	Ligands as published by Hausmann <i>et al.</i>
<b>JC</b>	Complex as published by Hausmann <i>et al.</i>
<b>RL</b>	Ligands as published by Hogue <i>et al.</i>
<b>RC#</b>	Complexes as published by Hogue <i>et al.</i> (# = number code)

## Chapter 1 Introduction

### 1.1 Cyclohelicates

The combination of metal ion and ligand allows complexes to self-assemble into supramolecular architectures. An interesting structure produced by this strategy is the cyclohelicate with a  $[M_xL_x]$  composition. In these structures, each ligand coordinates to one metal from “above” and to another metal from “below” (Figure 1.1).<sup>1,3,8</sup> These are typically formed by the self-assembly of a relatively rigid ligand system with a linear array of polydentate chelating pockets binding first row transition metal ions ( $3d$  metal ions).<sup>2</sup> The outcome of the self-assembly process is largely governed by the design of the bridging ligand and the often-predictable coordination geometry of the metal ion.<sup>1,9</sup> Due to the wide structural diversity of ligands and the different metal geometries it is possible to create cyclohelicates with various shapes, including but not limited to squares and triangles.<sup>1,2,9</sup>

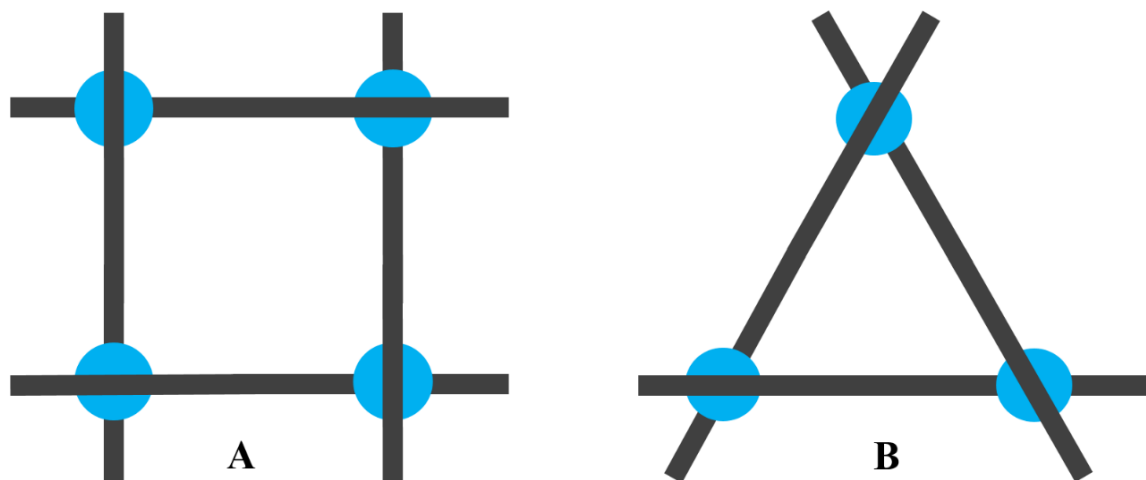


Figure 1.1. The cyclohelicate square (A) and triangle (B) complex.<sup>1-3</sup> The black lines represent the ligand and the blue circles represents the octahedral metal centre.

#### 1.1.1 Cyclohelicate squares and triangles

Cyclohelicate squares are tetrametallic  $[M_4L_4]$  systems and are an example of a chiral  $[2 \times 2]$  grid complex (Figure 1.1 - A). Cyclohelicate triangles are trimetallic  $[M_3L_3]$  systems (Figure 1.1 - B). The metals selected for the formation of these types of

complexes present an octahedral or tetrahedral binding geometry, where the ligands chosen are composed of two antiparallel bi- or terdentate chelating arms.<sup>3,8</sup> Cyclohelicates containing octahedrally coordinated metal centres are more commonly explored as they have displayed more exotic electrochemical properties, while tetrahedrally coordinated metal centres tend to alter their coordination geometry upon redox processes.<sup>10</sup> For the ligand, cyclohelicates with bis-terdentate arms will provide sufficient donor atoms to completely fill the octahedral metal centres.<sup>1</sup>

The formation of cyclohelicates can be understood by looking at the directional bonding approach and the molecular library model.<sup>11,12</sup> The self-assembly of 90 ° corners (metal centre – acceptor) with a rigid linear bridging ligand (donor) is expected to produce a square conformation (see Figure 1.2), however the formation of triangles have been reported.<sup>13</sup> As both cyclohelicates are synthesised under identical conditions, various factors determine which structure will be formed. Entropy favours the formation of the cyclohelicate triangle as more discrete molecules will be formed compared to the cyclohelicate square (4 triangles versus 3 squares from a 12M + 12L mixture). Cyclohelicate squares are more enthalpically favoured due to a smaller geometric strain.<sup>1</sup> Although the formation of cyclohelicate squares are more commonly reported, a bridging ligand with increased flexibility may favour a triangle conformation by distributing the geometric strain to smaller deformations in the ligand backbone.<sup>13</sup>

Cyclohelicate triangles are rarely formed complexes, meaning little is known about their applications. Cyclohelicate squares however have been known to be used in information storage and processing technology.<sup>14,15</sup> With the coordination of paramagnetic metal ions (containing unpaired electrons), these structures can provide intriguing magnetic and electrochemical exchange properties.<sup>1</sup> As minimal work has been done on the cyclohelicate triangles, further discussion into the magnetic and electrochemical properties of cyclohelicate complexes will cover only the cyclohelicate squares.

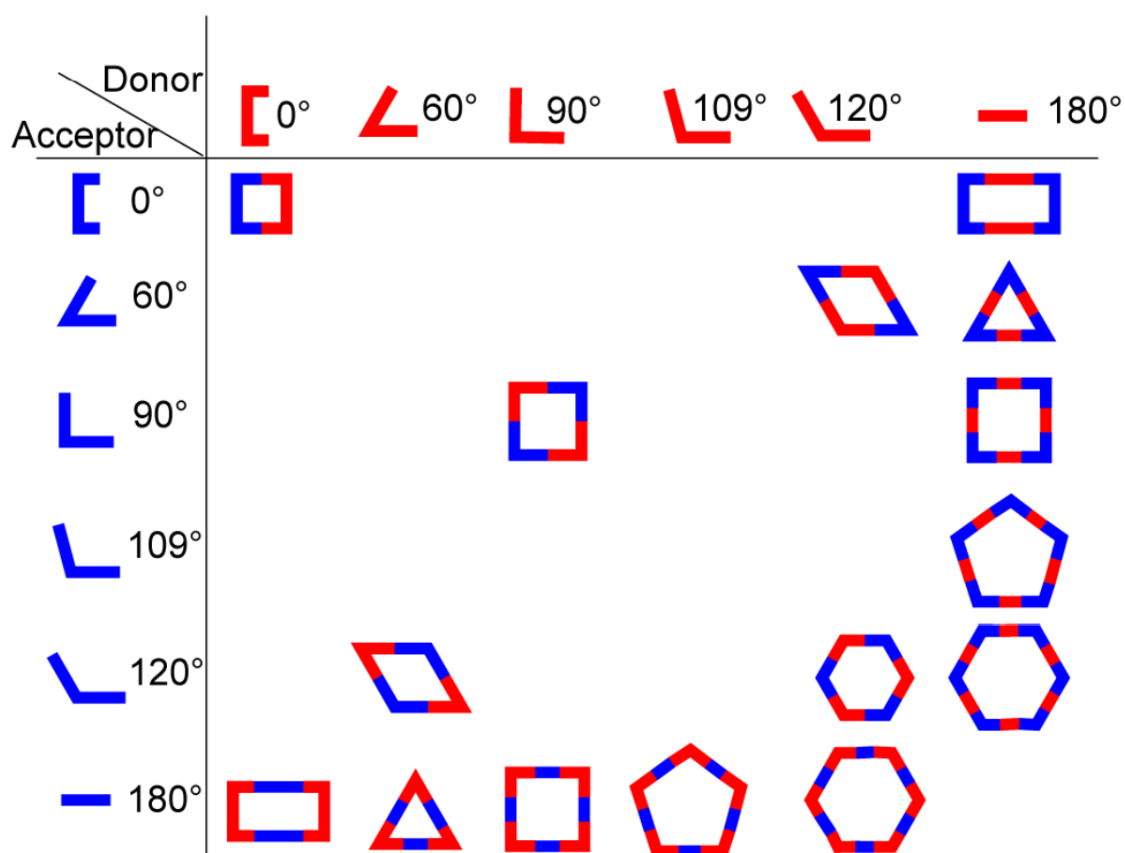


Figure 1.2. 2D Molecular library with various building units for creating supramolecular structures. Reprinted with permission from (Chakrabarty, R.; Mukherjee, P. S.; Stang, P. J. *Chemical Reviews* **2011**, 111, 6810). Copyright (2011) American Chemical Society.

## 1.2 Magnetism

The magnetism of a material arises largely from the magnetic moments generated by the electrons' intrinsic spin. When exposed to an external magnetic field, the spins of the ground state electrons will align with the applied field, exhibiting an attractive or repulsive response. Once removed from the magnetic field, thermal energy will restore the spins to a chaotic state. This reveals two central classes of magnetism: diamagnetism and paramagnetism. Diamagnetism arises from the response of a species with no unpaired electrons (no net spin) with an applied field, where the paired electrons repel in the opposite direction of the field. Paramagnetism is found in species containing unpaired electrons which will align with the magnetic field and display an attractive interaction with an applied magnetic field (Figure 1.3 – a). Further paramagnetic interactions can be observed in bulk materials.

### 1.2.1 Magnetic coupling

Paramagnetic metal centres in a complex may be capable of exhibiting intramolecular magnetic coupling with each other.<sup>14,16</sup> Below a certain temperature (see section 1.3.3 – Curie and Néel points, Figure 1.5), magnetic ordering can be seen in the spins of neighbouring paramagnetic metals once exposed to a magnetic field. The alignment of neighbouring spins in a uniform parallel direction gives rise to ferromagnetism (Figure 1.3 - b), where the alignment in an antiparallel direction

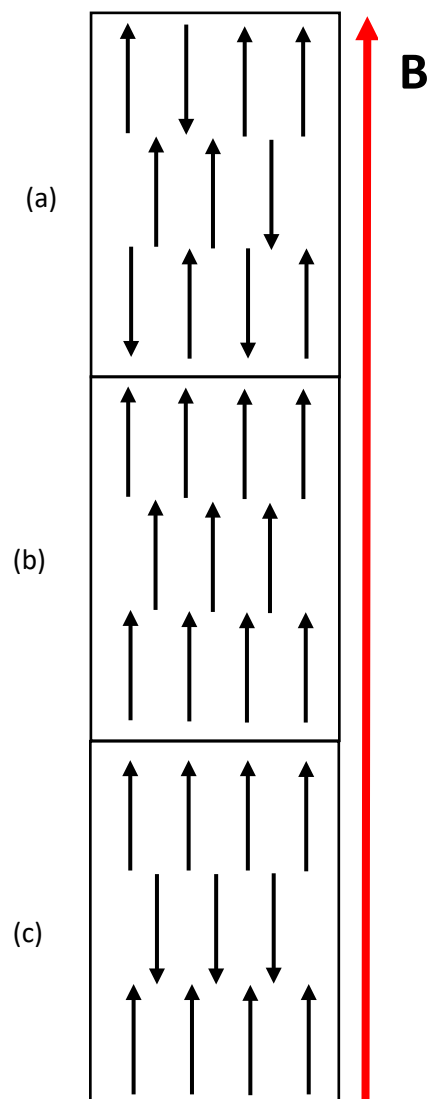


Figure 1.3. Theoretical view of neighbouring electron spins in (a) paramagnetic, (b) ferromagnetic and (c) antiferromagnetic upon exposure to magnetic field,  $B$ . Image was adapted from Orchard.<sup>4</sup>

gives rise to antiferromagnetism (Figure 1.3 – c). Most grid complexes containing paramagnetic  $3d$  metal centres exhibit antiferromagnetic behaviour.<sup>17-19</sup>

### 1.2.2 Superexchange

The dominant force in the spin coupling found in ferromagnetism and antiferromagnetism arises from the covalent bonding of the metal centres with their bridging ligand, leading to superexchange (see Figure 1.4).<sup>4,20-23</sup> This exchange is brought on by the unpaired electron on a metal centre interacting with a fully occupied orbital on the non-magnetic ligand (either  $p$ - or  $\pi$ -orbital). In response, partial donation of electron density is donated to each metal, where the donated spin is opposite to the lone pair on the metal (due to the

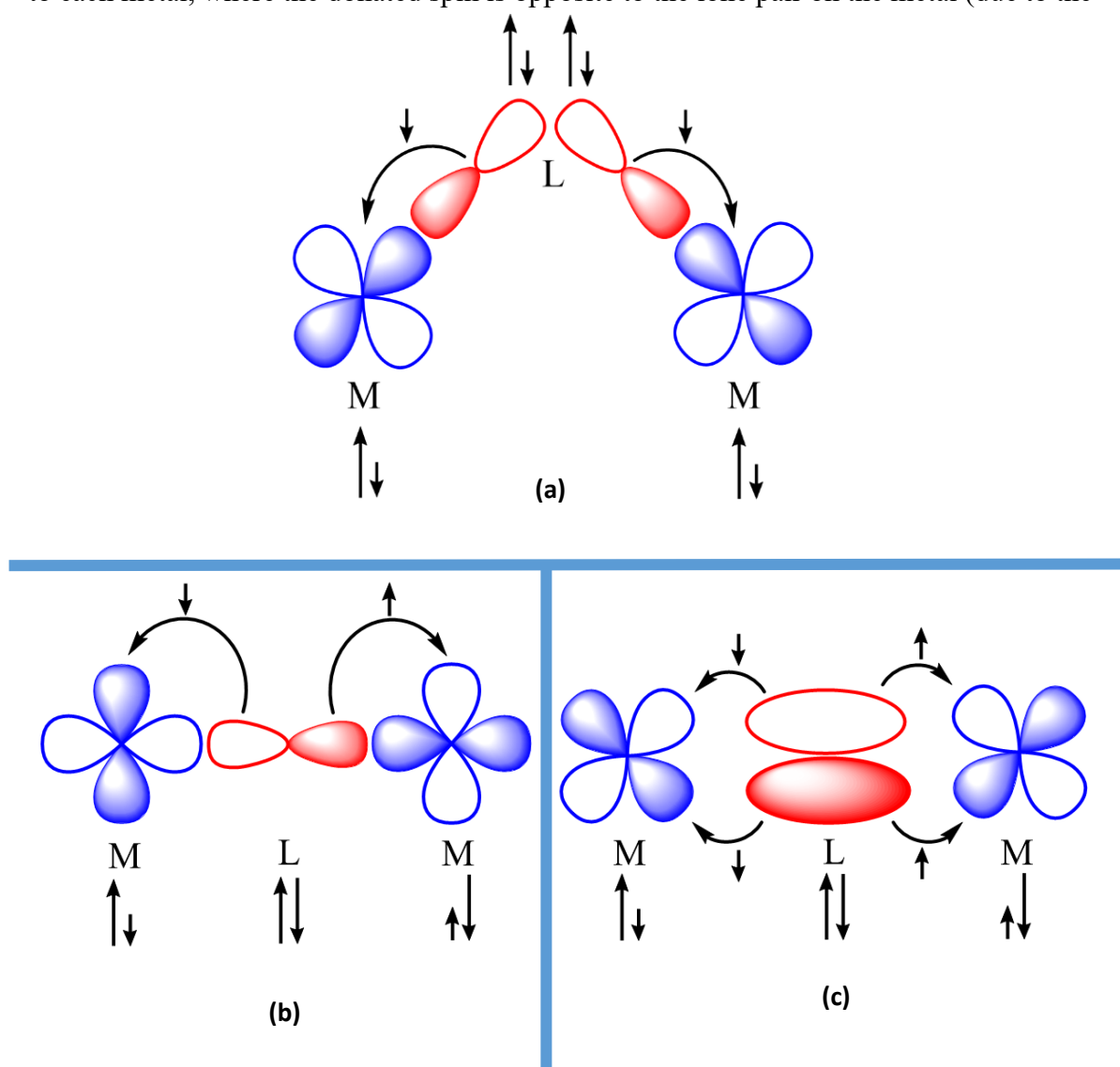


Figure 1.4.  $\sigma$ -type ferromagnetic (a),  $\sigma$ -type antiferromagnetic superexchange (b), and  $\pi$ -type antiferromagnetic superexchange (c). the orthogonal ligand  $p$ -orbitals shown for ferromagnetic superexchange with  $\sigma$ -bonding are separated for clarity. Image was reproduced from Orchard.<sup>4</sup>



Pauli exclusion principle prohibiting a fully occupied orbital containing electrons of the same spin).<sup>4,20,24</sup> The strength of superexchange is dependent on the orbital overlap where linear metal-ligand-metal (M-L-M) systems, presenting effective orbital overlapping, often exhibit antiferromagnetic exchange. The superexchange pathway for antiferromagnetic coupling will either go through a  $\sigma$ -type (Figure 1.4 – b) or  $\pi$ -type (Figure 1.4 – c) pathway, depending on which orbital in the bridging ligand is involved in the superexchange. As the M-L-M bond angle approaches  $90^\circ$ , the metal ion's d-orbitals will overlap with orthogonal p-orbitals on the bridging ligand, leading to superexchange favouring ferromagnetic coupling between the metal centres (Figure 1.4 – a).<sup>4</sup>

The Pauli exclusion principle also determines the likelihood of a particular coupling between metal centres with partially and filled orbitals. Antiferromagnetic coupling will be favoured between two metals with half occupied orbitals.<sup>25</sup> Ferromagnetism will also likely be observed in a system where coupling is present between a metal ion with a half filled orbital and another metal with a filled orbital, or a system presenting coupling between a metal ion with a half filled orbital and another metal ion with an unoccupied orbital.<sup>25</sup>

### 1.2.3 Characterisation of magnetism – SQUID

The use of superconducting quantum interference devices (SQUID) magnetometers have become increasingly common in measuring the magnetic coupling between paramagnetic centres.<sup>26</sup> SQUID magnetometers consists of superconductors, separated by sufficiently thin insulating layers known as Josephson junctions, which permit the electrons to flow through the junctions by quantum tunnelling (also known as the Josephson effect).<sup>26-28</sup> Squid magnetometers typically operate at liquid helium to liquid nitrogen temperatures (4.2 – 77 K).<sup>29</sup> As a current flows through the SQUID apparatus, the high sensitivity of

SQUID magnetometers allow for the detection of magnetic flux,  $\phi$  generated by the superconducting coil versus once a sample is placed within the setup. This is then translated into a voltage that can give information regarding a material's magnetic properties.<sup>30,31</sup>

SQUID magnetometers can provide information regarding the magnetic susceptibility,  $\chi$  (degree of magnetisation) and the effective magnetic moment,  $\mu_{eff}$  of a sample.<sup>31</sup> The anti-parallel spin configuration of antiferromagnetically coupled metal centres will present a negative  $\chi$  value below the Néel point, whereas a ferromagnetically coupled system will yield an increasing positive  $\chi$  value below the Curie point (Figure 1.5).

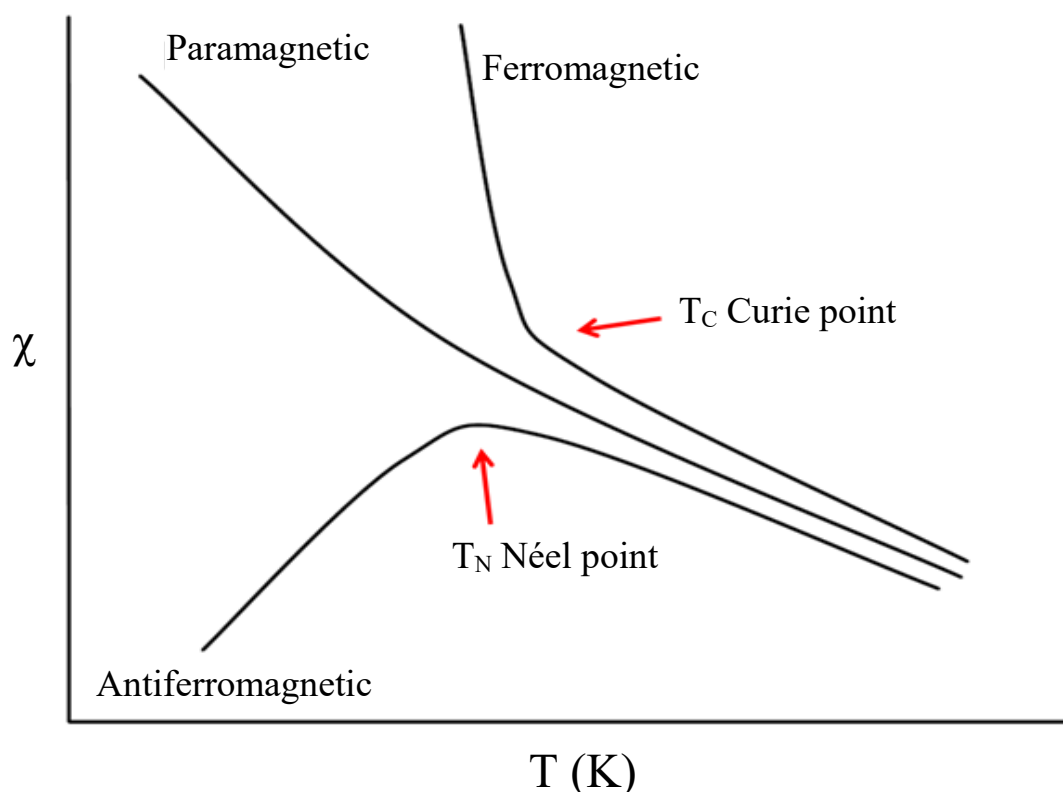


Figure 1.5. Magnetic susceptibility,  $\chi$  vs temperature,  $T$ , showing typical ferro-, antiferro- and paramagnetic slopes. Image was taken from Assoc. Prof. Paul Plieger.

### 1.3 Electronic coupling – Metal-Metal communication

Metallic centres within a cyclohelicate square complex can also exhibit electronic coupling through a bridging ligand.<sup>32</sup> This coupling is best assessed by measuring the influence one metal has on the redox potential of the other within chemically equivalent

environments.<sup>10,33-35</sup> Typically, to ensure electrostatic repulsions are minimised, metal centres at opposite corners of the complex will exhibit oxidation (or reduction) first, followed by a similar process occurring at the remaining two metals.<sup>6,10,36</sup> Electronically speaking, this metal-metal communication is observed when the loss of an electron from a metal centre changes the electron density within that metal, resulting in a positive charge. The change is communicated through the bridging ligand, causing the neighbouring metals to become more difficult to oxidise.<sup>32,33,37,38</sup>

### 1.3.1 Robin and Day classification of mixed-valence complexes

The degree of electronic coupling between the mixed-valence metal centres is described by the Robin and Day classification of mixed-valence systems.<sup>39-42</sup> There are three extremes: class I describes the mixed-valence metal centres as uncoupled with their valences localised to a single site, meaning there will be no electron transfer and no metal-metal interaction between the mixed-valence states.<sup>39,43-45</sup> Class II shows the valences as moderately localised due to the weak electronic coupling between the metals, leading to intervalence charge transfer being possible between the metal centres. The direction of electron transfer will proceed from the highest oxidation state metal to the lowest.<sup>33,43,44</sup> Class III displays a symmetrical delocalisation of the charge over the bridging ligand and through to the metal centres upon oxidation, making the metals essentially equivalent. This class presents the strongest coupling interactions between the two metals.<sup>33,40,43,44</sup> Most mixed-valence systems fall under one of these classes, however there are a select few compounds that can be classified as class II-III systems. This particular class embodies a mixed-valence complex with a sub-borderline delocalised system with strong electronic coupling.<sup>42,46-49</sup>

The electronic coupling between metal centres is mediated through the bridging ligand, so the design of this ligand is a crucial factor in determining the strength of metal-metal

communication. Various physical properties of a bridging ligand including its composition, length and electronic structure can affect the quality of metal-metal interaction.<sup>50</sup>

### 1.3.2 Measuring electrochemical properties – Cyclic voltammetry

Cyclic voltammetry (CV) is a popular technique for monitoring electron transfer processes in electroactive species in solution. It functions by measuring the current produced over a cycled voltage range.<sup>20</sup> A three-electrode

electrochemical cell (as shown in Figure 1.6) is commonly used in CV analysis, where the electrochemical cell consists of a working electrode, WE, the counter electrode, CE and a reference electrode, RE.

A cyclic sweeping voltage is imposed on the working electrode where oxidation of the analyte occurs as the voltage approaches in a positive direction, and reduction of the analyte occurs as the voltage approaches a negative direction.<sup>51</sup> To ensure that the redox profiles are accurate, both the working and counter electrodes are redox-inert over the desired voltage range being measured.<sup>51</sup> The reference electrode remains under a constant voltage and sets a ‘reference’ for the applied voltage to be measured against.<sup>51</sup>

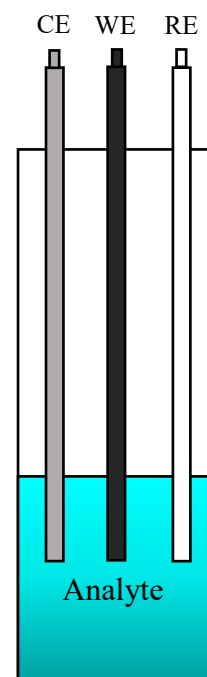


Figure 1.6. A three-electrode electrochemical cell.

Cyclic voltammetry is also used to determine the chemical and electrochemical reversibility of an analyte. Species that exhibit fast electron transfer processes are more likely to be electrochemically reversible.<sup>51</sup> Analytes that are electrochemically reversible will show a small separation between the oxidation and reduction peak ( $\leq 57$  mV for a one electron transfer process).<sup>51</sup> The ability to undergo redox processes and show

reversibility indicate a relatively stable complex that may be suitable for information storage applications.<sup>52</sup>

There are multiple practical considerations to address prior to performing a CV analysis. In preparing the sample (analyte), an appropriate solvent must be chosen. The solvent must be capable of dissolving the analyte and be stable to oxidation and reduction processes in the potential range of the experiment (the potential range of a solvent is described as the potential window).<sup>51</sup> Solvents commonly employed are dimethylformamide (DMF) and acetonitrile (MeCN). A supporting electrolyte is often dissolved in the analyte to decrease the solution's resistance to charge transfer. The supporting electrolyte achieves this by balancing the charge change caused by the electron transfer processes on the working electrode.<sup>51</sup> Ideal supporting electrolytes are highly soluble in the selected solvent and present electrochemical and chemical inertness in the experimental conditions.<sup>51</sup> Ammonium salts with counterions such as  $[\text{B}(\text{C}_6\text{H}_5)_4]^-$ ,  $[\text{PF}_6]^-$ ,  $[\text{BF}_4]^-$  and  $[\text{ClO}_4]^-$  are commonly employed in CV experiments.<sup>51</sup> Microelectrodes are a type of electrode which provide a small surface area (typically less than 20  $\mu\text{m}$ ).<sup>53</sup> This results in a large current density on the electrode surface, thus providing a higher signal-to-noise ratio compared to standard electrodes.<sup>51,53</sup> This means that the use of supporting electrolytes is unnecessary when using microelectrodes.<sup>53</sup>

## 1.4 Creutz-Taube ion

Interest in metal-metal communication can be traced back to the Creutz-Taube (CT) ion, which is now one of the most thoroughly studied complexes exhibiting this phenomenon. Synthesised in 1969, the CT ion,  $[(\text{NH}_3)_5\text{Ru}]_2\text{pz}^{5+}$  consists of two mixed-valence ruthenium metal cations ( $\text{Ru}^{2+}$  and  $\text{Ru}^{3+}$ ) within chemically identical environments (see Figure 1.7).<sup>33,37,54</sup>

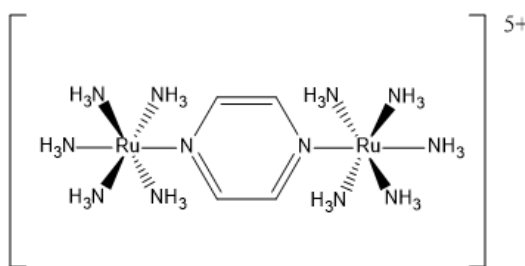


Figure 1.7. The Creutz-Taube Ion,  $[(\text{NH}_3)_5\text{Ru}]_2\text{pz}^{5+}$  where pz = pyrazine.

Initially proposed as a class II complex, the CT ion exhibits delocalisation similar to class III complexes. Later it was discovered that the CT ion belongs to the unique class II-III.<sup>46,55</sup> The  $\text{Ru}^{2+}/\text{Ru}^{3+}$  redox potentials of each metal in the CT ion were analysed, yielding a separation of 0.39 V between each oxidation peak. This clear separation indicates a distinct interaction occurring between the two ruthenium metal centres.<sup>33,37</sup> Magnetic measurements were also performed on the CT ion, showing a weak antiferromagnetic interaction on the fully oxidised CT ion ( $\text{Ru}^{3+}/\text{Ru}^{3+}$ ).<sup>56</sup> The electronic communication was brought on by the effective overlapping of the metals'  $d\pi$  orbitals ( $4d_{xz}$  and  $4d_{yz}$  for the CT ion) with pyrazine's delocalised  $\pi^*$  orbital, as shown by the  $\beta$ -HOMO in Figure 1.8.<sup>33,57,58</sup>

Extensive study has revealed trends between the electronic and magnetic coupling in systems exhibiting metal-metal communication. For example, antiferromagnetic coupling between transition metals often leads to an increase in the conductance for a given bridge, indicating a probable increase in metal-metal communication.<sup>59</sup> Likewise, para-connected bridging ligands often lead to antiferromagnetic coupling between transition metals.<sup>59</sup>

Considering these trends, it comes as no surprise that pyrazine was essential for enabling the metal-metal communication in the CT ion.

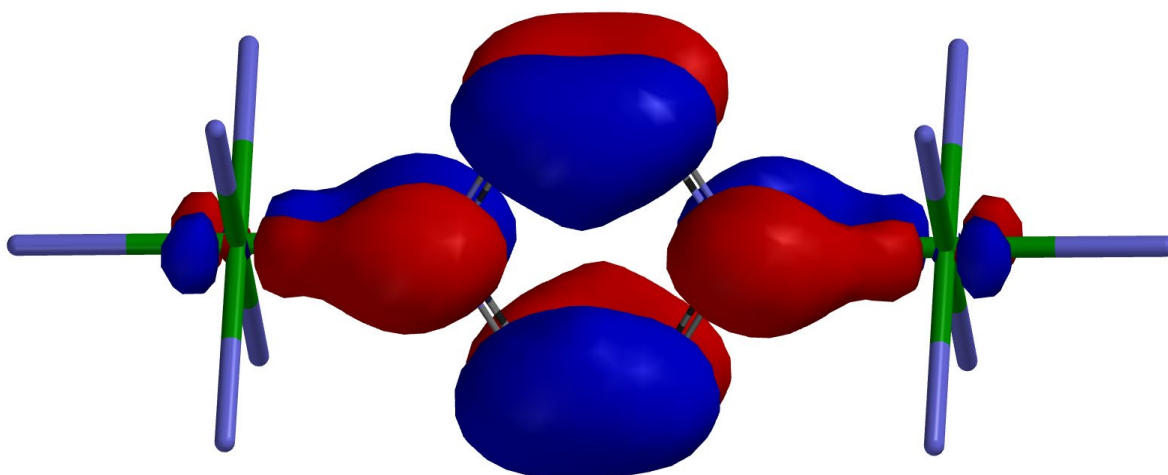


Figure 1.8. Calculated  $\beta$ -HOMO of the CT ion (isovalue = 0.04). Grey = carbon; purple = nitrogen; green = ruthenium. Hydrogens were removed for clarity. The image was generated using Spartan, using a unrestricted Hartree Fock calculation, with the 3-21\* basis set with a total of +5 whilst in a doublet state.

## 1.5 Pyrazine

Pyrazine (Figure 1.9 – C) is a six-membered, N-heterocyclic aromatic molecule belonging to a class of compounds called diazines (Figure 1.9).<sup>60</sup> Since the discovery of the CT ion, the use of pyrazine as a bridging ligand between two metal centres has increased in popularity. There are many advantages of using pyrazine as a bridging ligand between two metal centres. Pyrazine is known as a good  $\pi$ -acceptor ligand as it can accept electron density from the metal into the aromatic ring, strengthening metal-ligand interactions. Being a good  $\pi$ -acceptor ligand also provides the stabilisation of complexation of metal ions through  $\pi$ -backbonding.<sup>60-63</sup> In the case of the CT ion, this occurs when the lone pair of electrons from N-donor atoms in the ring are donated to an

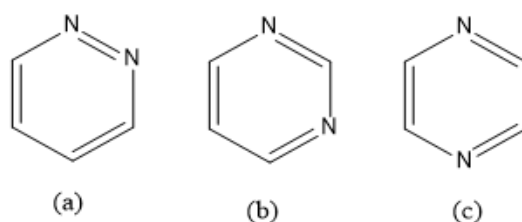


Figure 1.9. The three structural isomers of the diazine: Pyridazine (a), Pyrimidine (b) and Pyrazine (c).

unoccupied d-orbital on the ruthenium centres. In return, an electron lone pair from ruthenium's d-orbital is donated through to an unoccupied  $\pi^*$ -orbital on the pyrazine bridging ligand.<sup>24,54,64,65</sup>

### 1.5.1 Pyrazine as a bridging ligand

When utilised as a bridging ligand, pyrazine is well known for supporting antiferromagnetic coupling between metals up to 62 K.<sup>66</sup> The magnetic exchange occurs through superexchange mechanisms (Section 1.2.2) which can occur through a  $\sigma$ -pathway involving the nitrogen lone pair, or through the delocalised  $\pi$  system.<sup>67,68</sup> The effectiveness of a particular superexchange pathway is dependent on the metal-ligand distance and the degree of appropriate overlapping of the metal's magnetic orbitals with pyrazine's p- or  $\pi$ -orbitals which can be influenced by the presence of substituents on pyrazine.<sup>67,69</sup>

Pyrazine is electron deficient due to the electronegativity of the nitrogen atoms and this makes it susceptible to nucleophilic attack on the neighbouring carbons, therefore allowing functionality to be placed on pyrazine.<sup>70</sup> Functionalising the 2 and 5 (para) positions on pyrazine with arms containing suitable donor atoms will allow the formation of a relatively rigid ligand system (due to the steric hinderance of pyrazine)<sup>71</sup> with a linear, antiparallel array of bis-terdentate chelating pockets. Coordination of 3d metal ions with octahedral coordination geometries can result in the formation of cyclohelicite squares and triangles.

Below are a number of examples of pyrazine-containing complexes. These reveal the vitality of this system in the design of cyclohelicites.



## 1.6 Examples of cyclohelicate squares and triangles with pyrazine bridging ligands

### 1.6.1 Synthesis of cyclohelicate squares by Shen *et al.*

Shen *et al.* reported the synthesis of three cobalt(II) [2x2] grid complexes from three symmetrical 2,5-pyrazine hydrazones. The team were able to tune the ligand by incorporating functionality such as methyl and bromo substituents into the R<sub>1</sub> and R<sub>2</sub> position, giving **FL<sup>H</sup>**, **FL<sup>Me</sup>** and **FL<sup>Br</sup>** (Figure 1.10).<sup>6</sup>

The reactions of **FL<sup>H</sup>**, **FL<sup>Me</sup>** and **FL<sup>Br</sup>** with Co(ClO<sub>4</sub>)<sub>2</sub>·6H<sub>2</sub>O yielded the three [2x2] grid complexes which are shown in Figure 1.10. These complexes are [Co<sup>2+</sup><sub>4</sub>(**FL<sup>H</sup>**)](ClO<sub>4</sub>)<sub>4</sub>·6DMF·3H<sub>2</sub>O, **FC<sup>H</sup>**; [Co<sup>2+</sup><sub>4</sub>(**FL<sup>Me</sup>**)](ClO<sub>4</sub>)<sub>8</sub>·4MeCN·H<sub>2</sub>O, **FC<sup>Me</sup>** and [Co<sup>2+</sup><sub>4</sub>(**FL<sup>Br</sup>**)](ClO<sub>4</sub>)<sub>8</sub>·CH<sub>3</sub>OH·2MeCN·5H<sub>2</sub>O, **FC<sup>Br</sup>** (Figure 1.10 shows **FC<sup>H</sup>** as an example of the structure of **FC<sup>H</sup>**, **FC<sup>Me</sup>** and **FC<sup>Br</sup>**). Crystals suitable for single crystal x-ray diffraction (SCXRD) of all three complexes by vapour diffusion of diethyl ether into the reaction filtrate, confirming the grid structure.<sup>6</sup> The ligands in all three [2x2] grid complexes acted as N<sub>3</sub>-N<sub>3</sub> bi-terdentate chelates, where the cobalt centres were coordinated in a distorted octahedra geometry to the pyrazine N donor atom, the pyridine moiety and the unfunctionalised hydrazone N donor atom.

Magnetic susceptibility data was collected from the three complexes. **FC<sup>H</sup>** displayed a null magnetic susceptibility response to an applied magnetic field. This is indicative that the cobalt centres in the grid complex are low spin Co<sup>3+</sup>, implying a d<sup>6</sup> electron configuration, thus the metal centres are diamagnetic.<sup>6</sup> **FC<sup>Me</sup>** and **FC<sup>Br</sup>** both show a paramagnetic response, indicative of the presence of Co<sup>II</sup> species. Complexes **FC<sup>Me</sup>** and **FC<sup>Br</sup>** showed a decrease in the sample's magnetic susceptibility as the temperature was cooled below 40 K. This indicates that both **FC<sup>Me</sup>** and **FC<sup>Br</sup>** show weak antiferromagnetic coupling between the metal centres.<sup>6</sup>

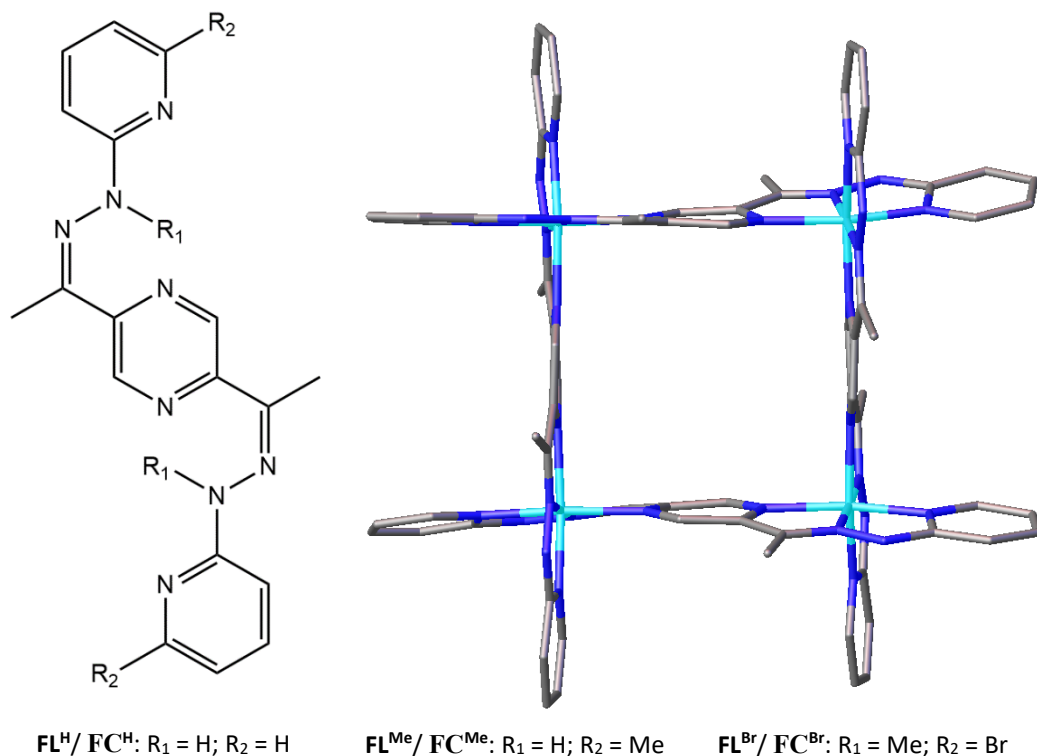


Figure 1.10. Framework of the ligand **FL** (left) and SCXRD structure of the cyclohelicate square, **FC<sup>H</sup>**. Ligand was reproduced from Shen *et al.*<sup>6</sup> SCXRD structure presented as tubes. Grey = carbon; purple = nitrogen; cyan = cobalt. Hydrogens and counterions were removed for clarity.

Electrochemical analysis was also performed by cyclic voltammetry (Figure 1.11). All three complexes showed four quasi-reversible one-electron oxidation processes, indicating that the electron transfer process is almost reversible, but the oxidation/reduction peak separation still exceeds 57 mV for a one electron transfer process (see section 1.3.2 for the importance of the reversibility of a complex). Shen *et al.* postulated that these processes correspond to the one-step oxidation from  $\text{Co}^{2+}$  to  $\text{Co}^{3+}$ , with the fourth oxidation peak (peak furthest to the right in voltammogram), leading to the  $\text{Co}^{3+}_4$  grid species. **FC<sup>H</sup>** and **FC<sup>Me</sup>** show two pairs of oxidation/reduction peaks separated by a large gap (more evident in complex **FC<sup>H</sup>**).<sup>6</sup> The first pair of peaks (left hand side peaks on voltammogram) for **FC<sup>H</sup>** and **FC<sup>Me</sup>** indicate the one-electron oxidations of two  $\text{Co}^{\text{II}}$  species into the  $\text{Co}^{\text{III}}$  species, resulting in a more thermodynamically stable mixed valence  $\text{Co}^{\text{II}}_2/\text{Co}^{\text{III}}_2$  complex, where it is assumed the two oxidation processes occur at opposite corners of the grid.<sup>6</sup> As the gap between the

two pairs of peaks in  $\text{FC}^{\text{H}}$  is quite large, it is thought that this is indicative of metal-metal communication as the formation of a  $\text{Co}^{2+}/\text{Co}^{3+}$  species is unfavourable compared to the  $\text{Co}^{2+}_2/\text{Co}^{3+}_2$  species. This interaction possibly arises from the deprotonation of the ligand in  $\text{FC}^{\text{H}}$ , causing a larger electron delocalisation throughout the complex.<sup>6</sup>  $\text{FC}^{\text{Me}}$  requires the greatest voltage to undergo the first oxidation step ( $\text{Co}^{2+}_4 \rightarrow \text{Co}^{2+}_3/\text{Co}^{3+}$ ). This is because the increase in delocalisation from  $\text{FC}^{\text{H}}$  and the presence of bromine (a known weak field ligand and  $\pi$ -donating substituent according to the spectrochemical series)<sup>20,24,72</sup> in  $\text{FC}^{\text{Br}}$  causes the ligand in both complexes to act as weaker  $\pi$ -acceptors.

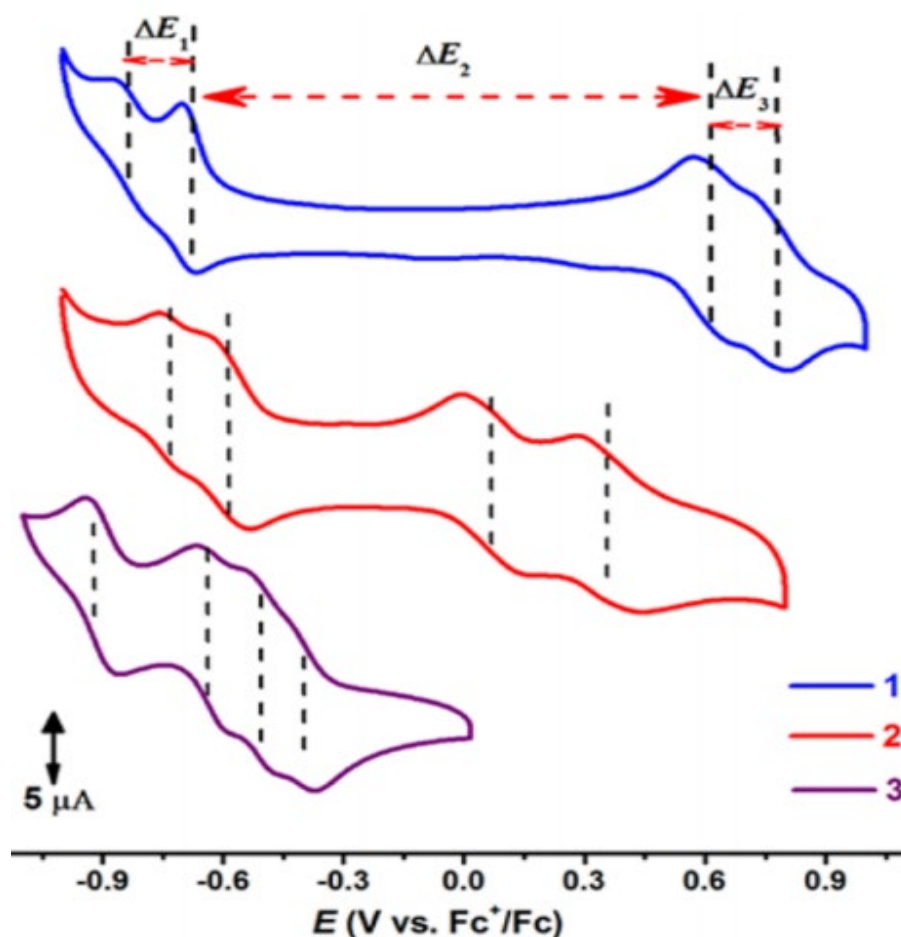


Figure 1.11. Cyclic voltammogram of  $\text{FC}^{\text{H}}$  (top voltammogram, 1),  $\text{FC}^{\text{Me}}$  (middle voltammogram, 2) and  $\text{FC}^{\text{Br}}$  (bottom voltammogram, 3) recorded in MeCN ( $M = 0.1 \text{ nM}$ ) and referenced against  $\text{Fc}^+/\text{Fc}$  ( $\text{Fc} = \text{ferrocene}$ ) at a scan rate of  $100 \text{ mV/s}$ .  $\text{nBu}_4\text{NPF}_6$  ( $0.1 \text{ M}$ ) was used as the supporting electrolyte. Reprinted with permission from Shen, F.; Huang, W.; Wu, D.; Zheng, Z.; Huang, X.-C.; Sato, O. *Inorganic Chemistry* **2016**, 55, 902. Copyright (2015) American Chemical Society.

This weakens the ligand strength in both  $\text{FC}^{\text{H}}$  and  $\text{FC}^{\text{Br}}$ , allowing for oxidation processes to occur at a smaller voltage than  $\text{FC}^{\text{Me}}$ .<sup>6</sup>

### 1.6.2 Synthesis of a cyclohelicate square by Hausmann *et al.*

Hausmann and Brooker reported the successful synthesis of a chiral Co(III) grid-type complex from the complexation of a diamide pyrazine ligand, **JL** and  $\text{Co}(\text{BF}_4)_2 \cdot 6\text{H}_2\text{O}$  in MeCN, followed by air oxidation  $[\text{Co}^{\text{III}}_4\text{JL}_4](\text{BF}_4)_4$  (**JC**) (Figure 1.12). The presence of two equivalents of triethylamine was necessary for the synthesis of **JC** to deprotonate the amide centres in the complex, as was shown by an increase in the yield of the isolated dark red crystalline solid  $\text{JC} \cdot 10\text{H}_2\text{O}$  from 30 % to 85%.<sup>8</sup> Vapour diffusion of diethyl ether into a MeCN solution containing  $\text{JC} \cdot 10\text{H}_2\text{O}$  gave dark red single crystals of  $\text{JC} \cdot 12.75\text{MeCN}$  (as reported by Hausmann *et al.*) suitable for SCXRD. This showed the cyclohelicate square complex where each of the four ligands act as a  $\text{N}_3\text{-N}_3$  bis-terdentate chelate, thus giving each cobalt centre a distorted octahedra geometry.<sup>8</sup> Interesting features of the grid include the non-linear pyrazine, as indicated by the angle between the cobalt centre and the pyrazine's nitrogens,  $\text{N}_{\text{pz}}$  where the bite/chelating angle is roughly

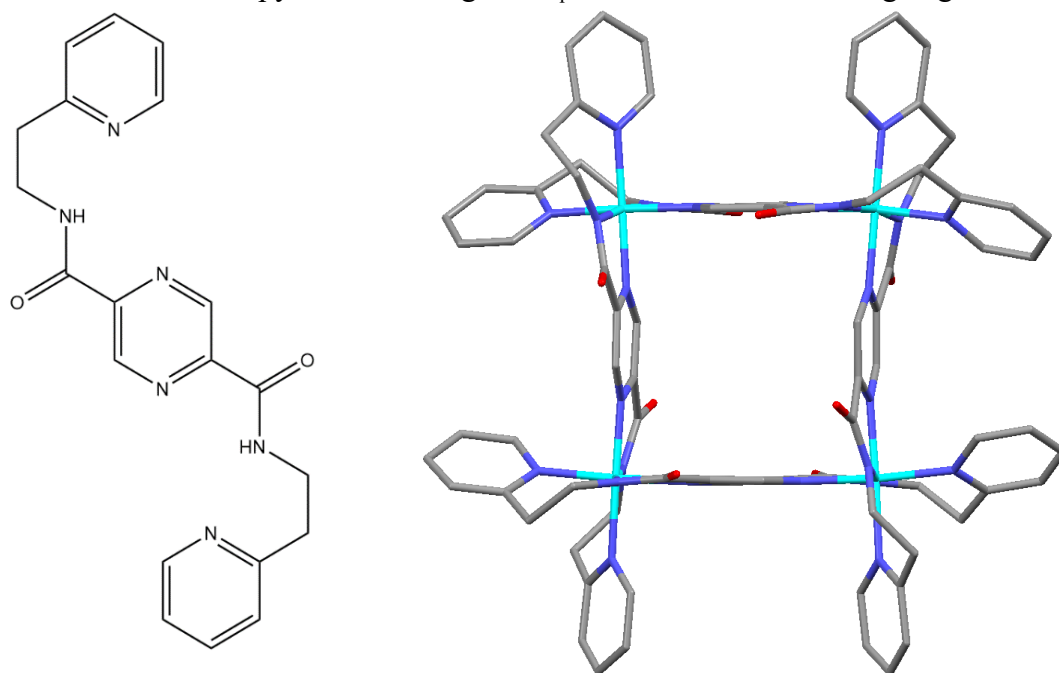


Figure 1.12. **JL** ligand structure (left) and SCXRD structure of the formed cyclohelicate square  $\text{JC} \cdot 12.75\text{MeCN}$  (right). SCXRD structure presented as tubes. Grey = carbon; purple = nitrogen; red = oxygen; cyan = cobalt. Hydrogens and counterions were removed for clarity.

172 ° (significantly less than the expected 180 °), giving the grid a slight astroid square shape (with each ligand adopting a concave geometry). The interwoven coordination of each chiral ligand to the metal centres provides a racemic mixture of ( $\Delta\Delta\Delta$ ) and ( $\Lambda\Lambda\Lambda$ ) enantiomers.<sup>8</sup> No magnetic or electrochemical data was collected on the complex.

### 1.6.3 Synthesis of cyclohelicate triangles by Hogue *et al.*

Hogue *et al.* recently attempted to synthesise iron(II) and zinc(II) [2x2] cyclohelicate square complexes with **RL** (an imine derivative of **JL** – see Figure 1.13), derived from a Schiff-base condensation between pyrazine-2,5-dicarbaldehyde and 2-(2-aminoethyl)pyridine.<sup>1</sup> Unexpectedly, the complexations with **RL** and  $M^{II}(\text{BF}_4)_2 \cdot x\text{H}_2\text{O}$  (**RC1**:  $M = \text{Zn}$ ,  $x = 1$ ; **RC2**:  $M = \text{Fe}$ ,  $x = 6$ ) in MeCN produced trimetallic triangular cyclohelicates  $[\text{Zn}_3\text{L}_3](\text{BF}_4)_6$  (**RC1**) and  $[\text{Fe}_3\text{L}_3](\text{BF}_4)_6$  (**RC2**) in moderate yields (**RC1**: 84 %; **RC2**: 52 %). This defies the expectations based on the molecular library model<sup>12</sup> and the directional bonding approach<sup>11</sup> (see section 1.1) which are used to predict the structural outcome of a supramolecular complex when a rigid ligand coordinates to a

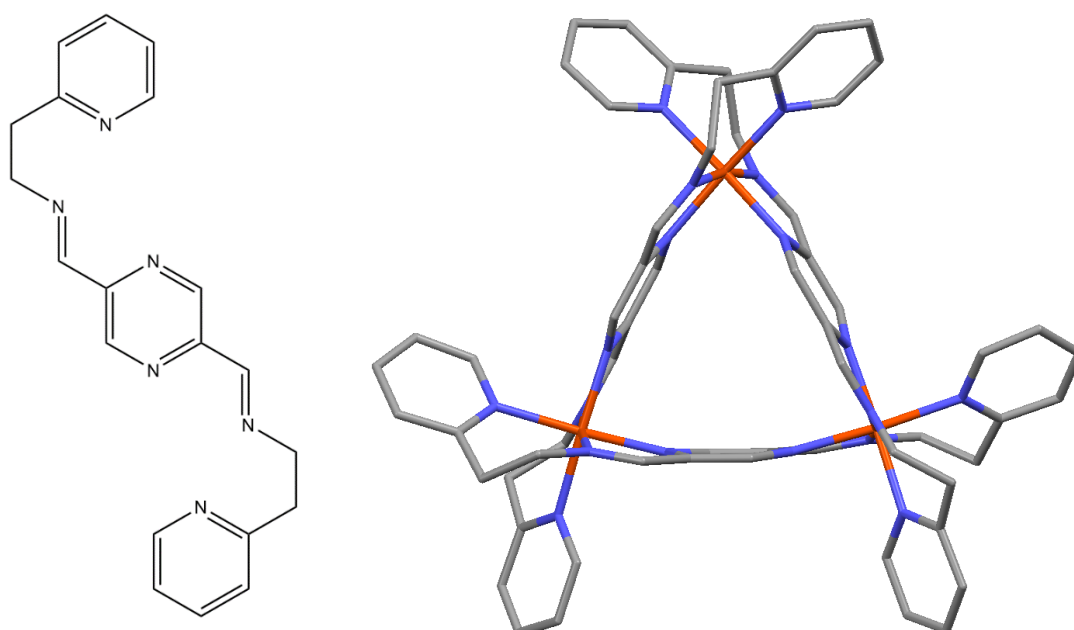


Figure 1.13. **RL** ligand structure (left) and SCXRD structure of the cyclohelicate triangle (right). SCXRD structure shown is **RC2**. SCXRD structure presented as tubes. Grey = carbon; purple = nitrogen; orange = iron. Hydrogens and counterions were removed for clarity.

transition metal centre, where the formation of a [2x2] grid-type complex was predicted.<sup>1,11,12</sup> Vapour diffusion of diethyl ether in solutions containing both complexes respectively in MeCN produced **RC1** and **RC2** as tan block-like and green plate-like single crystals, both of which were suitable for SCXRD. Similar to its grid predecessor, **RC1** possesses N<sub>3</sub>-N<sub>3</sub> bis-terdentate chelating pockets with anti-parallel coordinating vectors. This varies from the grid complex produced from the aforementioned **JC** as all the donor atoms within **RC1** are coordinating to the metal centres, as opposed to **JC** where the O<sub>am</sub> does not coordinate to the metal centre.<sup>1</sup> Much like the grid complexes mentioned earlier, the cyclohelical structure brings with it chirality, where each complex exists as a racemic mixture of ( $\Delta\Delta\Delta$ ) and ( $\Lambda\Lambda\Lambda$ ) enantiomers.<sup>1</sup> Although the complex is triangular-shaped, the N<sub>pz</sub> – M – N<sub>pz</sub> bite angles for both complexes average between ca. 80 – 85 ° (as opposed to the expected 60 °), meaning that the triangular shape is most likely attributed to the nonlinearity of the pyrazine bridge, as shown by the M – N<sub>pz</sub> – N<sub>pz</sub> bond angle (for M = Fe: ca. 162 – 167 °; M = Zn: ca. 163 – 167 °).<sup>1</sup> These deviations give the cyclohelicate triangles a reuleaux triangle shape (with each ligand adopting a convex geometry – see Figure 1.14). The X-ray data indicated that the iron(II) centres in the iron triangle complex would be low spin at 85 K, resulting in diamagnetic iron centres if subjected to a SQUID magnetometer. Minimal work was done to measure the magnetic and electrochemical properties of both the zinc and iron complexes.

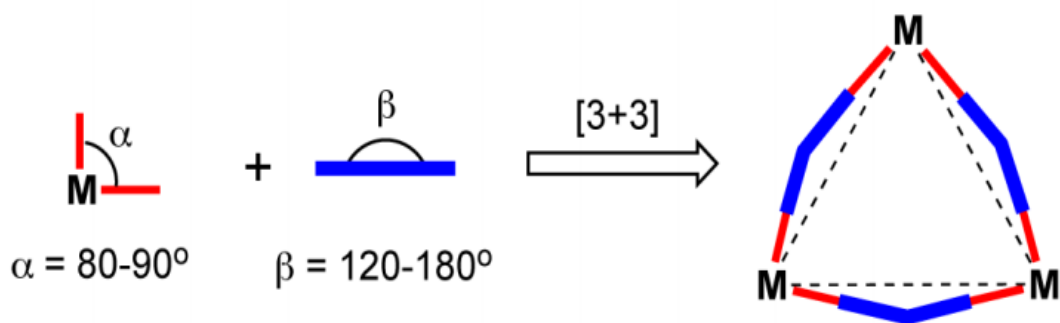


Figure 1.14. Directional-bonding approach for the synthesis of [M<sub>3</sub>L<sub>3</sub>] triangles, exhibiting conformational strain similar to cyclohelicate triangles **RC1-2**. Reprinted with permission from (Chakrabarty, R.; Mukherjee, P. S.; Stang, P. J. *Chemical Reviews* **2011**, 111, 6810). Copyright (2011) American Chemical Society.

## 1.7 Summary

Cyclohelicate squares and triangles are recently developed intricate architectures consisting of a rigid ligand system with an antiparallel array of polydentate arms, and a transition metal with an octahedral or tetrahedral configuration. Most of the research performed on cyclohelicates have been performed with octahedral  $3d$  metal centres. Studies show that these compounds are capable of exhibiting communal magnetic and electrochemical properties.<sup>10,14</sup> These structures have potential to be employed in applications in a variety of fields, including, but not limited to, information storage devices<sup>73</sup> and crystal engineering<sup>74</sup>. Not only that, but these structures have the possibility to exhibit properties not covered in this report, including spin crossover, pH-dependent optical switching, host-guest recognition and catalysis.<sup>6,73</sup>

Pyrazine is an N-heterocyclic ring that was involved in the pioneering work to observe metal-metal communication in the CT ion. Since this time, it has been incorporated into various complexes that display interesting magnetic and electrochemical phenomena. Its presence in cyclohelicate structures has become more popular in recent times, however the analysis on the electrochemical and magnetic properties brought on by the addition of pyrazine in these systems have been scarcely reported.

## 1.8 Research aims and hypothesis

The goal of this research is to synthesise a collection of symmetric bis-terdentate pyrazine-based ligands capable of coordinating to octahedral  $3d$  metal centres. To aid synthesis, the ligands will be prepared by Schiff base condensation analogues to Hogue *et al.* (see section 2.1 for more information regarding Schiff base reactions).<sup>1</sup> Following this, the ligands synthesised will undergo complexations with assorted  $3d$  metal salts in the hope of forming cyclohelicates. Investigations into the communication of the metals will be tested through analysing their electrochemical and magnetic properties.

Pyrazine is well known for its ability to mediate electronic and magnetic communication (examples include the CT ion), and has acted as a suitable bridging ligand in cyclohelicate structures previously reported.<sup>66</sup> It is therefore my hypothesis that with effective ligand design, unique pyrazine-based cyclohelicate structures can be synthesised, where electronic and magnetic communication should be observed between the metal centres.

## 1.9 Thesis outline

Chapter 2 details the design of Schiff base ligands and the various properties that must be considered in this process. It will include recapping the requirements necessary to form a cyclohelicate complex, as well as discussing the principles of a Schiff base reaction and how this reaction will be used to synthesise ligands. This chapter will also cover the various metals that will be considered to use for forming the cyclohelicate structures after synthesising the ligands. This chapter aims to show the necessary chemical components and conditions for the synthesis of Schiff base ligands incorporating pyrazine to be used for the formation of cyclohelicates.

Chapter 3 explores the previously established methods for synthesising the dialdehyde products required for the synthesis of ligands, as well as providing original routes as attempts to optimise/develop the formation of certain products. The synthesis of pyrazine-2,5-dicarbaldehyde will be discussed first, followed by the synthesis of pyrazine-2,5-diacetaldehyde. This chapter will discuss the general procedures followed and provide feedback on the results produced from each step. If any experiments reported no successful attempts, alternative courses of action will be advised in the case that efforts in this subject be made in the future. By the end of this chapter, the reader should have an understanding on the results obtained over the course of this study in regards to the synthesis of Schiff base precursors.



Chapter 4 examines the synthesis of original symmetric Schiff base ligands with pyrazine-2,5-dicarbaldehyde. This chapter includes the general synthetic method used to synthesise each ligand along with characterisation data collected to support the successful synthesis of these compounds. Any unsuccessful attempts in obtaining single crystals of suitable quality for SCXRD is reported, along with suggestions to investigate for future repeat attempts.

Chapter 5 covers the attempts to form cyclohelicates. This is done through complexations with a pure Schiff base ligand and assorted metal salts. This chapter will give details into the synthesis of each complex, as well as the techniques used to characterise the complexes. Following this, the various methods used to characterise the communication found within the complexes are discussed.

The appendices will delve into the synthetic routes taken in attempts to synthesise various products, but could not be isolated as pure product. Following this, the section discusses the preparation of reagents and solvents, the apparatus used and the information obtained from the SCXRD data of compounds that successfully produced single crystals of suitable quality. Lastly, the experiment procedure for synthesising all compounds that were successfully isolated as a pure product is recorded, as well as the characterisation data of the respective compounds. Providing this information will aid in the ability of replicating the results found in this report.

## Chapter 2 Ligand Design

In order to form cyclohelicates from octahedral metal ions, a linear, rigid ligand with antiparallel arms that create a bis-terdentate chelating environment is needed. An obvious choice for the construction of such a moiety is pyrazine as the two para nitrogens enforce the correct ligand geometry.<sup>75</sup> The inclusion of functionality to the 2 and 5 positions of pyrazine (Figure 2.1) must therefore provide two additional donor atoms to fully accommodate the coordination of octahedral 3*d* metal salts.

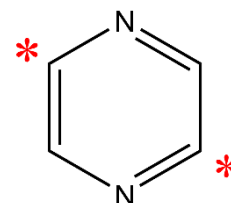
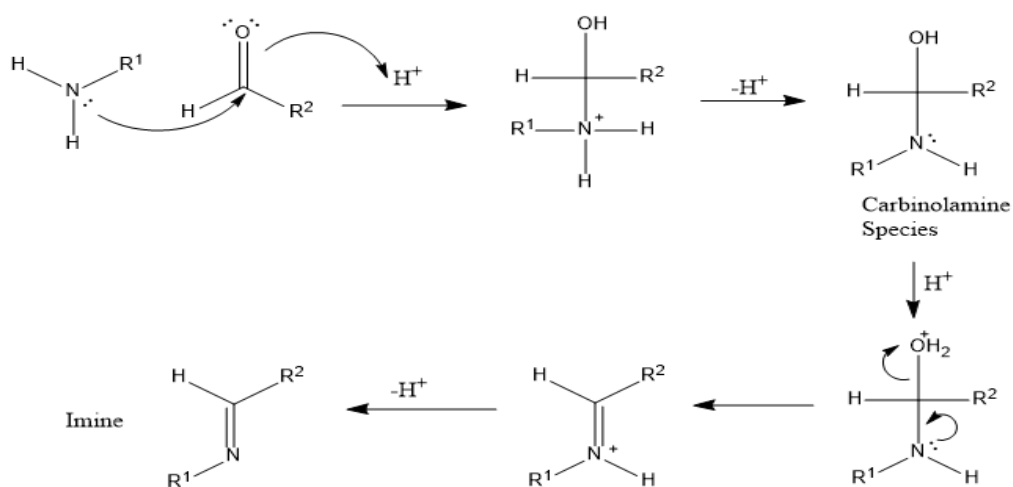


Figure 2.1. Pyrazine with 2 and 5 positions indicated.

### 2.1 Schiff base

The Schiff base condensation is a simple method for the construction of ligands and it has made a significant contribution to the library of cyclohelicate complexes synthesised largely due to their synthetic simplicity, often presenting high yields for a small economic cost.<sup>1,6,76-78</sup> The classic Schiff base condensation (See Scheme 2.1) involves the reaction of a primary amine and a carbonyl species (either an aldehyde or ketone). The nucleophilic attack of the amine on the electrophilic carbonyl carbon results in the development of a carbinolamine species. The dehydration of the water formed produces the characteristic imine, where R<sup>1</sup> and R<sup>2</sup> exist as identical or different alkyl, aryl or



Scheme 2.1. Mechanism for Schiff base condensation.

heteroaryl substituents. The imine can be hydrolysed back into its starting precursors in aqueous acidic conditions.<sup>79</sup>

A range of characterisation techniques can monitor the Schiff base condensation and determine the successful formation of the imine ( $C = N$ ). Using infrared (IR) spectroscopy, the presence of the peak corresponding to the imine ( $1690\text{-}1640\text{ cm}^{-1}$ ) and the absence of the carbonyl undergoing the Schiff base condensation ( $1720\text{-}1680\text{ cm}^{-1}$ ) are used to confirm the successful condensation.<sup>80</sup> Using an aldehyde as the carbonyl component for the Schiff base condensation can benefit from using  $^1\text{H}$  and  $^{13}\text{C}$  NMR spectroscopy to distinguish the imine bond by observing the disappearance of the carbonyl peak (usually around  $\delta = 9.5 - 10$  ppm) and the appearance of a singlet imine peak typically upshifted in the spectrum ( $\delta = 8 - 8.5$  ppm).

As a ligand for the formation of supramolecular constructions, Schiff base compounds provide many benefits. The simplicity of the Schiff base condensation in combination with a large number of suitable aldehyde and amine functionalities offers a vast series of possible ligands that can be synthesised.<sup>78</sup> The nature of the reaction allows for the insertion of supplementary functionality, providing a greater quantity of possible donor atoms. The chemical behaviour of the added donor atoms can allow for enhanced control of the coordination environment provided by the ligand.<sup>76</sup> Complexes formed with Schiff base ligands often exhibit interesting supramolecular and magnetic properties.<sup>81</sup>

By introducing functionality onto the 2 and 5 positions of pyrazine through a Schiff base condensation, any ligand will incorporate a bis-bidentate chelating environment from the nitrogens found on the imine and pyrazine. In order to favour the formation of a cyclohelicate structure with a completely occupied  $3d$  octahedral metal centre, an additional donor atom must be incorporated in the non-pyrazine precursor before the

Schiff base condensation can take place. Preferably, the inclusion of a donor atom with similar hard/soft properties (according to the hard and soft acid and base theory, or HSAB theory<sup>24,82,83</sup>) as the metals being coordinated to the ligand will aid in providing a bidentate chelating environment. As most *3d* metal centres generally exhibit intermediate/hard acid properties due to their high charge densities, an intermediate/hard donor atom must be included, where typical examples of functionality containing these donor atoms include pyridine and phenols.<sup>24</sup> With three suitable donors at either end of the ligand, *3d* metal ions that prefer an octahedral arrangement of donor atoms can be incorporated into the complex (Figure 2.2), this arrangement may lead to the formation of grid complexes using a 1:1 ligand:metal stoichiometry.

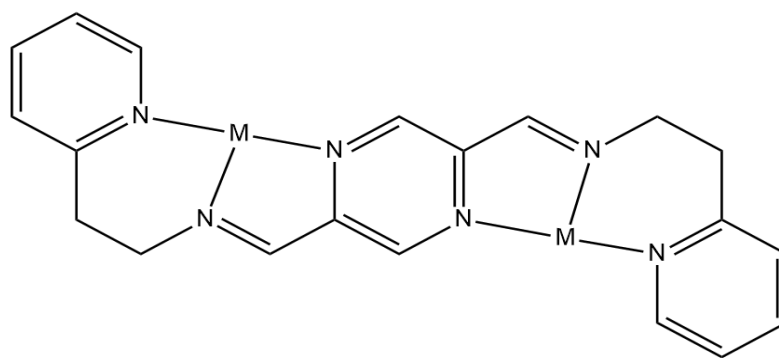
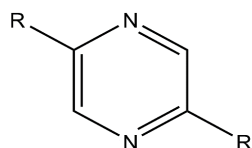


Figure 2.2. The expected coordination of a transition metal (M) to a pyrazine ligand (ligand L3 is shown as an example).

## 2.2 Schiff base with pyrazine

Limited research has been reported on the synthesis of pyrazine-derivative ligands containing Schiff base functionality at the 2 and 5 positions of pyrazine.<sup>1</sup> As discussed earlier, a Schiff base condensation requires a primary amine and a carbonyl species, implying that the pyrazine will need to incorporate either a primary amine or carbonyl species at the 2 and 5 positions. In this report, the route undertaken involves the incorporation of aldehyde species on the 2 and 5 positions of pyrazine. Reasons for this decision include the absence of reported literature describing the synthesis of the diamine derivative (until very recently by Zane Farrow from Massey University<sup>84</sup>) and the ease of synthesising the methyl dialdehyde species (Figure 2.3, R = CHO).

Since the beginning of this research project, new and improved methods have been provided for the synthesis of pyrazine-2,5-dicarbaldehyde, **A1** (Figure 2.3 - R = CHO).<sup>1,5,85,86</sup> The use of pyrazine-2,5-dicarbaldehyde as a precursor for a Schiff base condensation has proven to be effective as a synthetic building block, as was described by Hogue *et al.* in section 1.7.3. The synthesis of pyrazine-2,5-diacetaldehyde, **A2** (R = CH<sub>2</sub>CHO) was considered as another possible precursor for Schiff base condensation. The extension of the alkyl chains on the 2 and 5 positions will introduce a greater degree of flexibility in Schiff base ligands formed with this compound while still possessing the rigidity that pyrazine provides. This allows for a wider scope of research in the formation of cyclohelicates, including the incorporation of larger metal ions (such as 4f ions) and the formation of more intriguing cyclohelicate structures. Although the synthesis of pyrazine-2,5-diacetaldehyde (R = CH<sub>2</sub>CHO) is unexplored with no synthetic procedure provided, the synthesis of related pyridine structures have been reported.<sup>87-89</sup>



R = CHO (**A1**), CH<sub>2</sub>CHO (**A2**)

Figure 2.3. Pyrazine with 2 and 5 positions labelled with R substituents.

### 2.3 Summary

In order to provide a suitable bis-terdentate chelating environment for octahedral 3d metals capable of self-assembling into cyclohelical structures, functionality will be placed on pyrazine on the 2 and 5 positions. Schiff base condensations are excellent ways to introduce more donor atoms into a chemical system, where the imine produced can coordinate to a metal centre. The synthetic approach for the Schiff base condensation with pyrazine will require pyrazine-2,5-dialdehyde derivatives with pyridine or phenol arms to ensure each ligand postulated contains six donor atoms (three donor atoms per half of the ligand).

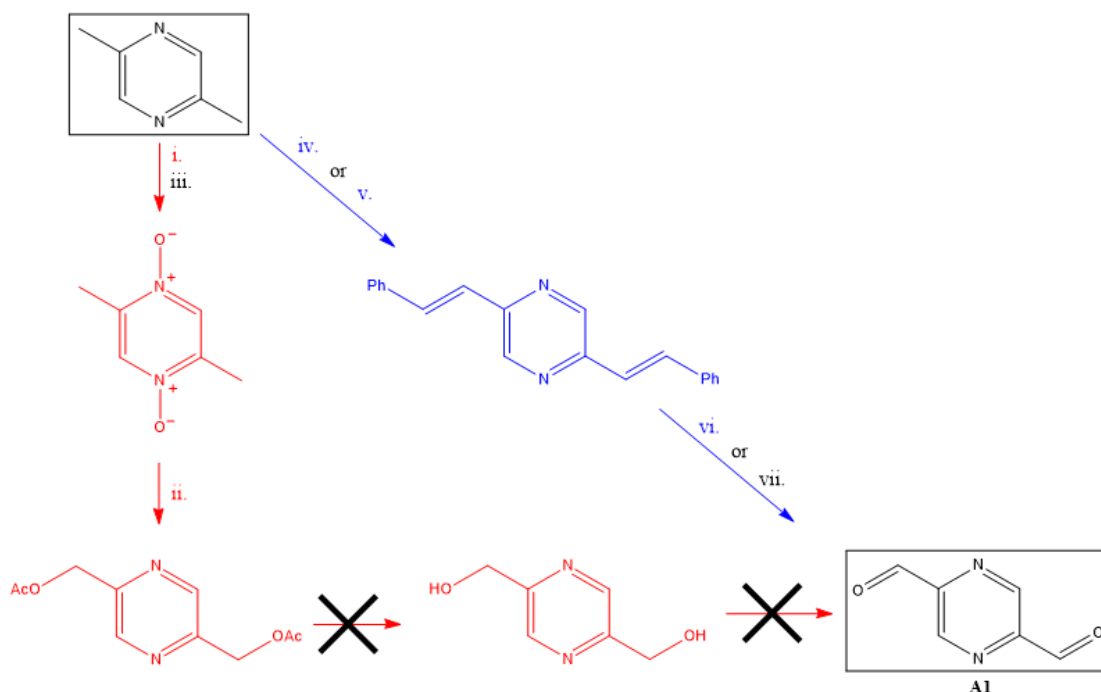
## Chapter 3 Synthesis of Schiff Base Precursors

### 3.1 Introduction

The reported syntheses of pyrazine dialdehyde derivatives is limited, with the bulk of publications focusing on pyrazine-2,5-dicarbaldehyde, **A1** (see section 2.2). The starting material often used for the formation of **A1** is 2,5-dimethylpyrazine. The following section will discuss the routes investigated to synthesise pyrazine-2,5-dicarbaldehyde, **A1** from 2,5-dimethylpyrazine. Attempts were also made to synthesise **A2**. Unfortunately, the desired product could not be isolated as a pure product. For this reason, information regarding the various attempts to synthesise **A2** are presented in Appendix B.

### 3.2 Synthesis of pyrazine-2,5-dicarbaldehyde

Within the last decade, there have been numerous procedures for the synthesis of pyrazine-2,5-dicarbaldehyde (**A1**) reported (Scheme 3.1), with the majority of them starting from 2,5-dimethylpyrazine. The initial route explored to synthesise the target



Scheme 3.1. Synthetic scheme for the synthesis of pyrazine-2,5-dicarbaldehyde (**A1**): (i) *m*-CPBA, rt, 24 h, 87 %. (ii) Ac<sub>2</sub>O, 158 °C, 7 h, rt, 12 o/n, 15 %. (iii) glacial CH<sub>3</sub>COOH, 30% H<sub>2</sub>O<sub>2</sub>, 95 °C, 24 hr, 20 %. (iv) Benzaldehyde, benzoic anhydride, reflux, 175 °C, 4 d, 54 %. (v) Benzaldehyde, benzoic anhydride, M.W., 175 °C, 6 h, 62 %. (vi) OsO<sub>4</sub>, NaIO<sub>4</sub>, rt, 2-3 d, 25 %. (vii) O<sub>3</sub>, -50 °C, 3 – 4 h, 30 %. The red scheme indicates the method by Das *et al.*, the blue scheme shows the method by Coufal *et al.* and the black roman numerals indicate alternative reaction routes.

molecule was based on the methodology of Das *et al.* (red procedure in Scheme 3.1) and involved a 4-step synthesis with an overall 8 % yield.<sup>85</sup> Although this is a low yield, this method was described as being simple to perform in most laboratories, therefore was an ideal first route to attempt.

### 3.2.1 Synthesis of pyrazine-2,5-dicarbaldehyde – Das method

The first step involved the formation of 2,5-dimethylpyrazine-1,4-dioxide. Two routes were investigated: the first (step i.) involved the oxidation of 2,5-dimethylpyrazine with meta-chloroperoxybenzoic acid, *m*-CPBA (77 % in H<sub>2</sub>O) in ethyl acetate.<sup>85</sup> The desired 2,5-dimethylpyrazine-1,4-dioxide precipitated as a white solid, which was isolated through filtration in 87 % yield. The purity of the white solid was determined by <sup>1</sup>H NMR spectroscopy (top spectrum in Figure 3.1), which matches the spectrum found in literature. The second route (step iii.) was the oxidation of 2,5-dimethylpyrazine with

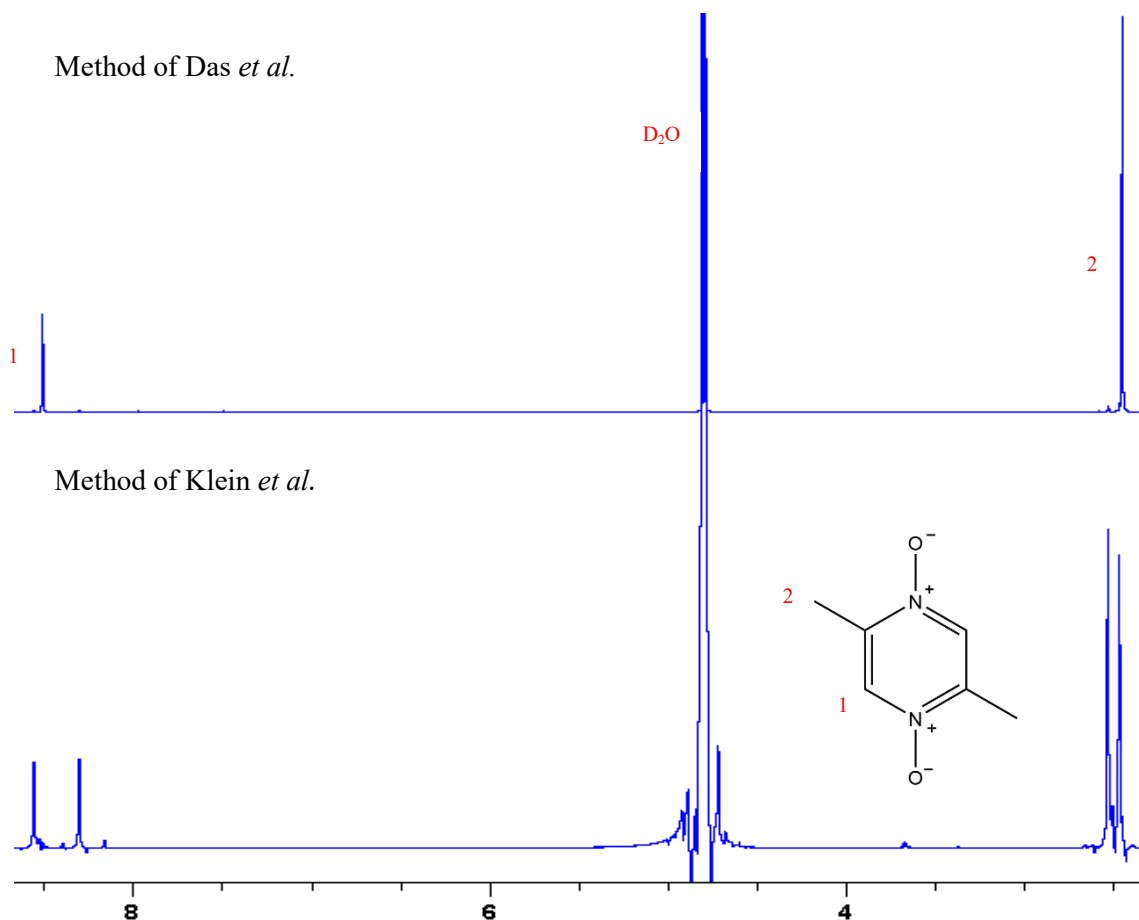
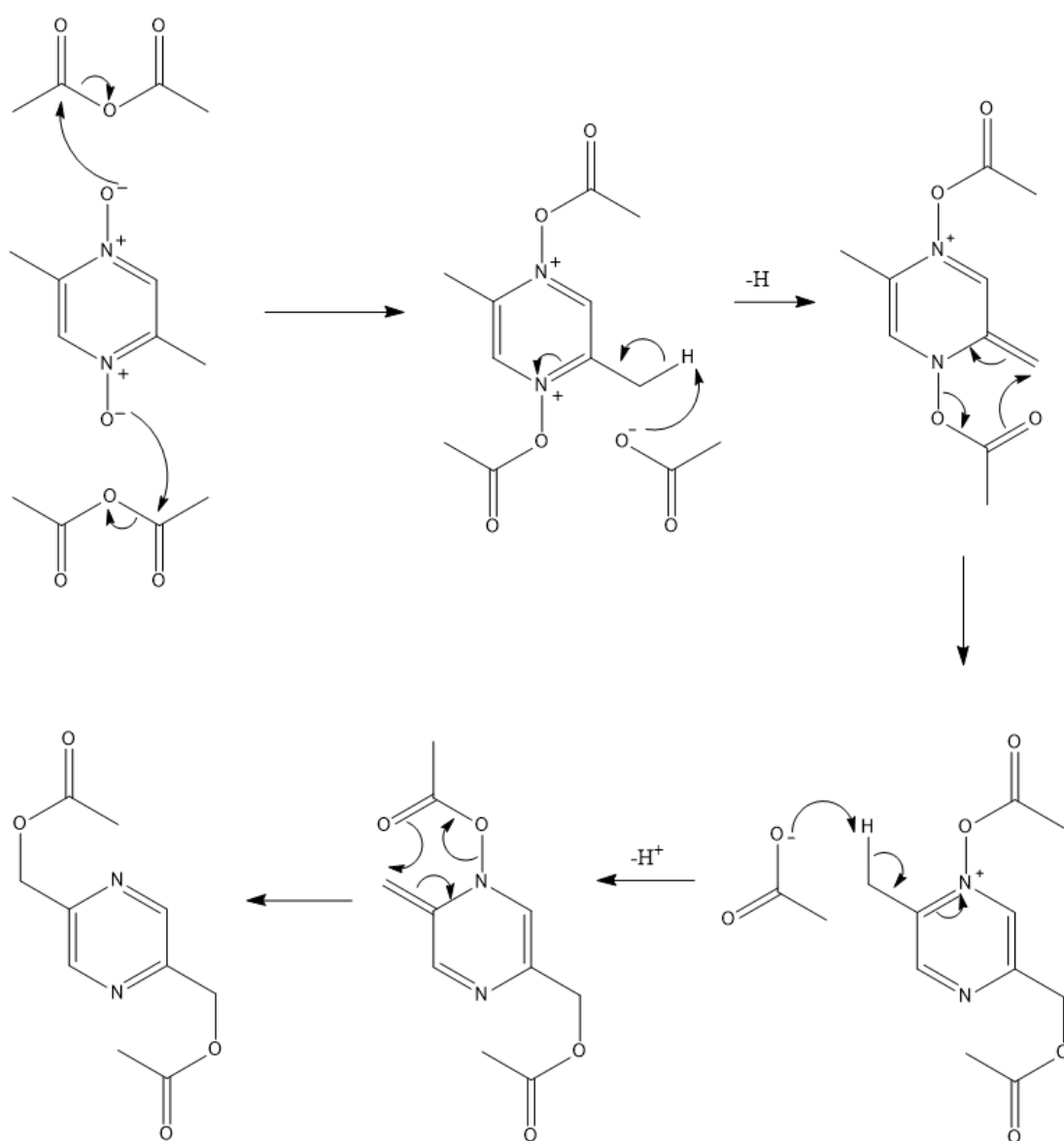


Figure 3.1. <sup>1</sup>H NMR spectra of 2,5-dimethylpyrazine-1,4-dioxide (in D<sub>2</sub>O) obtained from the methods provided by Das *et al.* (top) and Klein *et al.* (bottom).

hydrogen peroxide,  $\text{H}_2\text{O}_2$  (30 % in  $\text{H}_2\text{O}$ ) in glacial acetic acid.<sup>90</sup> The desired product was obtained with a notable decrease in the purity and yield of the white product. The  $^1\text{H}$  NMR indicated that the reaction frequently gave a mixture of desired 2,5-dimethylpyrazine-1,4-dioxide and 2,5-dimethylpyrazine (bottom spectrum in Figure 3.1). The low yield, coupled with a more challenging reaction work up meant route 1 was preferred.

The next step is the acetylation of 2,5-dimethylpyrazine-1,4-dioxide with acetic anhydride. The *N*-dioxide functionality allows the acetylation to occur on the methyl



Scheme 3.2. Proposed mechanism for the acetylation of 2,5-dimethylpyrazine-1,4-dioxide.



groups and is not a standard acetylation. Scheme 3.2 presents the proposed mechanism for the acetylation of 2,5-dimethylpyrazine-1,4-dioxide. The N-dioxide was heated to reflux in acetic anhydride for 7 hours and then stirred at room temperature overnight. The prolonged time was employed to ensure the starting material had come to completion, as opposed to only producing the monoacetate derivative (see Scheme 3.2).<sup>85</sup> Following purification by column chromatography (40 % ethyl acetate in *n*-hexane) and recrystallisation (50 % ethyl acetate in *n*-hexane), the desired pure product, 2,5-di(acetoxymethyl)pyrazine was isolated as a white crystalline solid in 15 % yield, as determined by <sup>1</sup>H NMR spectroscopy (Figure 3.2). The low yield was due to the formation of a large quantity of uncharacterised black polymeric solid. Due to the discovery of a less-time consuming and more efficient method, further research into the synthesis of pyrazine-2,5-dicarbaldehyde with this procedure was shelved.

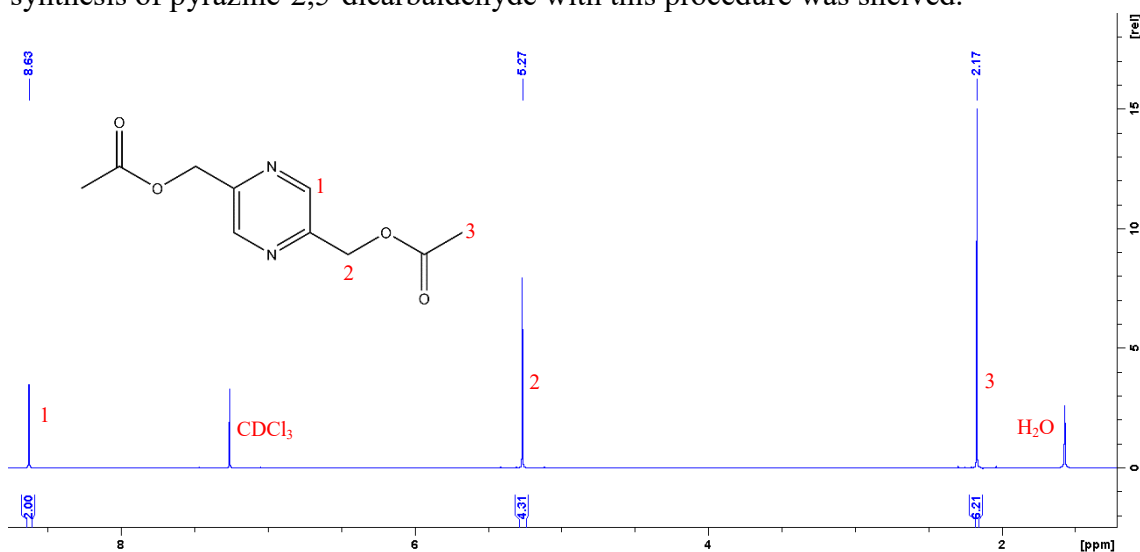
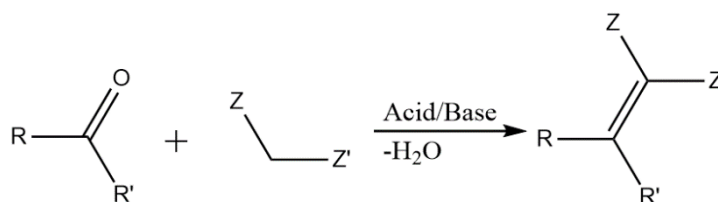


Figure 3.2. <sup>1</sup>H NMR spectrum of 2,5-di(acetoxymethyl)pyrazine (CDCl<sub>3</sub>) obtained from the method provided by Das *et al.* with assigned peaks.

### 3.2.2 Synthesis of pyrazine-2,5-dicarbaldehyde – Coufal method

In 2016, Coufal *et al.* developed a two-step synthetic route for producing pyrazine-2,5-dicarbaldehyde (**A1**) from 2,5-dimethylpyrazine (blue route in Scheme 3.1).<sup>5</sup> The methodology reported an overall yield of 30 – 35 %, quadrupling the expected yield from the Das *et al.* approach. Although each step required an increased reaction time, the reduction from four steps to two steps provided a greater overall efficiency.

The first reaction is a Knoevenagel-like condensation between 2,5-dimethylpyrazine and benzaldehyde in the presence of benzoic anhydride (step vi.), which was incorporated to act as a drying agent, as well as assisting in the dehydration necessary for the formation of the targeted alkene. This reaction differs from the Knoevenagel condensation as a typical Knoevenagel reaction (as shown in Scheme 3.3) is a modified acid or base catalysed aldol condensation between an aldehyde or ketone, and an activated methylene group (near an electron-withdrawing group).<sup>91,92</sup> The first reaction involved refluxing the reaction mixture at 178 °C for 4 days, which produced a brown solid upon completion.<sup>5</sup> Washing of the crude product with ethanol yielded the desired 2,5-*E,E*-distyrylpyrazine as a yellow crystalline solid, as indicated by <sup>1</sup>H NMR spectroscopy (see Appendix D). The presence of benzoic acid (the air-oxidised product of benzaldehyde) was required for the successful formation of 2,5-*E,E*-distyrylpyrazine, which was proven by a dramatic decrease in the yield upon repeating the reaction with distilled benzaldehyde. As the incorporation of impure benzaldehyde was shown to be successful in the formation of the desired product, as well as being an easily obtainable acidic source, impure benzaldehyde was used for further synthesis.



Scheme 3.3. General Knoevenagel condensation. Z and Z' are electron-withdrawing substituents.

In an attempt to improve this method, the reaction was trialled in a microwave. The reaction conditions for the microwave synthesis were similar to those above, except for changing the mode of heating and the duration of the reaction. Heating for 1 hour gave a brown solid that could be purified by washing with ethanol to give 2,5-*E,E*-distyrylpyrazine in 11 % yield. By optimising this procedure, it was found that a reaction time of 6 hours with no set pressure and filling the system with argon produced the greatest yield (62 %). The yellow product appeared to be photosensitive and underwent polymerisation if exposed to a light source for a significant period of time (evident by a colour change from yellow to gold).<sup>1</sup> For this reason, the synthesised product was stored in the dark for future use.

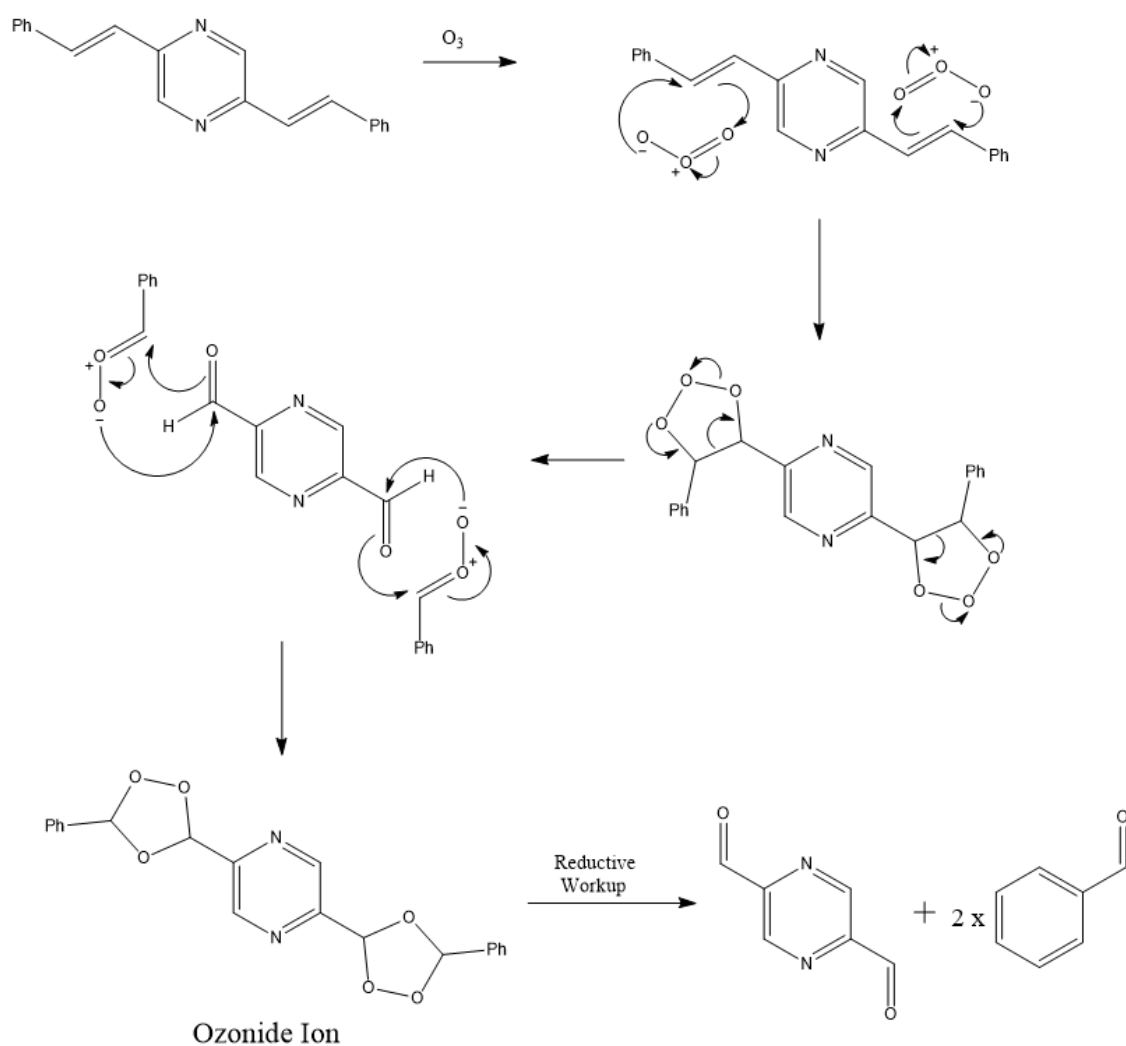
The second step in the Coufal method is the oxidative cleavage of 2,5-*E,E*-distyrylpyrazine to form pyrazine-2,5-dicarbaldehyde. This is achieved through the Lemieux-Johnson oxidation using osmium tetroxide (OsO<sub>4</sub>) and sodium periodate (NaIO<sub>4</sub>), where OsO<sub>4</sub> is used to oxidize the alkene to a diol. This reduces the Os(VIII) in osmium tetroxide to an Os(VI) species. Sodium periodate oxidatively cleaves the diol into two aldehydes, benzaldehyde and the desired pyrazine-2,5-dicarbaldehyde, as well as regenerates the Os(VIII).<sup>5</sup> As a result, a substoichiometric quantity of osmium tetroxide could be used.

This reaction was performed for 3 days, producing **A1** as a light brown solid. Initial attempts to purify the compound by silica gel column chromatography (dichloromethane), as proposed by Coufal *et al.*, were successful in isolating the desired product (as determined by <sup>1</sup>H NMR spectroscopy). Problems with this route include the low yield obtained (the greatest being 25 % of pure product versus the expected 40 %), the column chromatography purification showing inconsistency in being able to isolate

the desired product, and the associated hazards of osmium tetroxide. Due to these issues, an alternative oxidation that has been successfully utilised in the past was trialled.

### 3.2.3 Synthesis of pyrazine-2,5-dicarbaldehyde – Hogue *et al.* method

Following on from the synthesis of 2,5-*E,E*-distyrylpyrazine, Hogue *et al.* reported the synthesis of **A1** through ozonolysis.<sup>1</sup> This involves bubbling ozone gas into a suspension of 2,5-*E,E*-distyrylpyrazine in methanol at cold temperatures ( $\leq -50\text{ }^{\circ}\text{C}$ ), before subjecting the intermediate to a reductive workup to give pyrazine-2,5-dicarbaldehyde (**A1**) and benzaldehyde (see Scheme 3.4).<sup>1,93,94</sup> Due to the formation of the ozonide ion, a reactive/explosive intermediate (see Scheme 3.4), the reaction was approached with



Scheme 3.4. Criegee mechanism for the ozonolysis of 2,5-*E,E*-distyrylpyrazine, yielding pyrazine-2,5-dicarbaldehyde and benzaldehyde.

extreme precaution and was performed on a scale no greater than two grams of 2,5-*E,E*-distyrylpyrazine.<sup>5</sup>

Two reducing agents were investigated: triphenylphosphine (PPh<sub>3</sub>) and sodium metabisulfite (Na<sub>2</sub>S<sub>2</sub>O<sub>5</sub>). The latter reagent was more user-friendly. Reduction with PPh<sub>3</sub> results in the formation of triphenylphosphine oxide (Ph<sub>3</sub>P=O), which was hard to separate from the desired product. No such problems occur with Na<sub>2</sub>S<sub>2</sub>O<sub>5</sub>, as the addition of Na<sub>2</sub>S<sub>2</sub>O<sub>5</sub> resulted in the formation of a white precipitate, with the desired product (**A1**) remaining in solution. The white precipitate was easily separated by filtration.

The procedure used to synthesise the dialdehyde species was adapted from Brooker *et al.* where ozonolysis was performed on 3,6-distyrylpyridazine to synthesise 3,6-diformylpyridazine.<sup>95</sup> The modification was successful in producing the desired dialdehyde species **A1**, giving a yellow solid in 30 % yield, as confirmed by <sup>1</sup>H NMR spectroscopy (see Figure 3.3). With the product being unstable (decomposition at temperatures above 40 °C and exposure to air), the workup for the reaction is prompt, where the product is stored under argon in a freezer. As this route was shorter, and posed less associated hazards, the ozonolysis of 2,5-*E,E*-distyrylpyrazine was chosen over the Lemieux-Johnson oxidation as the preferred method to synthesise pyrazine-2,5-dicarbaldehyde.

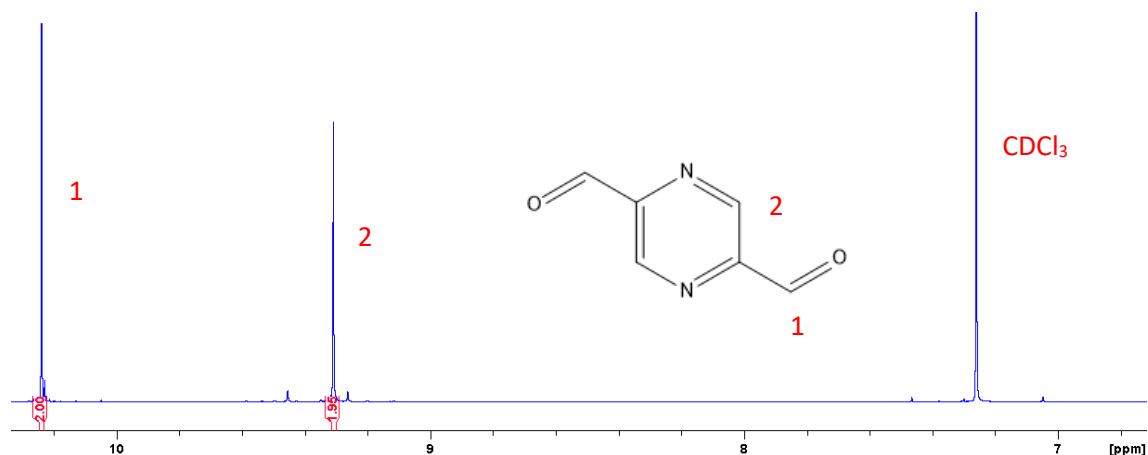
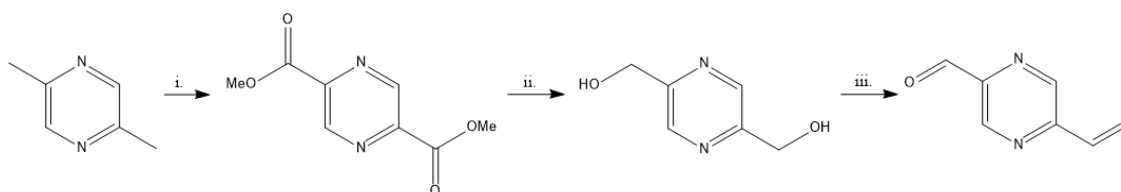


Figure 3.3.  $^1\text{H}$  NMR spectrum of pyrazine-2,5-dicarbaldehyde (**A1**) with assigned peaks ( $\text{CDCl}_3$ ).

### 3.3 Future work

Although this two-step procedure produces pure pyrazine-2,5-dicarbaldehyde in two days with an overall yield of 35 %, the reaction conditions imposed to limit the dangers associated with ozonolysis mean that only around 150 mg of **A1** can be produced at any time. Future efforts will investigate possible routes to increase the amount of **A1** produced at a time. A method provided by Hogue *et al.* involves a three-step procedure, taking roughly four days and producing **A1** in an overall yield of 20 % (Scheme 3.5).<sup>1</sup> This route however has the advantage of being upscaled to much greater extents than the ozonolysis route (up to at least 8 grams).<sup>1</sup> The first step involves the oxidation of 2,5-dimethylpyrazine with selenium dioxide ( $\text{SeO}_2$ ) and the esterification of the crude pyrazine-2,5-dicarboxylic acid with thionyl chloride, producing dimethylpyrazine-2,5-dicarboxylate in 61 % yield. As this step requires the use of toxic materials such as  $\text{SeO}_2$  and thionyl chloride, handling precautions will need to be undertaken before attempting this step to mitigate the risk. The next step involves the reduction of the ester with sodium borohydride ( $\text{NaBH}_4$ ), followed by the continuous extraction with chloroform for two days, producing 2,5-bis(hydroxymethyl)pyrazine in a 20-40 % yield. The long continuous extraction time is required as the desired product is highly soluble in the water used to

quench the reaction. The last step follows the oxidation of the diol species with manganese dioxide ( $\text{MnO}_2$ ). This is the same oxidation method provided by Das *et al.* and produces **A1** in an 84 % yield.<sup>1,85</sup>



Scheme 3.5. The three-step reaction scheme reported by Hogue *et al.* to produce **A1** from 2,5-dimethylpyrazine. (i)  $\text{SeO}_2$ , pyridine/water (10:1), reflux (61 %). (ii) a:  $\text{NaBH}_4$ , MeOH, b:  $\text{H}_2\text{O}$ , continuous extraction (40 %). (iii)  $\text{MnO}_2$ ,  $\text{CHCl}_3$ , reflux (84 %).

### 3.4 Summary

Several methods from recently published papers were investigated to synthesise **A1**. The optimal conditions found were a microwave-assisted Knoevenagel-like reaction between 2,5-dimethylpyrazine and benzaldehyde, followed by the ozonolysis of 2,5-*E,E*-distyrylpyrazine. This two-step procedure produced pure pyrazine-2,5-dicarbaldehyde in two days with an overall yield of 35 %. Unfortunately, due to the reaction conditions imposed to limit the dangers with the earlier described hazards associated with ozonolysis, only around 150 mg of **A1** was produced at any time. Nevertheless, this yield is suitable for the synthesis of pyrazine-based Schiff base ligands.

## Chapter 4      Synthesis of Ligands

### 4.1      Introduction

Following the successful synthesis of **A1**, a pyrazine dialdehyde species (see section 3), a series of symmetrical ligands can now be synthesised using a Schiff base condensation reaction between **A1** and a series of primary amines incorporating additional N – or O – atoms. This design provides a bis-terdentate chelating environment for selected 3*d* metal ions to octahedrally coordinate to the ligand. The following section will discuss the synthesis of various ligands from pyrazine-2,5-dicarbaldehyde (**A1**) through Schiff base condensation reactions, as well as elaborate on the various characterisation methods used to verify the successful formation of each ligand.

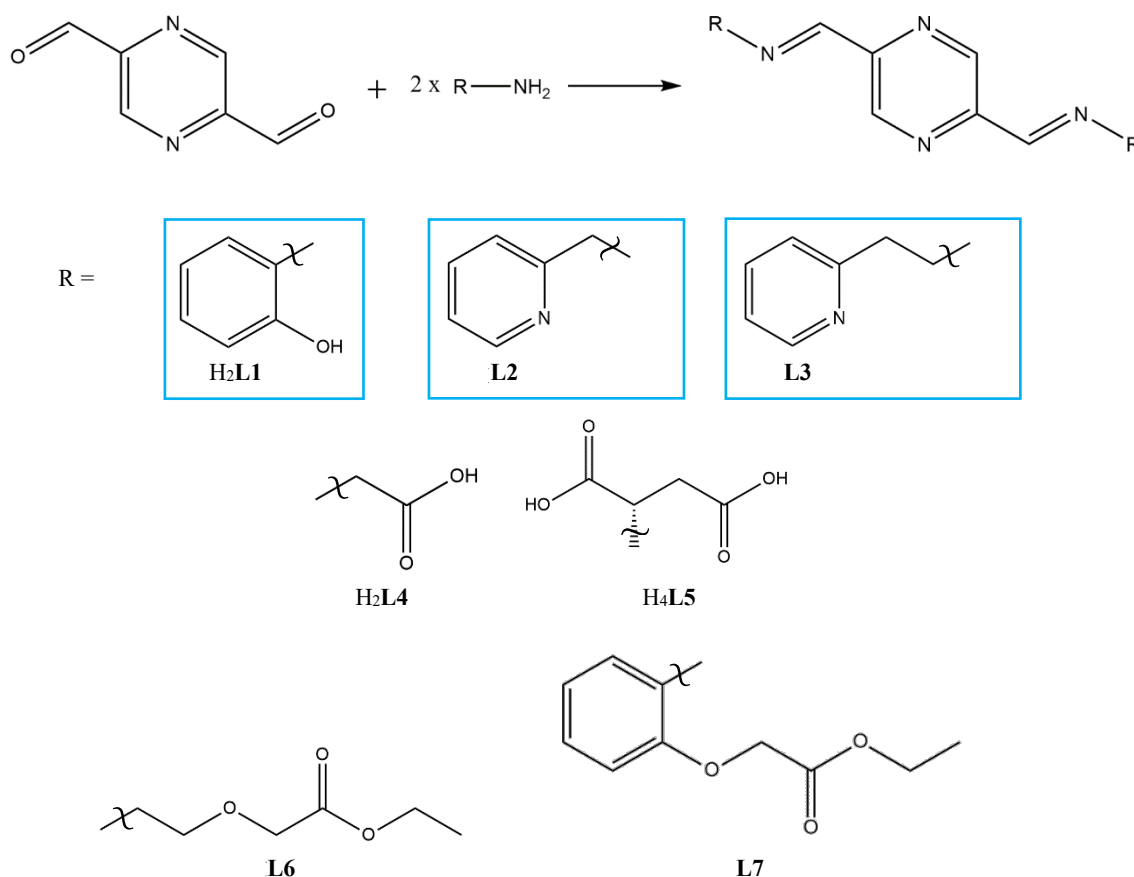
### 4.2      General protocol for the synthesis of Schiff base ligands

As **A1** degrades at temperatures  $\geq 40\text{ }^{\circ}\text{C}$ , careful consideration was undertaken during the synthesis of these ligands. For this reason, the use of a Dean-Stark apparatus (glassware commonly used in Schiff base synthesis for the azeotropic removal of water) was not used as this apparatus requires the reaction mixture to be refluxed for a period of time.

A modification of Brooker's methodology for the synthesis of various Schiff base ligands was used.<sup>96</sup> Pyrazine-2,5-dicarbaldehyde (1 equivalence) and a primary amine which consisted of additional N- or O-donors (2 equivalence) was stirred at room temperature in an appropriate solvent system, such that the desired ligand crashed out of solution. The mixture was stirred for 30 minutes and left to stand at room temperature until no more solid crashed out of solution (typically 2-3 hours). The product was then filtered and washed with ice cold solvent (to deter the dissolution of the solid back into the mother liquor), yielding the desired Schiff base ligand in a moderate yield and high purity. Using this method,<sup>96</sup> three pyrazine-based Schiff base ligands were synthesised (**H<sub>2</sub>L1**, **L2**, **L3** in



Scheme 4.1), where **H<sub>2</sub>L1** possesses two phenol groups, while **L2** and **L3** containing pyridines with differing length linkers. A further four ligands were considered (**H<sub>2</sub>L4**, **H<sub>4</sub>L5**, **L6** and **L7**), but time constraints coupled with synthetic problems meant these groups will be investigated in the future. The attempts made to synthesise these four ligands can be found in appendix A.



Scheme 4.1. The general reaction scheme of a Schiff base condensation between pyrazine-2,5-dicarbaldehyde (**A1**) and a primary amine. The three ligands enclosed in the blue boxes (**H<sub>2</sub>L1**, **L2** and **L3**) were successfully synthesised and isolated as pure ligands. The four ligands not enclosed in a blue box (**H<sub>2</sub>L4**, **H<sub>4</sub>L5**, **L6** and **L7**) were not successfully isolated as pure ligands.

### 4.3 Characterisation of Schiff base ligands

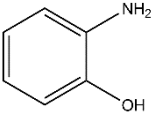
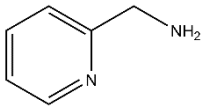
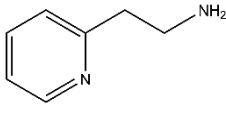
The proposed ligand systems (**L1-7**) are all unique. It was therefore necessary for each ligand successfully synthesised to be characterised with a variety of methods. To determine the success of a Schiff base reaction, <sup>1</sup>H NMR spectroscopy (both 400 and 500 MHz) was employed as the primary method of characterisation. The presence of a new singlet peak around 9 – 10 ppm indicated the successful formation of the imine. The

respective assignment of each ligand was supported by  $^{13}\text{C}$  NMR and HMQC spectroscopy (see additional spectra section) This technique also measured the completeness of each condensation reaction by investigating the intensity of the aldehyde singlet peak associated with **A1** ( $\delta = 10.24$  ppm). If no peak was present in this region, it was likely that the reaction had come to completion. The results obtained from this technique were verified with attenuated total reflectance – infrared spectroscopy (ATR-IR spectroscopy). ATR-IR spectroscopy was chosen over IR spectroscopy with KBr pellets or Nujol mulls due to the high resolution spectrum obtained and the simplicity in sample preparation. Prior to IR analysis, each sample was dried in vacuo before being placed on the ATR-IR spectrometer for measurement. The appearance of a sharp peak around  $1640\text{ cm}^{-1}$  reassured that the imine had been formed. The disappearance of the aldehyde peak (found around  $1700\text{ cm}^{-1}$ ) proved that the reaction had come to completion. Following these techniques, each successfully formed ligand was further characterised with UV-visible spectroscopy, elemental analysis, mass spectrometry and melting point determination. The results obtained from these techniques can be found in the experimental section. Attempts to grow single crystals of each ligand was made, with several crystallisation techniques employed to maximise the chances of success. This was done in hopes to analyse the ligands through single crystal X-ray diffraction (SCXRD) and examine various structural features that the ligand possesses. This was successfully achieved for the ligand **L3**. The remaining ligands did not crystallise and the failed attempts at crystallising these ligands are elaborated in the experimental section.

#### 4.4 Synthesis and characterisation of H<sub>2</sub>L1, L2 and L3

The synthesis of each ligand was performed by following the general protocol above with appropriate solvents, yielding the desired ligands in moderate yields, as shown in Table 4.1. Full details of the results obtained from the various characterisation methods are presented in the Appendix 4 (section A4.2), with the most relevant data concerning the successful Schiff base formation presented in Table 4.1.

Table 4.1. The synthesis and appearance of ligands H<sub>2</sub>L1, L2 and L3 with the selected characterisation data used to verify the successful formation of these ligands. The yields shown in green indicate the solvent that was used to produce the greatest yield of their respective ligand system.

	H <sub>2</sub> L1	L2	L3
R =			
Solvent Used (with corresponding yield obtained)	MeCN (72 %) EtOH (90 %)	MeCN (54 %) EtOH (failed)	MeCN (62 %)
Product Description	Yellow/orange solid	Solid (purple on one face, yellow on the other face)	White crystalline solid
<sup>1</sup> H NMR imine peak (ppm) vs solvent	9.70 (DMSO-d <sub>6</sub> )	9.31 (CDCl <sub>3</sub> )	9.14 (CDCl <sub>3</sub> )
IR imine peak (cm <sup>-1</sup> )	1621	1642	1644

Both <sup>1</sup>H NMR and IR spectroscopy confirmed the presence of the imine in ligands H<sub>2</sub>L1, L2 and 3. Interestingly, the deshielding nature of the pyrazine ring and the neighbouring substituents led to the low field shift of the imine peaks to ppm ranges higher than anticipated (see Table 4.1). This effect was also observed in the IR spectra of H<sub>2</sub>L1, L2 and 3, presenting the characteristic imine peak below or at the lower expected range of the imine peak. The disappearance of the aldehyde peak indicated the reaction had come to completion.

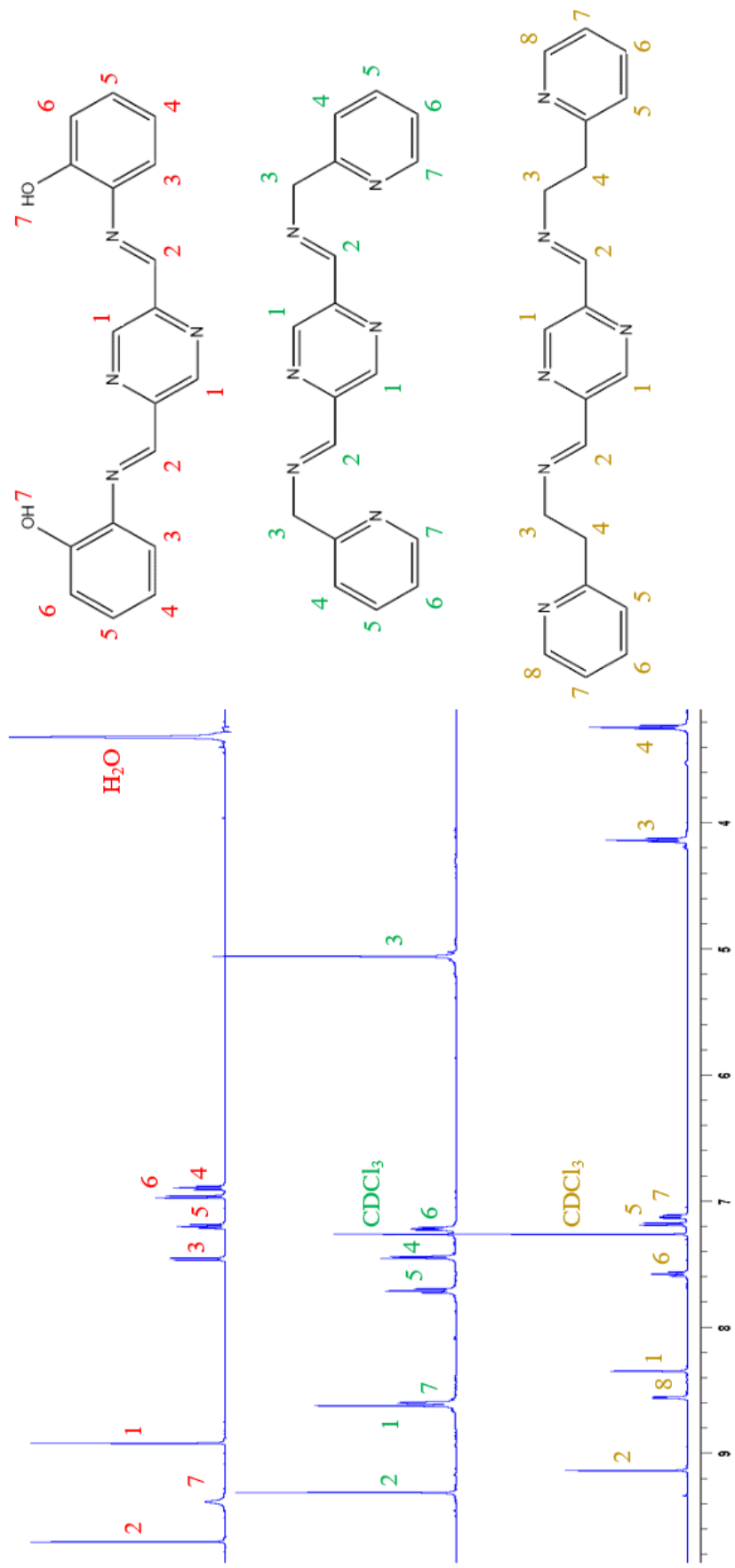
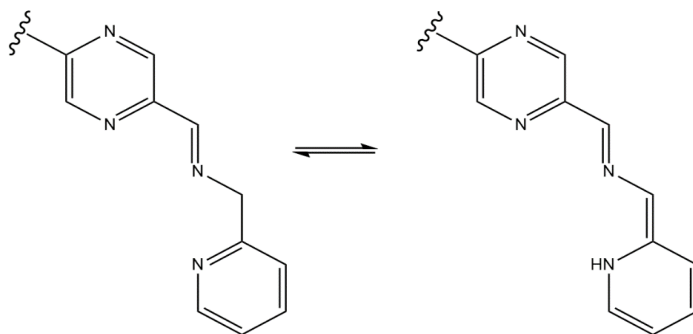


Figure 4.1. Assigned <sup>1</sup>H NMR spectra (top <sup>1</sup>H NMR spectrum (H<sub>2</sub>L1): DMSO-d<sub>6</sub>, middle <sup>1</sup>H NMR spectrum (L2): CDCl<sub>3</sub>; bottom <sup>1</sup>H NMR spectrum (L3): CDCl<sub>3</sub>).

Ligand **L2** behaved unexpectedly. The dry solid was a purple colour, but if the compound was wet or in solution, it became yellow. It is possible that tautomerisation allows the solid to be highly conjugated, but conformation freedom when dissolved breaks this (Scheme 4.2).



Scheme 4.2. Tautomerism exhibited in **L2**.

Several attempts were made to grow crystals of suitable quality of  $H_2L1$ , **L2** and **L3** for SCXRD, typically involving vapour diffusion of diethyl ether into a solution of the dissolved ligand, or hot recrystallisation. Although some techniques did show signs of crystallising  $H_2L1$  and **L2** (see section A4.2 – Table A4.2.1), crystals of  $H_2L1$  or **L2** suitable for SCXRD were not obtained.

Hot recrystallisation of the ligand **L3** in MeCN produced white needle-shaped single crystals suitable for SCXRD upon placing the boiling solution in a freezer (-15 °C) over 30 minutes. The crystal was solved in the monoclinic space group ( $P 2_1/c$ ) and confirms the successful synthesis of ligand **L3** (Figure 4.2). The asymmetric unit contains one-half of the molecule (indicated by the dashed line in Figure 4.2). The structure of the full molecule was generated by inversion centred on the pyrazine ring. The diimine units lie flat with respect to the pyrazine ring, as indicated by virtually no displacement between the pyrazine and imine atoms. Both the pyrazine and pyridine rings are planar, where each pyridine ring are parallel to each other. The pyrazine ring however does not lie parallel with respect to the pyridine rings, where a 12.12 ° offset found between them. The imine bond adopts a trans conformation, which assists in providing intermolecular pyrazine-

imine  $\pi$ -stacking interactions within the packed structure (as seen in Figure 4.3), with a distance of 3.451 Å between the centre of the pyrazine ring and the imine C=N bond (a in Figure 4.3). The packing presents a zig-zag appearance with alternating ligands (when viewed down the a-axis) where the alternating ligands are between 83.18 ° (with respect to the pyrazine rings) and 85.95 ° (with respect to the pyridine rings). Although the ethyl chain in the ligand possesses free rotation, the structure presents this chain with an antiperiplanar geometry (Figure 4.3), which positions one of the hydrogen atoms in one molecule fairly close to the centre of the pyridine ring in an adjacent molecule within the packed structure (2.841 Å – b in Figure 4.3). This arrangement is presumably an artefact of the close packing.

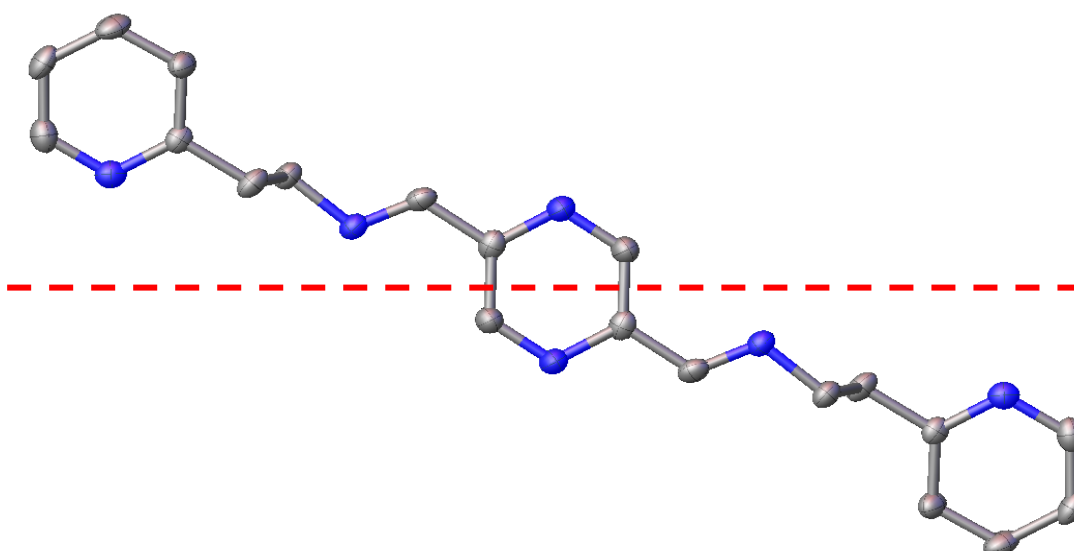


Figure 4.2. Molecular structure of **L3**. All hydrogens have been omitted for clarity. Atoms are represented as ellipsoids. Grey = carbon, blue = nitrogen. The red line indicates the asymmetric unit.

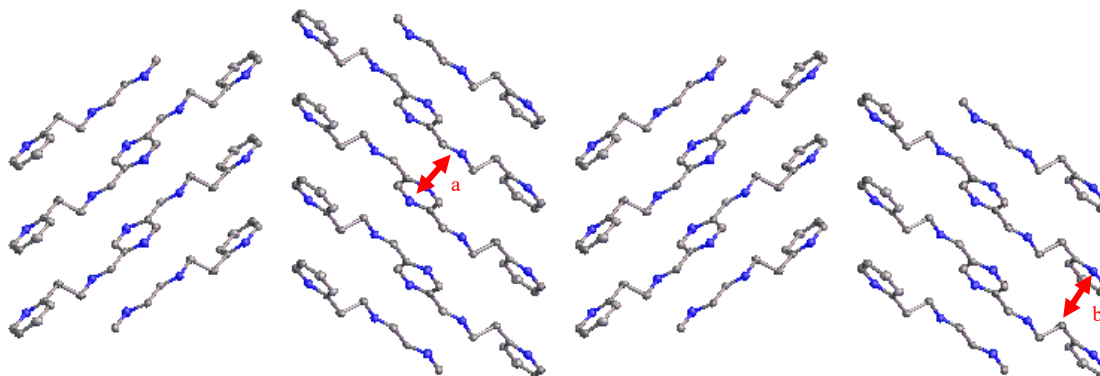


Figure 4.3. Packed structure of **L3** (viewed down the a-axis), revealing a zigzag appearance stabilised by pyrazine-imine  $\pi$ -stacking interactions (as indicated by a) and the interactions between the alkane hydrogen and pyridine (as indicated by b).

#### 4.5 Future work

The data collected from the SCXRD of **L3** provided structural information of the ligand, and can be used to assess its usefulness as a bis-terdentate chelator for *3d* metals. Although the attempted crystallisation methods of **H<sub>2</sub>L1** or **L2** produced no suitable crystals, other crystallisation systems will be investigated. Following this, the synthesis of a larger library of pyrazine-based Schiff base ligands containing other functionalities with intermediate N- and O-donor atoms may be explored. With the recent synthesis of the diamine derivative of **A1** by Zane Farrow (of the Gareth Rowlands group at Massey University, Manawatu), pyrazine may act as the primary amine, where efforts can be also be directed to the synthesis of unique ligands by Schiff base condensations with suitable aldehyde/ketone species with additional N- or O-donor atoms.

#### 4.6 Conclusions

Three ligands (**H<sub>2</sub>L1**, **L2** and **L3**) with chelating environments capable of coordinating assorted *3d* metal ions were synthesised through Schiff base condensations. Using a collection of characterisation techniques, the successful formation of each ligand was verified, with several methods indicating the formation of the desired imine moiety and the removal of the dialdehyde functionality found in the precursor **A1**. Multiple attempts were made to obtain single crystals of each ligand (of suitable quality) for SCXRD, with varying solvent conditions and recrystallisation methods, however, most attempts failed to produce any crystals. Single needle-shaped crystals of **L3** were successfully produced by hot recrystallisation of a solution of **L3** in MeCN. The SCXRD of **L3** was obtained, revealing intermolecular pyrazine-imine  $\pi$ -stacking interactions within the packed structure and presenting a zigzag appearance.

## Chapter 5 Synthesis of Complexes

### 5.1 Introduction

As mentioned in section 1.8, following the successful synthesis of a library of symmetric pyrazine-based Schiff base ligands with antiparallel bis-terdentate chelating environments (**L1-3**), efforts were directed toward the synthesis of cyclohelicate structures containing assorted  $3d$  octahedral metal ions. Due to the design of the ligands synthesised, it was expected that any cyclohelicates formed would adopt either the square or triangle configuration (as mentioned in section 1.8). The following chapter describes the synthetic attempts in producing cyclohelicate structure from the pyrazine-based Schiff base ligands synthesised (**L1-3**) and assorted  $3d$  metal ions, as well as the methods used to characterise the structural and chemical properties of each complex formed.

### 5.2 General protocol for the synthesis of complexes

Attempts to synthesise the cyclohelicate  $[M_xL_x]$  systems were made by reacting the ligands **H<sub>2</sub>L1**, **L2** or **L3** and a  $3d$  metal salt capable of octahedral coordination in a 1:1 ratio in an appropriate solvent system (typically MeCN, EtOH or MeOH). The preferred counterion was the perchlorate anion ( $ClO_4^-$ ) due to its propensity to crystallise and act as a non-coordinating counterion.<sup>97,98</sup> Unfortunately, dry perchlorate complexes are known to be shock sensitive. Therefore, a cautious approach was necessary when dealing with these materials. Mixing the reactants together at room temperature resulted in an immediate colour change. The mixture was stirred for 30 minutes, whereupon the solvent was almost completely removed under reduced pressure. Care was taken not to dry out the reaction mixture. Vapour diffusion of diethyl ether into the reaction solution containing the complex was performed twice: first to isolate the desired complex and second to obtain single crystals suitable for SCXRD. If no crystals of suitable quality were possible to obtain, other techniques were employed to provide structural information about the synthesised complexes.



## 5.3 Characterisation of complexes

### 5.3.1 Structural characterisation of complexes

ATR-IR, taken in the range of 4000 – 700  $\text{cm}^{-1}$ , provided information on the effectiveness of the  $\text{N}_2\text{O}-\text{N}_2\text{O}$  coordination pocket found in **H<sub>2</sub>L1** and the  $\text{N}_3-\text{N}_3$  binding environment found in **L2** and **L3** in coordinating the selected metal ion. This was determined by monitoring changes in functional group bond stretches of the donor atoms upon complexation. These include the imine, pyrazine and pyridine/phenol infrared stretching frequencies. IR analysis was also used to determine the coordination nature of the counterions to a given complex. This was achieved by ATR-IR and IR spectroscopy with KBr pellets, taken in the range of 4000 – 500  $\text{cm}^{-1}$ . The latter was employed for analysis of complexes containing perchlorates as the counterion as the desired bands in question are present at  $\sim 1089$  and  $625 \text{ cm}^{-1}$ .<sup>97,98</sup>

Mass spectrometry was employed as a means of speculating on the possible structures obtained from the various complexations. A key feature in a complex's mass spectrum is the fragmentation patterns associated with the complex (as indicated by a multitude of closely-bundled peaks with differing heights in the  $M+2$  peak throughout the spectrum). Due to the design of the ligands used in the complexation and the expected coordination geometry of the metal ions, fragmented peaks to search for included simple  $\text{M}_2\text{L}$  systems and possible polymorphic  $[\text{M}_3\text{L}_3]^{x+}$ ,  $[\text{M}_4\text{L}_4]^{x+}$  and  $[\text{M}_2\text{L}]^{x+}_2$  systems. The assignments of particular fragmentation patterns in the complexes was achieved by comparison with theoretical fragmentation patterns generated by the ChemDraw software and an isotope distribution calculator.<sup>99</sup>

Conductivity measurements were used to determine the number of counterions present with each complex in solution by using Equation 1 (where  $\Lambda$  is the molar conductivity,  $\kappa$  is the measured conductivity of the sample,  $\kappa_s$  is the measured conductivity of the solvent used and  $c$  is the concentration of the sample – see the following page). A comparison of values obtained by Geary in 1971<sup>100</sup> indicate a correlation between the molar conductance,  $\Lambda$  of coordination complexes in a particular solvent and the number of counterions present. Using acetonitrile as the solvent system, the expected approximate molar conductivity for a particular complex:counterion ratio given by Geary are as follows: 120 – 160 S cm<sup>2</sup> mol<sup>-1</sup> for 1:1 systems, 220 – 300 S cm<sup>2</sup> mol<sup>-1</sup> for 1:2 systems, 340 – 420 S cm<sup>2</sup> mol<sup>-1</sup> for 1:3 systems and ~500 S cm<sup>2</sup> mol<sup>-1</sup> for 1:4 systems.<sup>100</sup> As ligands **H<sub>2</sub>L1**, **L2** and **L3** were designed to form cyclohelicate squares and/or triangles upon complexation with octahedral 3d metal ions, it was expected that the multiple metal ions present would require more than four counterions per complex. Unfortunately, no studies since then have explored coordination complex systems with larger ratios; therefore, any expected molar conductivity values for coordination complexes with 1:5 or higher systems can only be predicted by following the trend for the other known systems. A plot of this trend is presented in Figure 5.1, where the molar conductivity values for each previously mentioned ratio is averaged.

$$\Lambda = \frac{1000(\kappa - \kappa_s)}{c}$$

*l*

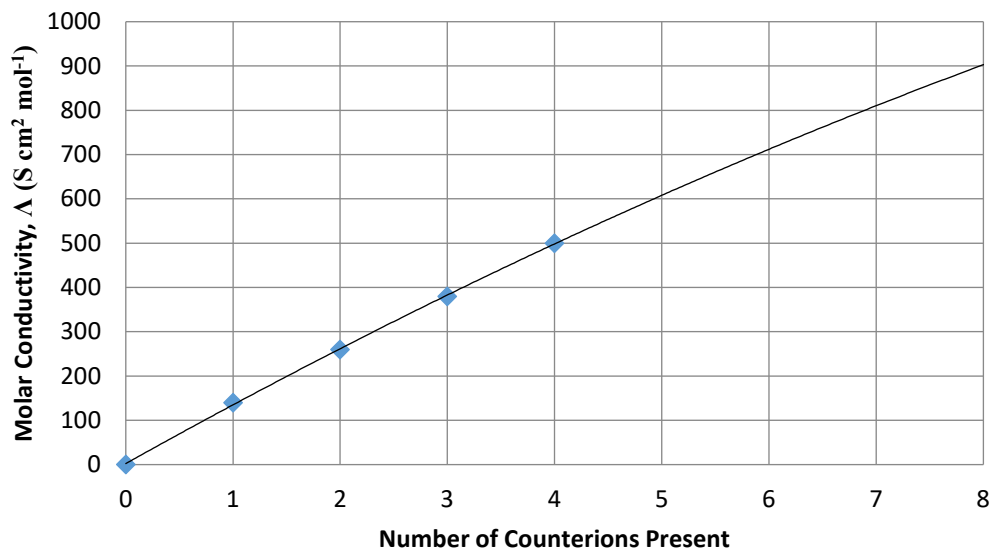


Figure 5.1. A plot of the molar conductivity of coordination complexes in acetonitrile as a function of the number of counterions per complex present.

For complexes that produced suitable crystals and generated an X-ray crystal structure; these samples were characterised using a variety of additional methods. These include the characterisation techniques mentioned above, as well as elemental analysis and thermogravimetric analysis (see appendix 3 for the generic use of these two techniques) and UV visible spectroscopy. Characterisation data for each complex synthesised is summarised in the experimental section.

### 5.3.2 Electrochemical analysis of complexes

Following the structural characterisation of a number of complexes, the electrochemical properties of these were explored with cyclic voltammetry. The overall goal was to see if any cyclohelicate structure containing a pyrazine ligand framework would exhibit metal-metal communication between neighbouring metal centres. The experimental set up for cyclic voltammetry on a given complex system resembles Figure 1.6 shown in section 1.3.2. Both platinum working micro- and macroelectrodes were used for this analysis,

however, microelectrodes produced no visually acceptable spectrum. Platinum macroelectrodes were therefore the designated electrodes of choice and only the spectra obtained with the platinum macroelectrodes are presented in this report. This meant that the presence of a supporting electrolyte was necessary for electrochemical analysis. Tetrabutyl ammonium perchlorate,  $[\text{NBu}_4][\text{ClO}_4]$  ( $\geq 0.2 \text{ mol L}^{-1}$ ) was selected to act as the supporting electrolyte as it is soluble in MeCN, is electrochemically inert in the experimental conditions, and possesses the same counter ion as is found in the complex (**C3A** and **C3B** – see section 5.4.1). Tetrabutyl ammonium perchlorate was recrystallized in EtOH prior to addition in the respective solution. The counter electrode selected was the platinum electrode due to the electrode being redox inert within the given electrochemical window. An Ag/AgCl (3M NaCl) reference electrode was used for these experiments. Argon was purged through the system prior to any analysis to remove any dissolved oxygen. Samples were analysed between 2 and -2 V, typically starting at 0 V. The scan rates used to measure the redox profiles of **C3A** and **C3B** were run at 0.01, 0.05, 0.1, 0.2 and 0.4  $\text{V s}^{-1}$ . The altering of the scan rate was done to control the adsorption of the electrochemically active species to the electrode surface, where faster scan rates led to a decrease in the diffusion of the species into solution. This would in turn produce a greater current and make minuscule peaks more pronounced.<sup>51</sup> To provide a reference check, ferrocene crystals were added at the conclusion of the electrochemical experiment. The  $\text{Fc}/\text{Fc}^+$  couple occurred at 0.45 V with  $\Delta E = 0.17 \text{ V}$ .

Unfortunately, no information regarding the magnetic properties of any complex is given in this report. Although some samples were sent for magnetic analysis (see section 5.4), it can be deduced that the samples have not been investigated at the time of writing this report.

#### 5.4 Synthesis and characterisation of complexes with **L3**

A square cyclohelicate has been prepared from the diamide analogue of **L3** (see section 1.6.3). Based on this precedent, we attempted to form a complex from **L3** and  $M(\text{ClO}_4)_2 \cdot 6\text{H}_2\text{O}$  ( $M = \text{Co}^{2+}$ ; **C3A** or  $\text{Mn}^{2+}$ ; **C3B**) in MeCN. This produced a dark green and dark red colour change upon the addition of the metal salt respectively. Removing the solvent produced dark green crystals for **C3A** and a dark red powder for **C3B**. Both complexes were both subjected to crystallisation by vapour diffusion of diethyl ether into a solution of the corresponding complex in acetonitrile. Over 4 days, dark green (**C3A**) and dark red (**C3B**) crystals suitable for SXCRD were obtained from both complexation attempts. SCXRD analysis revealed a cyclohelicate triangle structure for both complexes, as opposed to the expected cyclohelicate square structure. The cyclohelicate triangles observed were  $[\text{M}_3\text{L}_3](\text{ClO}_4)_6$  systems, with each metal centre coordinated to one  $\text{N}_3$  pocket on two separate **L3** ligands. The anti-parallel design of ligand **L3** allowed each ligand to coordinate to one metal centre from “above” and to another metal centre from “below” (as shown in Figure 5.2).

When these complexes were first produced, they were unique. Unfortunately, Hogue *et al.* published an analogous complex just a month later (see section 1.8 for further information about the structures generated in this paper).<sup>1</sup> While disappointing, this publication provided a proof of comparison to our new molecules to compare and contrast **C3A** and **C3B** with the complexes synthesised by Hogue *et al.* with  $\text{Zn}^{2+}$  (**RC1**) and  $\text{Fe}^{3+}$  (**RC2**) tetrafluoroborate salts.

Both **C3A** and **C3B** are isomorphous, indicating that both complexes are essentially identical other than the different metals contained in each complex. This indicates that any differences in bond lengths and/or bond angles are due to the metal centres. The asymmetric unit of both complexes contain one  $\text{M}^{2+}\text{L}_3$  component, representing one-

third of the triangle. The other two-thirds are generated by 3-fold rotation through the centre of the triangle (as indicated by the R-3c space group). In these complexes, the three metal ions are octahedrally coordinated to all of the donor atoms in the N<sub>3</sub> pockets from two **L3** ligands. The R-3c space group indicates a racemic mixture with inversion generating a 50:50 mixture of ΔΔΔ and ΛΛΛ enantiomers.<sup>1</sup> The arrangement of these enantiomers can be seen in Figure 5.3. Figure 5.3 also shows three perchlorates per complex sitting outside of the cavity of the triangle, and three perchlorates sitting within the bisecting point of the triangle (the middle perchlorate on the right image in Figure 5.3). The generated structures shows lots of disorder throughout the complex. This disorder is present in both the ligand system (in particular, one pyridine moiety in each ligand), and the perchlorate anions (see Figures 5.2, 5.3 and 5.4). The application of the SQUEEZE masking command was implemented, reducing the crystal's R1 value for **C3A** and **C3B** from 8.39 % and 8.32 %, to 4.95 % and 3.79 %. Further details can be found in the experimental section.

Table 5.1. Comparison of selected bond angles (°) for compounds **C3A**, **C3B**, **RC1** and **RC2**. [a] disorder present in py1/py2 on ligand **L3**. [b] disorder present in Fe1/Fe2 on ligand **RL**.

	[Co <sup>2+</sup> <sub>3</sub> <b>L3</b> ](ClO <sub>4</sub> ) <sub>6</sub> ( <b>C3A</b> ) [a]	[Mn <sup>2+</sup> <sub>3</sub> <b>L3</b> ](ClO <sub>4</sub> ) <sub>6</sub> ( <b>C3B</b> ) [a]	[Zn <sup>2+</sup> <sub>3</sub> <b>L3</b> ](BF <sub>4</sub> ) <sub>6</sub> ( <b>RC1</b> )	[Fe <sup>2+</sup> <sub>3</sub> <b>L3</b> ](BF <sub>4</sub> ) <sub>6</sub> ( <b>RC2</b> ) [b]
Reference	This work	This work	[1]	[1]
Space Group	R-3c	R-3c	R-3c	C 2/m
N <sub>pz</sub> – M <sup>2+</sup> – N <sub>pz</sub> (°)	81.648	81.131	79.6(1)	84.33(13)/85.87(9)
N <sub>pz</sub> – N <sub>pz</sub> – M <sup>2+</sup> Range; [av.] (°)	163.969 – 166.608; [165.289]	164.546 – 167.017; [166.282]	163.470 – 167.017; [165.244]	163.278 – 167.211; [165.245]

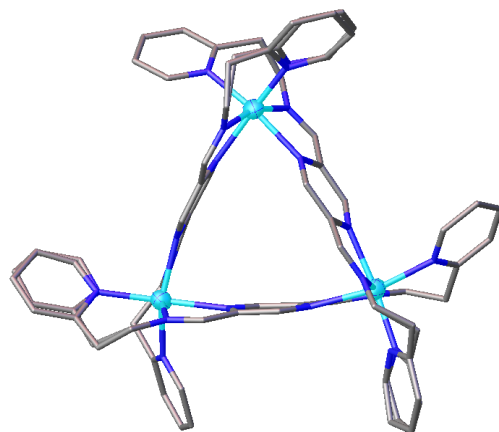


Figure 5.2. SCXRD generated molecular structure of  $[M_3L_{33}](ClO_4)_6$ . The metal centres are shown as ellipsoids, whereas the rest of the complex is shown as tubes. The hydrogens and perchlorate counterions were omitted for clarity. Disorder is shown in one-half of the pyridine rings Grey = carbon, blue = nitrogen, cyan = metal (either manganese or cobalt).

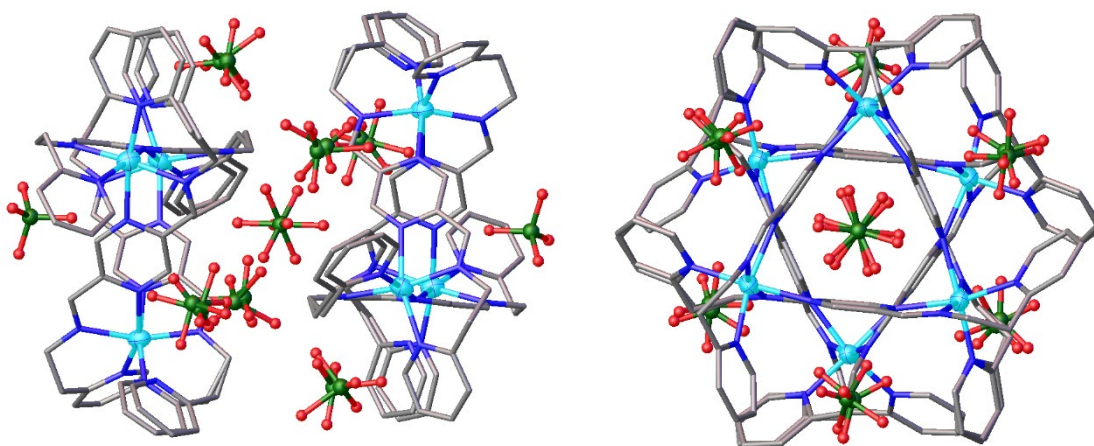


Figure 5.3. SCXRD generated molecular structure of two neighbouring  $[M_3L_{33}](ClO_4)_6$  viewed from the side (left) and the front (right). The metal centres are shown as ellipsoids, the perchlorate anions are shown as balls and sticks, and the rest of the complex is shown as tubes. Disorder is shown in one-half of the pyridine rings and in the perchlorate anions. The hydrogens were omitted for clarity. Grey = carbon, blue = nitrogen, cyan = metal (either manganese or cobalt).

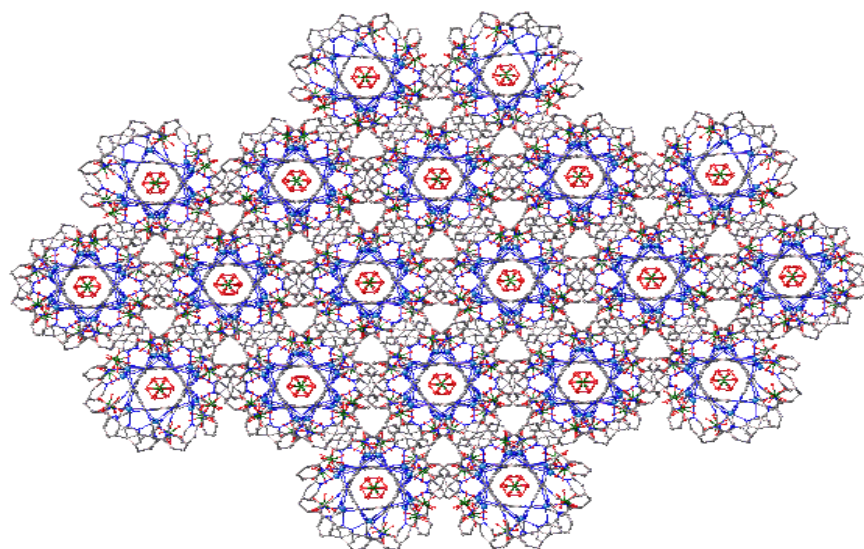


Figure 5.4. Packed structure of triangle complex (viewed down the c-axis). The metal centres are shown as ellipsoids, and the remaining atoms are shown as tubes. Hydrogens were omitted for clarity. Grey = carbon, blue = nitrogen, cyan = metal (either manganese or cobalt).

The cyclohelicate square was the expected structure to be formed from these complexations. This prediction was supported by using the molecular library model and the directional binding approach mentioned in section 1.2 to anticipate the self-assembly of an octahedral  $3d$  metal ion with **L3**.<sup>11,12</sup> For these complexes to self-assemble into cyclohelicate triangles, deformations would likely be found at either the pyrazine ring directional angle (as noted by the  $N_{pz} - N_{pz} - M$  angle), the corners of the supramolecular triangle (as noted by the  $N_{pz} - M - N_{pz}$ ), or a combination of both. The respective bonding angles can be found in Table 5.1. These measurements showed a significant decrease in the  $N_{pz} - N_{pz} - M$  angle in both **C3A** and **C3B** compared to the expected  $180^\circ$  (**C3A**: av.  $165.289^\circ$ ; **C3B**: av.  $166.282^\circ$ ). It also showed a decrease in the  $N_{pz} - M - N_{pz}$  bond angle compared to the expected  $90^\circ$  square corners (**C3A**:  $81.648^\circ$ ; **C3B**:  $81.131^\circ$ ). As the  $N_{pz} - M - N_{pz}$  corner bond angles more closely resemble corner angles found in a square than in a triangle, the deviation of the binding pyrazine is most likely responsible for the cyclohelicate triangle produced.<sup>1,13</sup> Comparable bonding angles were also obtained by Hogue *et al.* (see Table 5.1) where similar conclusions regarding the formation of the cyclohelicate triangle were reached.<sup>1</sup>

With the successful formation of the cyclohelicate triangles **C3A** and **C3B**, both of these complexes were also characterised by elemental analysis (by CHN analysis), thermogravimetric analysis (TGA), ATR-IR spectroscopy and conductivity measurements. Attempts to characterise these complexes by mass spectrometry and  $^1H$  NMR spectroscopy failed due to degradation of the complexes and the issues with paramagnetic material in the NMR apparatus respectively. Issues with the mass spectrometry were overcome by Hogue *et al.* by use of a cryospray mass spectrometer, allowing for the sample to be run at much colder temperatures ( $-60^\circ C$  to  $20^\circ C$  versus  $300^\circ C$  of our instrument). The use of  $^1H$  NMR spectroscopy to characterise paramagnetic



complexes is not commonly employed due to the low resolution spectra obtained.<sup>101</sup> To obtain the greatest quality spectrum, <sup>1</sup>H NMR spectroscopy was run between -40 and 40 °C (in 20 °C increments) as a decrease in temperature increases the NMR sensitivity.<sup>102</sup> Unfortunately, no suitable data was obtained from this form of analysis.

The elemental analysis of **C3A** differs from what was expected of the complex. This difference can be attributed to the presence of five water molecules for every complex, as shown in Table 5.2. The sample likely picked up atmospheric water over time. The results obtained from the elemental analysis of **C3B** were inconclusive. Multiple samples were sent for analysis, but gave similar results. While the results obtained were self-consistent, they did not correspond to any reasonable formulation.

Table 5.2. CHN analysis data of **C3A** with expected molecular formulas for [Co<sub>3</sub>L<sub>3</sub>](ClO<sub>4</sub>)<sub>6</sub> and [Co<sub>3</sub>L<sub>3</sub>](ClO<sub>4</sub>)<sub>6</sub> · 5H<sub>2</sub>O.

		% C	% H	% N
<b>C3A</b>	Found	37.69	3.34	13.02
	Expected (C <sub>60</sub> H <sub>60</sub> N <sub>18</sub> Co <sub>3</sub> Cl <sub>6</sub> O <sub>24</sub> )	39.89	3.35	13.95
	Expected (C <sub>60</sub> H <sub>60</sub> N <sub>18</sub> Co <sub>3</sub> Cl <sub>6</sub> O <sub>24</sub> ) + 5 H <sub>2</sub> O	37.99	3.72	13.29

To further investigate this discrepancy, **C3A** and **C3B** were subjected to thermogravimetric analysis (TGA). Heating **C3A** to 80 °C and holding for 20 hours showed a 5 % weight decrease. This is in agreement with the TGA analysis of **RC1** by Hogue *et al.* as the weight loss was due to the loss of 5 non-coordinated water molecules per complex<sup>1</sup>. Repeat analysis of **C3A** performed one month after the initial TGA showed a 6 % weight decrease, likely arising from atmospheric water picked by the sample overtime. Hogue *et al.* also detected **RC1** taking up atmospheric water upon re-examination of the product one week after initial analysis. The steady linear decline observed below 94 % is likely due to sample degradation. TGA of **C3B** presented a very different plot to **C3A**. A 6 % weight loss was observed after 40 minutes, which could

have been attributed to the loss of six non-coordinated water molecules per complex. Over two hours however, the sample lost another 5 % in weight, where the sample then lost 7 % instantly and varied very little over the remained of the time. This slow decline and dramatic drop was likely due to the decomposition of **C3B**, along with potential ‘popping’ of the compound off of the thermobalance. This may help to understand why no suitable CHN analysis result was obtained for **C3B** as CHN analysis requires the heating of the samples (see section A3.1.3).

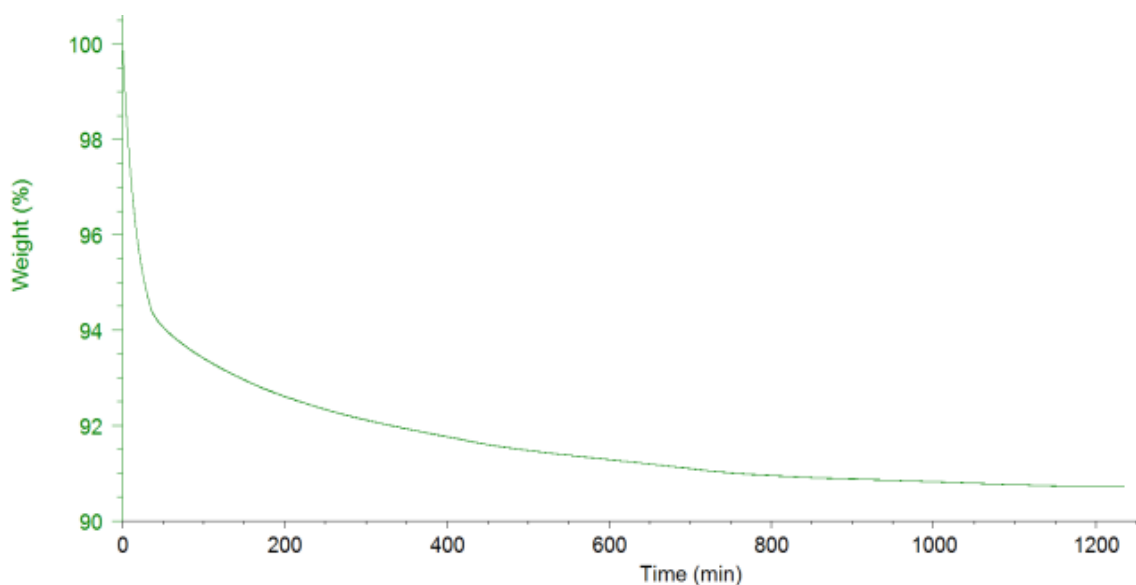


Figure 5.5. TGA plot of cobalt triangle **C3A**. The sample (6.8080 mg) was heated to 80 °C at a rate of 2 °C min<sup>-1</sup> and held at a constant temperature for 20 hours. The final temperature of 80 °C was reached after 36 minutes. Note that this TGA of **C3A** was performed one month after the initial TGA, where the mass lost was equivalent to 6 H<sub>2</sub>O water molecules.

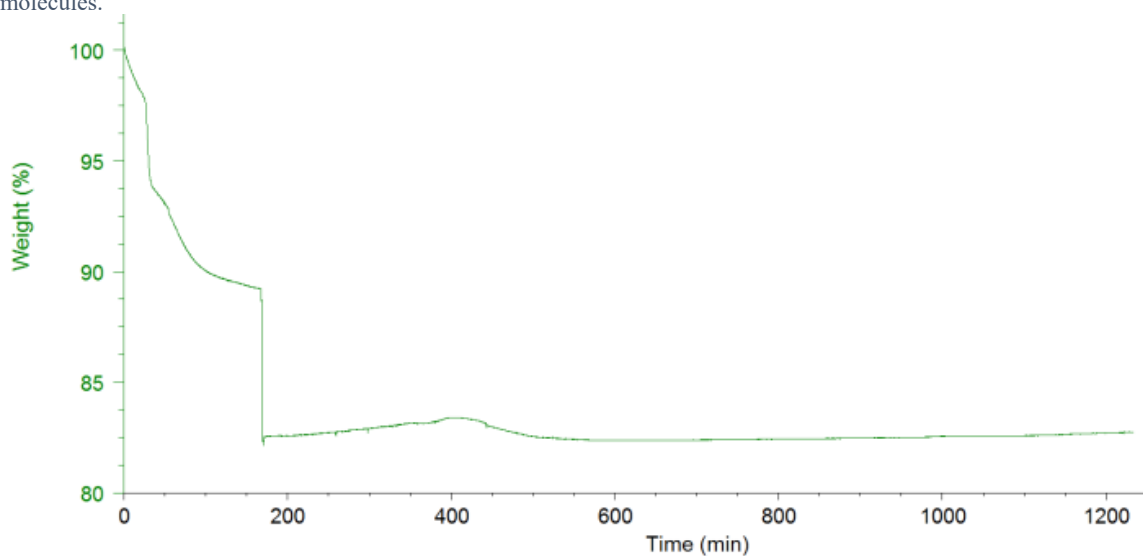


Figure 5.6. TGA plot of manganese triangle **C3B**. The sample (1.0160 mg) was heated to 80 °C at a rate of 2 °C min<sup>-1</sup> and held at a constant temperature for 20 hours. The final temperature of 80 °C was reached after 36 minutes.

As both complexes contain paramagnetic metal centres, variable temperature magnetic measurements were organised. Samples of both **C3A** and **C3B** were sent to Otago University, New Zealand for this measurement nearly a year ago. We have recently been informed they are unable to now be done at Otago University and it is now too late to send samples elsewhere.

#### 5.4.1 Electrochemical analysis of **C3A** and **C3B**

The electrochemical properties of **C3A** and **C3B** were analysed with cyclic voltammetry. Prior to this, the cyclic voltammogram of **L3** in MeCN ( $2.93 \times 10^{-3} \text{ mol L}^{-1}$ ) with tetrabutyl ammonium perchlorate,  $[\text{NBu}_4][\text{ClO}_4]$  ( $\geq 0.2 \text{ mol L}^{-1}$ ) was run to provide an additional reference spectrum.

Several redox processes were revealed in the ligand **L3** (see Figure 5.7). Scanning in the negative direction first from 0 V, two quasi-reversible reduction peaks are shown at -1.64 V. These are tentatively assigned as the reduction of the imines to secondary amines. This was compared to the pyridazine analogue of **L3** prepared by Plieger *et al.*, where the respective reduction peak was found at -1.88 V (pyridazine is 1,2-diazine). The presence of an irreversible oxidation peak is seen at 1.65 V.<sup>96,103</sup> This is assigned as the oxidation of the pyrazine ring or the secondary amines. Amine oxidation occurs in benzylamine above 1.0 V versus Ag/AgCl (3M NaCl)<sup>104</sup>, however has been shown to be as low as 0.897 V versus Ag/AgCl (sat. KCl)<sup>105</sup>. Yaman *et al.* reported the oxidation of pyrazine to be found at 2.10 V versus Ag/AgBF<sub>4</sub>. It is expected that the presence of electron donating groups on **L3** will lower the oxidation potential of pyrazine.<sup>96,103,106</sup> Further analysis is required to confirm the tentative assignment. The voltammogram obtained by travelling in the positive direction first revealed no additional peaks, nor any loss of peaks.

Between -1.30 V and -0.20 V, three quasi-reversible redox processes can be seen. The nature of these peaks are unknown as similar ligands do not present this set of quasi-reversible peaks. The origin of this set of peaks likely arises from impurities in the solvent or from other sources. Although dry HPLC grade MeCN was used for CV analysis, no further methods of purifying the solution was carried out prior to analysis.

As no electrochemical measurements have been performed on any trimetallic cobalt triangles consisting of a pyrazine diimine ligand backbone, comparisons were drawn from other sources. The closest comparison that can be made for **C3A** is with the cyclic voltammograms obtained by Shen *et al.* on tetrametallic cobalt cyclohelicate squares comprised with a pyrazine dihydrazone ligand backbone (see section 1.7.1). Other systems used for comparison included both mono- and diamide derivatives of **L3**.<sup>68,107</sup> As no similar manganese complexes could be found, the cyclic voltammogram of **C3B** was compared with the voltammograms of **C3A**.

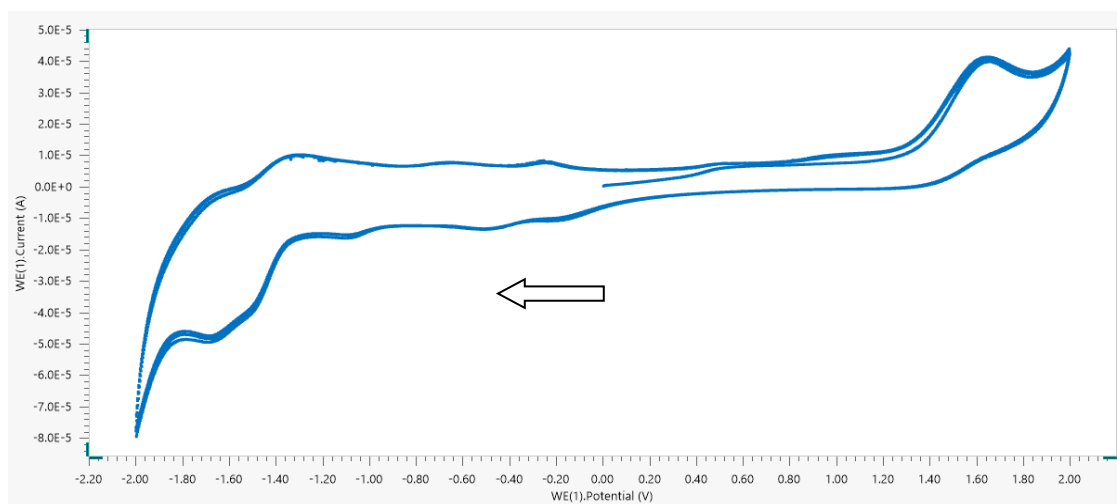


Figure 5.7. Cyclic voltammogram of **L3** in MeCN ( $2.93 \times 10^{-3} \text{ mol L}^{-1}$ ) with  $[\text{NBu}_4][\text{ClO}_4]$  ( $\geq 0.2 \text{ mol L}^{-1}$ ) at  $50 \text{ mV s}^{-1}$  in MeCN. The voltammogram was produced by scanning to more negative potentials first, with the starting point at 0 V (as indicated by the arrow).

Cyclic voltammograms of **C3A** in MeCN ( $3.21 \times 10^{-4} \text{ mol L}^{-1}$ ) showed various redox processes (see Figure 5.8). Scanning at  $0.1 \text{ V s}^{-1}$  in the negative direction first, the reduction of the imine was present at  $-1.42 \text{ V}$ . Two quasi-reversible processes can be found at  $-1.00 \text{ V}$  and  $-0.16 \text{ V}$ , followed by the presence of an irreversible oxidation peak at  $0.44 \text{ V}$ . The oxidation processes are tentatively assigned as three one-electron oxidations of the three metal centres to be  $\text{Co}^{2+}\text{Co}^{2+}\text{Co}^{2+} \rightarrow \text{Co}^{3+}\text{Co}^{2+}\text{Co}^{2+} \rightarrow \text{Co}^{3+}\text{Co}^{3+}\text{Co}^{2+} \rightarrow \text{Co}^{3+}\text{Co}^{3+}\text{Co}^{3+}$ . Oxidation and reduction peaks at similar voltages can be found by Shen *et al.* in the complexes **FC<sup>H</sup>** and **FC<sup>Me</sup>**.<sup>6</sup> These differences can likely be attributed to the different donors present in each complex. Interestingly, the separation between the two most negative of the three oxidation processes appears to be greater than the separation between the two most positive oxidation processes ( $0.88$  versus  $0.31 \text{ V}$ ), which is vaguely similar to the redox profile of the complexes that Shen *et al.* presented. This difference could be indicative of possible metal-metal communication between the cobalt metal centres through the pyrazine ligand **L3**.

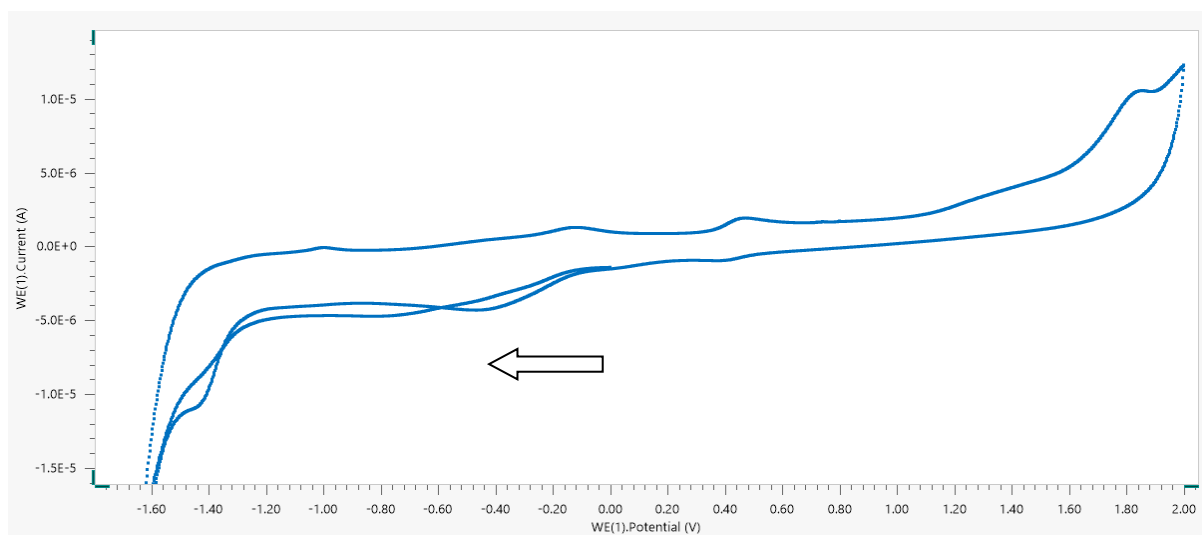


Figure 5.8. Cyclic voltammogram of **C3A** in MeCN ( $3.21 \times 10^{-4} \text{ mol L}^{-1}$ ) with  $[\text{NBu}_4][\text{ClO}_4] (\geq 0.2 \text{ mol L}^{-1})$  at  $10 \text{ mV s}^{-1}$  in MeCN. The voltammogram was produced by scanning to more negative potentials first, with the starting point at  $0 \text{ V}$  (as indicated by the arrow).

Cyclic voltammograms of **C3B** in MeCN ( $2.25 \times 10^{-4} \text{ mol L}^{-1}$ ) showed the imine reduction peak at -1.40 (Figure 5.9). The spectrum also presented two irreversible oxidation and reduction processes, as well as one quasireversible redox process (see Table 1). Similar to **C3A**, the oxidation processes are well separated with the first oxidation process (far left peak) being separated from the other two oxidation processes to a much greater extent. This is potentially indication of metal-metal communication between the manganese metal centres. Further investigation will have to be carried out on these redox processes to confirm the initial assignments. Such investigations will include the use of controlled potential coulometry, allowing for in-depth insights into the redox processes occurring at specific voltages, thus allowing for the determination of the number of electrons being transferred per peak observed.

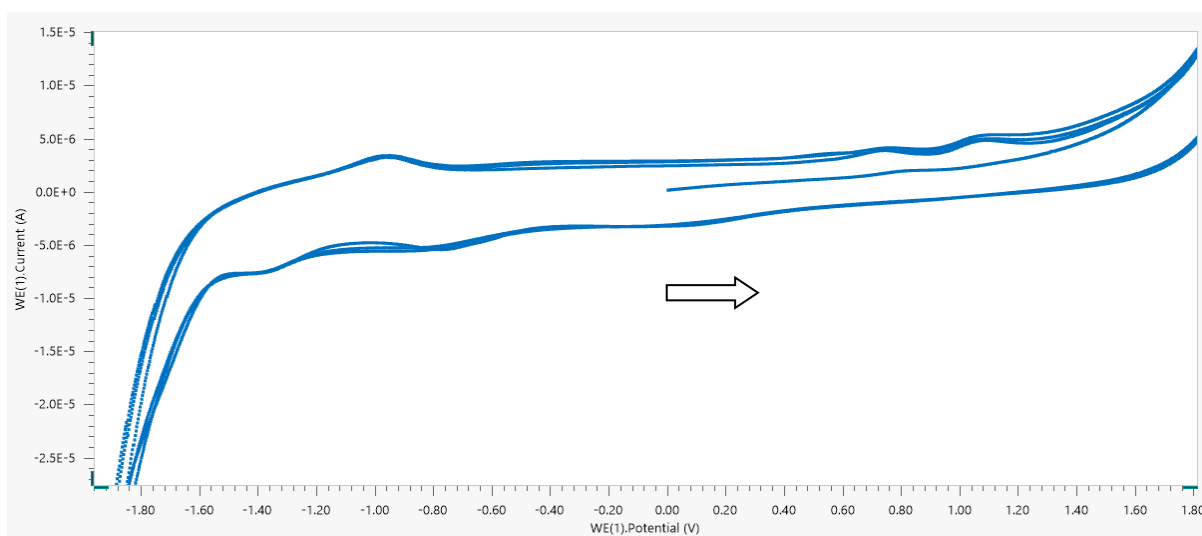


Figure 5.9. Cyclic voltammogram of **C3B** in MeCN ( $2.25 \times 10^{-4} \text{ mol L}^{-1}$ ) with  $[\text{NBu}_4][\text{ClO}_4] (\geq 0.2 \text{ mol L}^{-1})$  at  $50 \text{ mV s}^{-1}$  in MeCN. The voltammogram was produced by scanning to more positive potentials first, with the starting point at 0 V (as indicated by the arrow).

## 5.5 Synthesis and characterisation of complexes with **L2**

Due to time constraints, limited efforts were put into the complexation of **L2**. The incorporation of a methyl chain in **L2** (as opposed to an ethyl chain in **L3**) restricts the flexibility of the ligand. It was thought that these restrictions would not allow for the same deformations that allowed the triangle to be formed in **C3A** and **C3B**, and would therefore

favour the formation of a cyclohelicate square upon complexation with an octahedral 3d metal ion. To test this hypothesis,  $\text{Co}(\text{ClO}_4)_2 \cdot 6\text{H}_2\text{O}$  and  $\text{Mn}(\text{ClO}_4)_2 \cdot 6\text{H}_2\text{O}$  were also used for the complexation of **L2**. The complexations with  $\text{Co}(\text{ClO}_4)_2$ , **C2A** and  $\text{Mn}(\text{ClO}_4)_2$ , **C2B** in acetonitrile produced reaction mixtures dark blue and dark red in colour respectively. The solutions were dried under reduced pressure, yielding a dark blue solid for **C2A** and a dark red solid for **C2B**. Attempts were made to crystallise the two potential complexes. Vapour diffusion of diethyl ether into a solution of the dissolved complex in MeCN was investigated, but to no avail.

As no suitable crystals were formed, **C2A** and **C2B** were characterised by IR spectroscopy (both ATR-IR and with KBr pellets), UV-visible spectroscopy, mass spectrometry and conductivity measurements. The manganese complex **C2B** unfortunately changed colour to a dark green colour with a sludgy texture upon evaporation of the red solution, indicating that the complex may have undergone an oxidation process. As this colour change was observed near the end of the project, the characterisation techniques mentioned above were performed on the dark green manganese product, as opposed to the original dark red product. No attempts were made to crystallise this new product.

Table 5.3. Assigned peaks observed in the ATR-IR spectra and IR with KBr pellets spectra of **L2**, **C2A** and **C2B**. A question mark (?) indicates the absence of an expected peak. <sup>a</sup> indicates the peaks shown was obtained from ATR-IR spectroscopy. <sup>b</sup> indicates the peaks shown was obtained from IR spectroscopy with KBr pellets.

Compound	$\nu_{\text{pz}}$ ( $\text{cm}^{-1}$ ) <sup>a</sup>	$\nu_{\text{imine}}$ ( $\text{cm}^{-1}$ ) <sup>a</sup>	$\nu_{\text{py}}$ ( $\text{cm}^{-1}$ ) <sup>a</sup>	$\nu_{\text{ClO}_4^-}$ ( $\text{cm}^{-1}$ ) <sup>b</sup>
<b>L2</b>	?	1642	1590	-
<b>C2A</b>	2946	1614	1587	1086, 626
<b>C2B</b>	2928	1627	1595	1086, 626

The spectra obtained by ATR-IR presents the imine peak in both complexes at 1614 (**C2A**) and 1627  $\text{cm}^{-1}$  (**C2B**). These peaks are respectively lower than that of **L2** (1642  $\text{cm}^{-1}$ ). In **C2A** and **C2B**, miniscule peaks were found just below 3000  $\text{cm}^{-1}$ , which were assigned as the pyrazine C=N stretching peak, as well as sharp peaks just below 1600  $\text{cm}^{-1}$ , which were assigned as the pyridine C=N stretching peaks. The latter assignment was justified by the presence of the sharp peak in the ATR-IR spectrum of **L2** at 1590  $\text{cm}^{-1}$  (see Table 4.1). Unfortunately, the pyrazine C=N stretching peak was unidentifiable in the IR spectrum obtained for **L2**. This was likely due to the presence of a broad peak representing non-coordinated water at 3282  $\text{cm}^{-1}$  masking this peak frequency. This miniscule response in the pyrazine C=N stretching is also observed in **C2A** and **C2B**.

Both **C2A** and **C2B** complexes exhibit a strong broad peak at 1083  $\text{cm}^{-1}$ , indicative of the perchlorate Cl – O stretch. The shape of the perchlorate peak obtained resembles the IR spectra of the  $\text{Co}(\text{ClO}_4)_2 \cdot 6\text{H}_2\text{O}$  and  $\text{Mn}(\text{ClO}_4)_2 \cdot 6\text{H}_2\text{O}$  metal salts. This suggests that the perchlorates are present as non-coordinating anions. An IR using KBr pellets was performed on **C2A** to further support this claim through observing the second indicative peak (Cl – O bend) found around 625  $\text{cm}^{-1}$ . The IR spectrum with KBr discs obtained for **C2A** presented an additional set of peaks at 626  $\text{cm}^{-1}$  for **C2A** which also resembled that of  $\text{Co}(\text{ClO}_4)_2 \cdot 6\text{H}_2\text{O}$ , further indicating that the perchlorates do not coordinate to the complex. Like **C3B**, **C2B** had difficulties in precipitating the desired product when subjected to vapour diffusion of  $\text{Et}_2\text{O}$  into a solution of **C2B** in MeCN. Although multiple attempts were made to isolate the complex as a solid, this produced insufficient product to perform both ATR-IR and IR spectroscopy with KBr pellets. Therefore, it is assumed that the perchlorate is present as a non-coordinating species due to the previous claim. Future testing will be needed to confirm this inference.



To determine the structure of the complexes formed, both mass spectrometry and conductivity measurements were used. The mass spectra of **C2A** and **C2B** present similar fragmentation patterns. Patterns with varying heights in the  $M + 2$  peak indicated species with various number of perchlorate species, and so were of interest. Some peaks identified include  $M_2L(ClO_4)_x$  with peaks corresponding to hydrated species, and a dimerised fragment  $(M_2L)_2$ . Due to this, a  $M_2L$  system, or even a supramolecular system (such as a cyclohelicate square or triangle) cannot be ruled out.

Given that **L2** is a neutral molecule, the presence of a supramolecular structure would likely produce a significantly large molar conductivity ( $\geq 420 \text{ S cm}^2 \text{ mol}^{-1}$ ) due to the large number of counterions ( $ClO_4^-$  in this case) needed to produce a neutral charge. Various systems that could exist with the expected number of counterions were accounted for, including  $M^{2+}L_2(ClO_4^-)_2$ ,  $M^{2+}_2L_2(ClO_4^-)_4$ ,  $M^{2+}_3L_3(ClO_4^-)_6$  (cyclohelicate triangle) and  $M^{2+}_4L_4(ClO_4^-)_8$  (cyclohelicate square) systems, as well as including the  $M^{3+}$  variants for **C2B** due to the potential oxidation of **C2B** previously mentioned. Conductivity measurements of both **C2A** and **C2B** were performed, giving values of 0.527 and 0.661  $\text{mS cm}^{-1}$  respectively. Substituting these numbers as  $\kappa$  in equation 1 gives large molar conductivities for each system (as seen in Table 5.4), which would suggest the presence of a large number of counterions. This suggests that based on this analysis, no ratios can be ruled out and therefore, it is possible that the samples analysed do form a cyclohelicate square or triangle. Further investigation will need to be carried out to confirm this interpretation.

Table 5.4. Possible structures of **C2A** and **C2B** and the respective calculated molar conductivity of **C2A** (0.0436 g) in MeCN (25 mL) and **C2B** (0.0456 g) in MeCN (25 mL). The estimated complex:counterion ratio is derived from the plot presented in section 5.2.

Compound	Predicted structure formed	Expected complex: counterion ratio	Calculated $\Lambda$ and expected systems ( $\text{S cm}^2 \text{ mol}^{-1}$ )	Estimated complex: counterion ratio
<b>C2A</b>	$\text{Co}^{2+}\text{L2}(\text{ClO}_4^-)_2$	1:2	172	1:1 – 1:2
	$\text{Co}^{2+}_2\text{L2}(\text{ClO}_4^-)_4$	1:4	250.39	1:2
	$\text{Co}^{2+}_3\text{L2}_3(\text{ClO}_4^-)_6$	1:6	518.39	1:4 – 1:5
	$\text{Co}^{2+}_4\text{L2}_4(\text{ClO}_4^-)_8$	1:8	691.19	1:5 – 1:6
<b>C2B</b>	$\text{Mn}^{2+}\text{L2}(\text{ClO}_4^-)_2$	1:2	206.20	1p:1 – 1:2
	$\text{Mn}^{2+}_2\text{L2}(\text{ClO}_4^-)_4$	1:4	298.00	1:2
	$\text{Mn}^{2+}_3\text{L2}_3(\text{ClO}_4^-)_6$	1:6	618.61	1:5 – 1:6
	$\text{Mn}^{2+}_4\text{L2}_4(\text{ClO}_4^-)_8$	1:8	824.81	1:7 – 1:8
	$\text{Mn}^{3+}\text{L2}(\text{ClO}_4^-)_3$	1:3	242.17	1:2
	$\text{Mn}^{3+}_2\text{L2}(\text{ClO}_4^-)_6$	1:6	369.93	1:3
	$\text{Mn}^{3+}_3\text{L2}_3(\text{ClO}_4^-)_9$	1:9	726.50	1:6
	$\text{Mn}^{3+}_4\text{L2}_4(\text{ClO}_4^-)_{12}$	1:12	968.67	1:8 – 1:9

## 5.6 Synthesis and characterisation of complexes with **L1**

Using the general protocol for complexations described at the start of this chapter, six complexations were attempted with  $\text{H}_2\text{L1}$ , each changing colour upon addition of the dissolved metal salt. The particular metal salts, solvent used and respective colour changes of each complex are presented in Table 5.5. Unfortunately, no SCXRD quality crystals were produced for any of the attempted complexations described in Table 5.5.

Table 5.5. Complexations with **L1** and various metal salts, with the respective solvent system used, the colour changes observed and the complexation code.

Metal Salt	Solvent	Colour Change?	Complex Code
$\text{Co}(\text{ClO}_4)_2 \cdot 6\text{H}_2\text{O}$	MeCN	Brown	<b>C1A</b>
$\text{Mn}(\text{ClO}_4)_2 \cdot 6\text{H}_2\text{O}$	MeCN	Red	<b>C1B</b>
$\text{Zn}(\text{CH}_3\text{COO})_2 \cdot 2\text{H}_2\text{O}$	In MeOH- $d_4$	Dark Blue	<b>C1C</b>
$\text{Co}(\text{CH}_3\text{COO})_2 \cdot 4\text{H}_2\text{O}$	EtOH	Dark Brown	<b>C1D</b>
$\text{Fe}(\text{ClO}_4)_3 \cdot \text{H}_2\text{O}$	EtOH	Dark Brown	<b>C1E</b>
$\text{Mn}(\text{NO}_3)_2 \cdot 4\text{H}_2\text{O}$	MeCN	Dark Brown	<b>C1F</b>

Due to other priorities and time constraints, only the samples **C1A-C** were subjected to further characterisation as complexations with both  $\text{Mn}(\text{ClO}_4)_2$  and  $\text{Co}(\text{ClO}_4)_2$  proved to be useful with **L3**, whereas  $\text{Zn}(\text{OAc})_2$  provided a diamagnetic metal centre which can be studied with  $^1\text{H}$  NMR spectroscopy. These complexes were characterised with mass spectrometry, UV-visible spectroscopy, infrared spectroscopy (both ATR-IR and KBr discs) and conductivity measurements.

Using ATR-IR spectroscopy, all three complexes exhibit the imine peak at 1626 (**C1A**), 1620 (**C1B**) and 1657  $\text{cm}^{-1}$  (**C3C**). The absence of a sharp phenol stretch peak at 3429  $\text{cm}^{-1}$  in **L1** disappears under the presence of a broad peak between 3000-3500  $\text{cm}^{-1}$  indicating non-coordinated water. These peaks arise at 3519 and 3263  $\text{cm}^{-1}$  for **C1A**, 3521  $\text{cm}^{-1}$  for **C1B** and 3374  $\text{cm}^{-1}$  for **C1C**. The second peak found in **C1A** may indicated the presence of coordinated water within the complex (see Table 5.7).

Table 5.6. Assigned peaks observed in the ATR-IR spectra and IR with KBr pellets spectra of H<sub>2</sub>L1, C1A, C1B and C1C. A question mark (?) indicates the absence of an expected peak. <sup>a</sup> indicates the peaks shown was obtained from ATR-IR spectroscopy. <sup>b</sup> indicates the peaks shown was obtained from IR spectroscopy with KBr pellets

Compound	$\nu_{pz}$ (cm <sup>-1</sup> ) <sup>a</sup>	$\nu_{imine}$ (cm <sup>-1</sup> ) <sup>a</sup>	$\nu_{phenol}$ (cm <sup>-1</sup> ) <sup>a</sup>	$\nu_{ClO_4^-}$ (cm <sup>-1</sup> ) <sup>a,b</sup>	$\nu_{CH_3COO^-}$ (cm <sup>-1</sup> ) <sup>a</sup>
H <sub>2</sub> L1	3073	1620	3407	-	-
C1A	2958	1626	?	1079, 627	-
C1B	2957	1620	?	1074, 627	-
C1C	2953	1657	?	-	1585, 1447

The presence of a strong broad band between 1070 – 1080 cm<sup>-1</sup> in the spectra of C1A-B indicates the presence of the perchlorate anion; prompting further IR studies with KBr pellets (similar to C2A-B). The latter produced intermediate bands at 626 and 634 cm<sup>-1</sup>, which were assigned as asymmetric Cl-O bends. The bands present at both 1070 – 1080 cm<sup>-1</sup> and 626 – 634 cm<sup>-1</sup> resemble stretching and bending bands found in the metal salts used. The bands are not split, which indicates that the perchlorates are not coordinated to either complex C1A or C1B.

The mass spectra of C1A and C1B presented similar fragmentation patterns. Both complexes exhibited dimerised fragment [M<sub>2</sub>L]<sub>2</sub> (from comparing predicted spectra of this complex). From this, the possibility of a polymorphic cyclohelicate structure with L1 was not out of the question. Conductivity measurements were performed on these two complexes to determine the likelihood of a supramolecular structure by figuring out the number of perchlorate counterions present. As the coordination of a metal to H<sub>2</sub>L1 would result in a -2 charge, the formation of a cyclohelicate M<sup>2+</sup><sub>x</sub>L1<sup>2-</sup><sub>x</sub> system wouldn't possess any counterions. As a non-zero value was measured for both complexes, it is safe to assume that neither complex were present as a M<sup>2+</sup><sub>x</sub>L1<sub>x</sub> cyclohelicate structure. Equation 1 was used to determine the number of counterions that may be present in possible M<sup>3+</sup><sub>x</sub>L<sub>x</sub>

or  $M^{3+}_2L$  systems for both **C1A** and **C1B**. The molar conductivities calculated for the various structures indicated that the likely structure for **C1A** to be a  $M^{2+}_2L$  system, where **C1B** is a  $M^{3+}_2L$  system (although no observation was noted in the appearance of **C1B** for any signs of oxidation).

For complex **C1C**, the presence of two bands in the ATR-IR, assigned the symmetric and asymmetric stretches of the acetate anion, is to be expected. Broad peaks were found at  $1585\text{ cm}^{-1}$  and  $1447\text{ cm}^{-1}$ . Sharp peaks were found around this area in the ATR-IR spectrum of the original ligand **L1**, but appear to have broadened upon complexation. A correlation between the magnitude of the difference between the symmetric and asymmetric acetate stretches ( $\Delta\nu$ ) can be used to determine the nature of the coordination of the acetate counterion. The acetate ion can coordinate in three possible ways: as a unidentate ligand ( $\Delta\nu \leq 200\text{ cm}^{-1}$ ), **A** in Figure 5.10, bidentate ligand ( $\Delta\nu \leq 150$ ), **B** in Figure 5.10 or a bridging ligand ( $150 \leq \Delta\nu \leq 200\text{ cm}^{-1}$ ), **C** in Figure 5.10.<sup>96,108</sup> Due to the size of the complex and the location of the metal centres, it will not coordinate as a bridging ligand. As the gap between the symmetric and asymmetric C-O stretch is  $137\text{ cm}^{-1}$ , initial assignment implies that the acetates coordinate in a bidentate fashion (**B**).

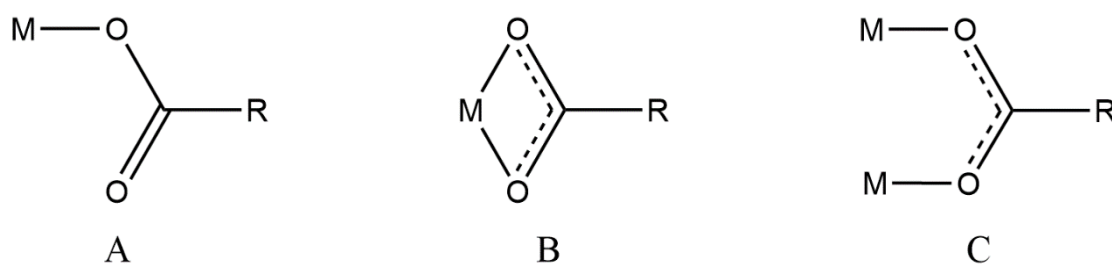


Figure 5.10. The unidentate (**A**), bidentate (**B**) and bridging (**C**) coordination fashion of acetate anions to a metal centre.

As mentioned previously, the purpose of attempting a complexation with **L1** and a zinc metal salt was to investigate the complexation by  $^1\text{H}$  NMR spectroscopy. This reaction was performed in an NMR tube, where  $^1\text{H}$  NMR spectra were collected before and after the addition of  $\text{Zn}(\text{OAc})_2 \cdot 2\text{H}_2\text{O}$  in  $\text{MeOD-d}_4$  to a solution of  $\text{H}_2\text{L1}$  in  $\text{MeOD-d}_4$  (see Figure 5.11). The spectrum of the complex showed noticeable shifts compared to the spectrum of  $\text{H}_2\text{L1}$ , with the most significant differences observed in the peaks assigned to the pyrazine  $\text{CH}=\text{N}$  and pyridine  $\text{CH}=\text{COH}$  moieties. This likely indicates that the respective N- and O-donor atoms are involved with the coordination of the zinc metal in

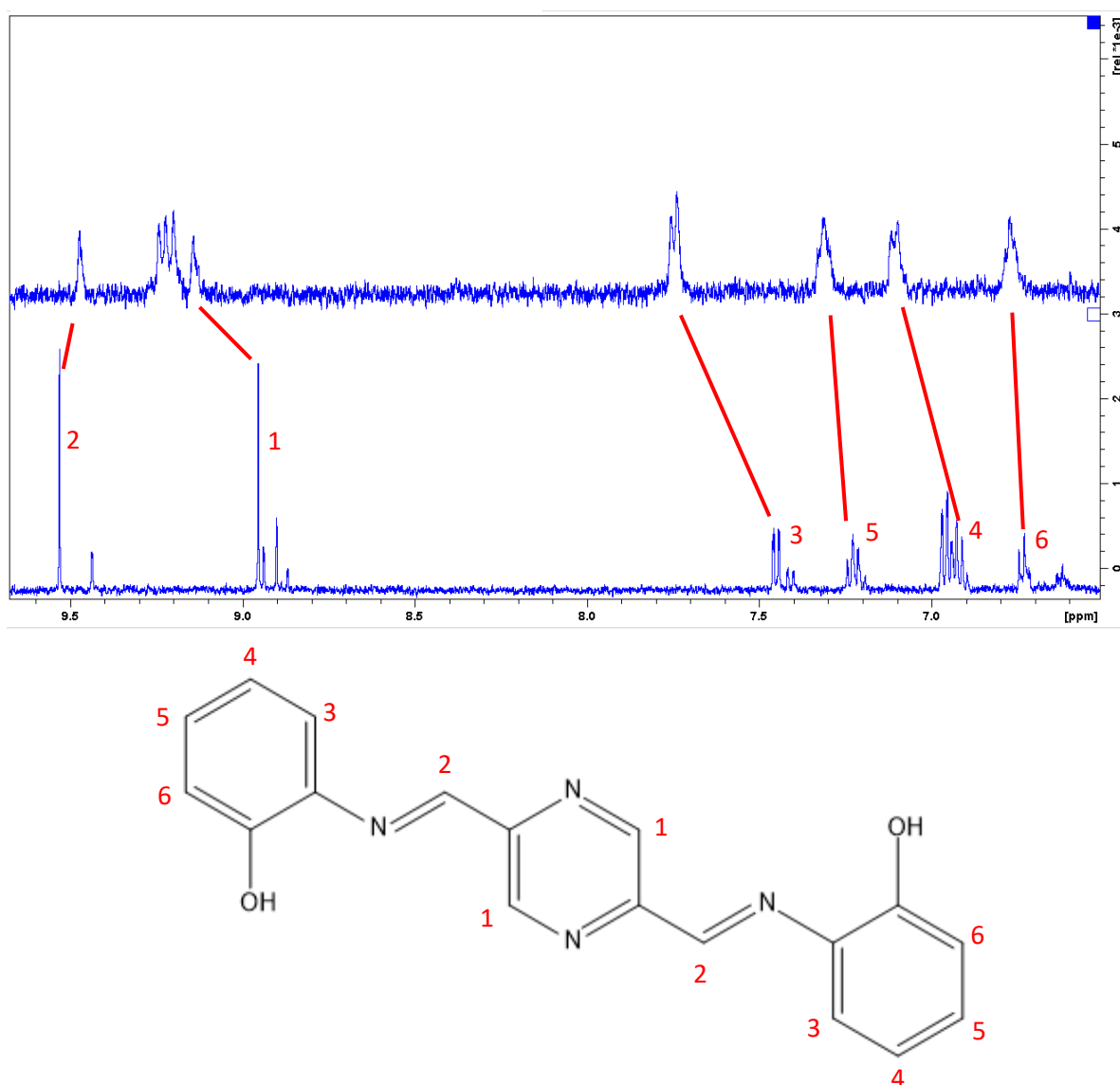


Figure 5.11. The ligand  $\text{H}_2\text{L1}$  with assigned hydrogens (bottom) and the comparison of the assigned  $^1\text{H}$  NMR spectrum of **L1** (bottom spectrum) against the assigned  $^1\text{H}$  NMR spectrum of the zinc acetate coordinated complex **C1C** (top spectrum). The spectra were ran in  $\text{MeOH-d}_4$ .

the complexation reaction. The obtained  $^1\text{H}$  NMR spectrum of **C1C** does not suggest that the imine group is involved with the coordination of the zinc metal ion. It also presents no noticeable shift in the acetate peak (found at 1.99 ppm – not shown) compared to a solution of  $\text{Zn}(\text{OAc})_2 \cdot 2\text{H}_2\text{O}$  in  $\text{MeOH-d}_4$ . This suggests that the acetate groups are not coordinating to the metal centre. With the ATR-IR and  $^1\text{H}$  NMR spectrums of **C1C** contradicting each other, in regards to the coordination nature of the acetate groups, further analysis was necessary to provide a final answer.

The mass spectrum of **C1C** presented different fragmentation pattern to **C1A** and **C1B** due to the difference in counterions present. By using the same isotope distribution prediction software used for **C2A** and **C2B**, a pattern assigned as a  $\text{M}_2\text{L}$  system with four acetate moieties was found. To further determine the coordination nature of the acetate groups (as previously unresolved by ATR-IR spectroscopy,  $^1\text{H}$  NMR spectroscopy and mass spectrometry), conductivity measurements were run. Systems investigated included  $\text{M}^{2+}\text{L}$  systems, with varying number of acetate groups coordinated to the complex, and  $\text{M}^{2+}_x\text{L}_x$  cyclohelicate structures. The value of  $\kappa$  and  $\kappa_s$  for **C1C** were almost identical, indicating that no counter ions was present in the solution and the acetate groups are in fact coordinating to the metal centres. This therefore rules out the likelihood of the formation of a cyclohelicate structure with **C1C** as the metal centres in a cyclohelicate must be completely coordinated to the donors provided in the original ligand system (in this case: **L1**).

## 5.7 Conclusion

Attempts were made to synthesise cyclohelicate structures from complexations with ligands **H<sub>2</sub>L1**, **L2** and **L3** and various octahedral metal salts. Two related cyclohelicate triangles with **L3** as the backbone were produced from the complexation with  $\text{Mn}(\text{ClO}_4)_2 \cdot 6\text{H}_2\text{O}$  and  $\text{Co}(\text{ClO}_4)_2 \cdot 6\text{H}_2\text{O}$  (as determined by SCXRD), and show that both

complexes were isostructural to one another. Although cyclic voltammetry showed potential communication between the metal centres in their respective complexes, further analysis is necessary to verify these observations. The complexation between the same metal salts and the other two ligands ( $H_2L1$  and  $L2$ ) were attempted, however the structure of the complex could not be determined by SCXRD. Other techniques were therefore employed to implement an educated guess into the obtained products. In the case for  $L2$ , mass spectrometry and conductivity measurements suggested that a cyclohelicate may have been formed, whereas for  $H_2L1$ , it appears that a  $M_2L$  system is more likely the product obtained.



## 6 Conclusion

Overall, this project has provided new knowledge surrounding the synthesis of unique pyrazine-based ligand systems, as well as demonstrating their effectiveness in producing both simple and polymorphic inorganic systems. On top of this, preliminary electrochemical analysis provided evidence of possible metal-metal communication within tri-cobalt and tri-manganese pyrazine-based cyclohelicate triangles. To produce these pyrazine-based ligand systems, a suitable method of synthesising the precursor **A1** needed to be established.

Several routes were explored for the synthesis of **A1**, where procedures by Das *et al.*<sup>85</sup>, Klein *et al.*<sup>90</sup> and Coufal *et al.*<sup>5</sup> were all trialled. Eventually, an original method was established in a two-step method, where 150 mg of **A1** could be produced over a two day period. The first step in this procedure reduced the time to synthesise 2,5-distyrylpyrazine from three days to just six hours in a 62 % yield with the incorporation of a microwave synthesiser. The second step adapted the reaction by Brooker *et al.*, where 3,6-distyrylpyridazine underwent oxidation by ozonolysis.<sup>95</sup> This successfully produced **A1** in a 35 % yield.

The Schiff base condensation of **A1** with various primary amine reactants produced three unique ligand systems. The confirmed synthesis of these ligands was verified with a large variety of characterisation techniques. Unfortunately, a single crystal structure could only be generated for one ligand system (**L3**), which revealed both imine –  $\pi$  stacking interactions, as well as alkane hydrogen – pyridine interactions. These resulted in the formation of columns of zig-zag arrays (as shown in Figure 4.3).

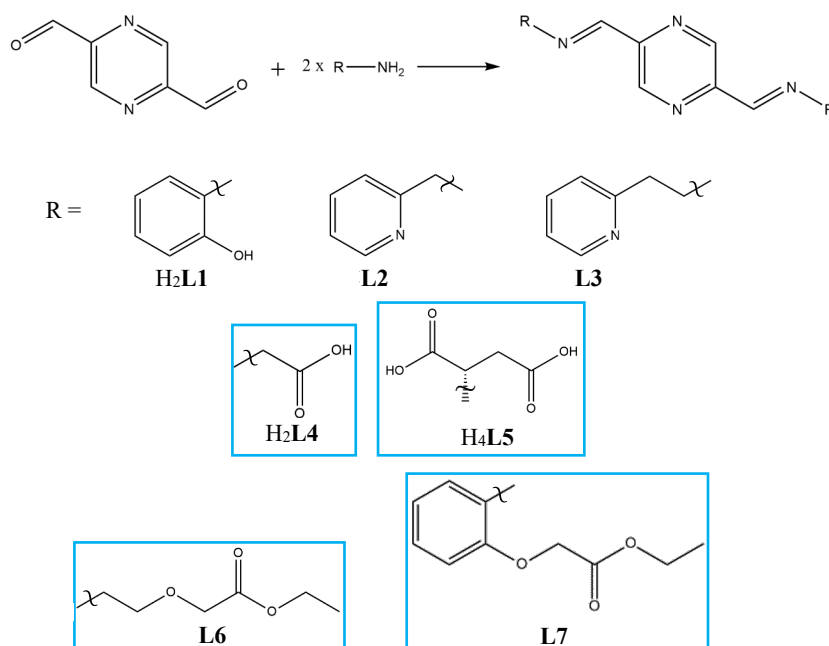
Several complexations were attempted with the three ligand systems synthesised. Although the list of metals trialled for complexation with **L3** is short, the single crystal structures generated showed cyclohelicate triangles, which were unique at the time. The

electrochemical analysis of these complexes in MeCN showed similar redox processes as was seen in the electrochemical analysis of **L3**. Signs of possible metal-metal communication within the cyclohelicate triangles was also noticed, with oxidation (and reduction) processes unevenly spaced apart from one another. Further analysis is necessary to verify these interpretations, including magnetic analysis. Complexations with identical metal salts and **L2** could not be characterised by SCXRD. Future work will attempt crystallisation with other solvent systems. Other techniques such as mass spectrometry and conductivity measurements indicated the likely formation of a polymorphic – potentially cyclohelical structure. To confirm this initial assessment, future efforts into the crystallisation of these complexes will be beneficial. Complexations with **H<sub>2</sub>L1** incorporated the inclusion of a larger collection of metal salts. Unfortunately, due to time constraints, only three complexes were suitably characterised. From the various characterisation methods used, it was deduced that all three complexes were likely simple **M<sub>2</sub>L1** systems, where the coordination of the 6-coordinate *3d* metal centres were accompanied by the coordination of either water, solvent (MeCN), counterion or a combination of these. Similar to the complexations with **L2**, further analysis will aid in confirming these conclusions.

The findings presented in this thesis will hopefully provide a suitable platform that can assist in any future work involving the synthesis of pyrazine-based imine ligands, and the subsequent formation of cyclohelicates upon complexation with octahedral *3d* metal ions. Although new cyclohelical systems were produced during the course of this project, the truly remarkable surprises are still to come.

## Appendix 1                      Synthesis of L4 – L7

As mentioned in Chapter 4.2, the synthesis of seven pyrazine-based Schiff base ligands (**H<sub>2</sub>L1** - **L7**) were attempted. The synthesis and characterisation of **L4-7** was not discussed in chapter 4 due to synthetic issues and time constraints. Ligands **L4-7** were designed to possess a multitude of hard donor atoms, such as O-donor atoms found in carboxylic acids, esters and ether functionalities. The hard donors favour coordination to lanthanide (4f) metal ions as they are considered to be hard Lewis acids (according to HSAB theory) with coordination numbers up to nine.<sup>24</sup> In this project, Schiff base condensations were also attempted with glycine (**L4**) and L-aspartic acid (**L5**) as these were easily obtainable precursors. Schiff base condensations with 2-(2-aminoethoxy)acetic acid ethyl ester (**L6**) and 2-(2-aminophenoxy)acetic acid ethyl ester (**L7**) were not attempted due to issues regarding the synthesis of these precursors. The following appendix section describes the synthetic attempts at producing pyrazine-based Schiff base ligands with **H<sub>2</sub>L4** and **H<sub>4</sub>L5**, as well as the attempts to produce the **L6** and **L7** precursors in this respective order (see Scheme A1.1).



Scheme A1.1. The general reaction scheme of a Schiff base condensation between pyrazine-2,5-dicarbaldehyde (**A1**) and a primary amine. The three ligands not enclosed in boxes (**H<sub>2</sub>L1**, **L2** and **L3**) were successfully synthesised and isolated as pure ligands. The four ligands enclosed in a blue box (**H<sub>2</sub>L4**, **H<sub>4</sub>L5**, **L6** and **L7**) were not successfully isolated as pure ligands and will be the discussion point for this section.

### A1.1 Synthesis of H<sub>2</sub>L<sub>4</sub> and H<sub>4</sub>L<sub>5</sub>

Glycine (R = H<sub>2</sub>L<sub>4</sub>) and *L*-aspartic acid (R = H<sub>4</sub>L<sub>5</sub>) are both amino acids that are produced within the human body. These amino acids were specifically selected for their simple chemical structure with multiple hard O-donor atoms, along with the presence of only one primary amine, thus preventing the formation of multiple Schiff base products.

The introduction of amino acids as the primary amine component of a Schiff base condensation does present several issues. Firstly, due to the chemical nature of amino acids, they are only soluble in water-based solvents and slightly soluble in a small number of organic solvents.<sup>109</sup> As was described in section 2.1, Schiff base condensation is a reversible reaction. The presence of water shifts the equilibrium towards the starting materials. Unfortunately, due to the thermal stability of **A1**, refluxing the reaction mixture (to promote dissolution of the amino acids in the selected solvent) was not possible. Instead, mixtures containing water-miscible solvents and water were used for the reaction.

Due to the focus of the research, being directed toward the ligand systems in section 4, and the various complexations attempted, limited work was performed in this area. As the solubility of the amino acids is poor in most organic solvents, mixtures with high or low water content (compared to the water-miscible organic solvent) were used in the various attempts. Solvent systems trialled for H<sub>2</sub>L<sub>4</sub> were 3:1 H<sub>2</sub>O:MeOH for 3 days and 4:1 MeOH:H<sub>2</sub>O for 1 week. Due to these solvent mixtures showing no signs of success, they were not used in the attempted synthesis of H<sub>2</sub>L<sub>5</sub>. For the synthesis of H<sub>2</sub>L<sub>5</sub>, only 1:1 EtOH:pyridine was used, but this too was unsuccessful.

### A1.2 Conclusion

As this aspect of research was shortly lived, there are still plenty of routes to undertake that can influence the successful synthesis of the desired ligands. Firstly, by repeating the

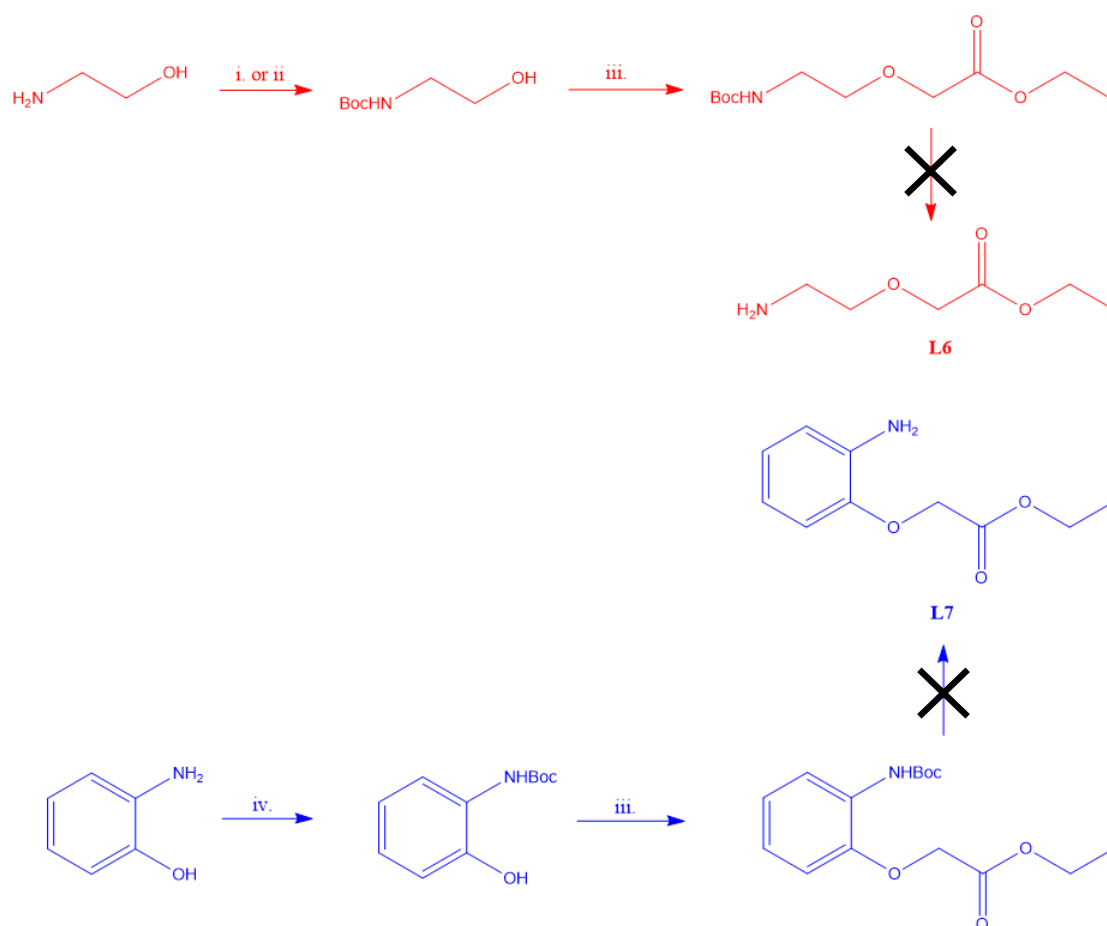
Schiff base reaction with the above mentioned amino acids in a more acidic solution, this will encourage the amino acids to dissolve in solvents such as EtOH or MeOH.<sup>109</sup> Although a Schiff base reaction is an acid-catalysed reaction, it has been shown that the addition of a base (such as NaOH or KOH) to reduce the acidity of the solution has been effective in producing Schiff base compounds with amino acids like glycine and L-aspartic acid.<sup>110-113</sup> Another method that would be worth investigating would be altering the pressure of the reaction system to decrease the boiling point of the solvent used in the reaction. If the optimal pressure solvent combination is achieved, the solubility issue of the amino acids may be overcome, whilst avoiding the degradation of **A1**. This outcome would allow the reaction mixture to receive more energy (likely by refluxing the reaction mixture), thus increasing the likelihood of the successful formation of the desired ligands.

### A1.3 Synthesis of **L6** and **L7**

The synthesis of **L6** was reported by Späth *et al.* who used a two-step method starting from *N*-Boc-2-aminoethanol (red method starting from step iii. in Scheme A1.2).<sup>7</sup> First, the amine was protected with a *tert*-butyloxycarbonyl (Boc) group to prevent the nucleophilic amine interfering with the ether formation. According to Späth *et al.*, the acidic hydrolysis of the newly formed ether product cleaves the Boc protecting group, yielding **L6**.<sup>7</sup> Unfortunately, due to time constraints and synthetic issues, this step was not attempted (black cross in the red method in Scheme A1.2). The following procedure was also adapted for the synthesis of the precursor **L7** from *N*-Boc-2-aminophenol (blue procedure starting from step iii. in Scheme A1.2). The synthesis of *N*-Boc-2-aminoethanol and *N*-Boc-2-aminophenol required for the formation of **L6** and **L7** saw 2-aminoethanol and 2-aminophenol stirred at room temperature in water for 3 – 4 hours with di-*tert*-butyl dicarbonate (step i. and iv. in Scheme A1.2).<sup>114,115</sup> Although the desired product was obtained (proven by <sup>1</sup>H NMR spectroscopy), unreacted di-*tert*-butyl

dicarbonate, or (Boc)<sub>2</sub>O was not removed during the workup process. Attempts to wash the crude N-Boc-2-aminoethanol with NaOH to remove the excess (Boc)<sub>2</sub>O was found to be unsuccessful. Due to this, another route to making N-Boc-2-aminoethanol by Devine *et al.* was trialled.<sup>116</sup> Although this procedure requires a longer reaction time (15 minutes at 0 °C followed by stirring at room temperature overnight), the final product obtained, a colourless oil (85 % yield), had a more complete reaction (see bottom <sup>1</sup>H NMR spectra in Figure A1.1). Due to the successful synthesis of N-Boc-2-aminoethanol and known literature describing the synthetic route to **L6**, efforts in synthesising N-Boc-2-aminophenol were put on hold until the synthesis of **L6** was optimised.

Following the successful Boc protection of 2-aminoethanol, a Williamson ether synthesis was attempted on N-Boc-2-aminoethanol with ethyl bromoacetate. Under an inert atmosphere, potassium *tert*-butoxide (*t*-BuOK) in THF and ethyl bromoacetate were added together in small portions, producing an orange mixture that was stirred at 0 °C for 3 hours, and following work-up produced an orange oil. <sup>1</sup>H NMR spectroscopy and mass spectrometry (see Figures AS8 and AS9) indicated that the desired product was present within the crude material. TLC of the crude material with the column conditions indicated by Späth *et al.* (1:1 petroleum ether: ethyl acetate) was attempted, however yielded no spots under UV light.<sup>7</sup> Subjecting the TLC plate to ninhydrin caused a dark brown spot to appear half way up the plate ( $R_f = 0.5$ ), likely indicating the desired product as ninhydrin stain is used to detect primary (and secondary) amines. Unfortunately, the silica gel column run with said conditions only partially separated the desired product from the crude material and so attempts were abandoned.



Scheme A1.2. Reaction scheme for the synthesis of L6 and L7. (i) (Boc)<sub>2</sub>O, H<sub>2</sub>O, rt, 4 hr, 99 % (i). (ii) (Boc)<sub>2</sub>O, dry DCM, 0 °C, Et<sub>3</sub>N, 87 %. (iii) *t*-BuOK, dry THF, CH<sub>2</sub>BrCOOCH<sub>2</sub>CH<sub>3</sub>, 0 °C, 3 hr, n/a. (iv) (Boc)<sub>2</sub>O, H<sub>2</sub>O rt, 2 hr, 74 %. (i): incomplete reaction. n/a: unable to obtain a yield.

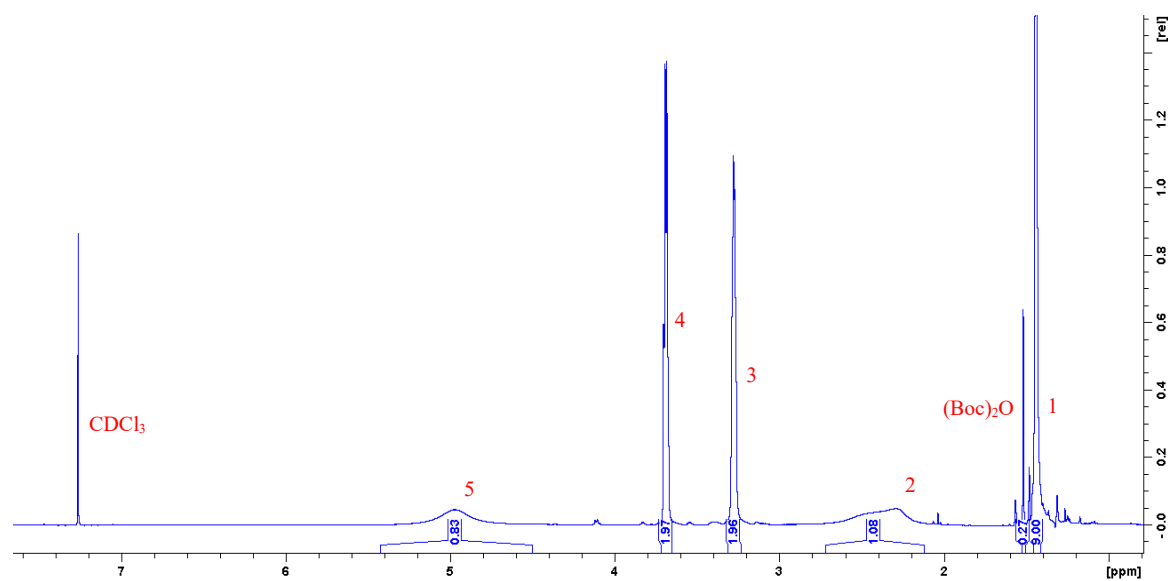
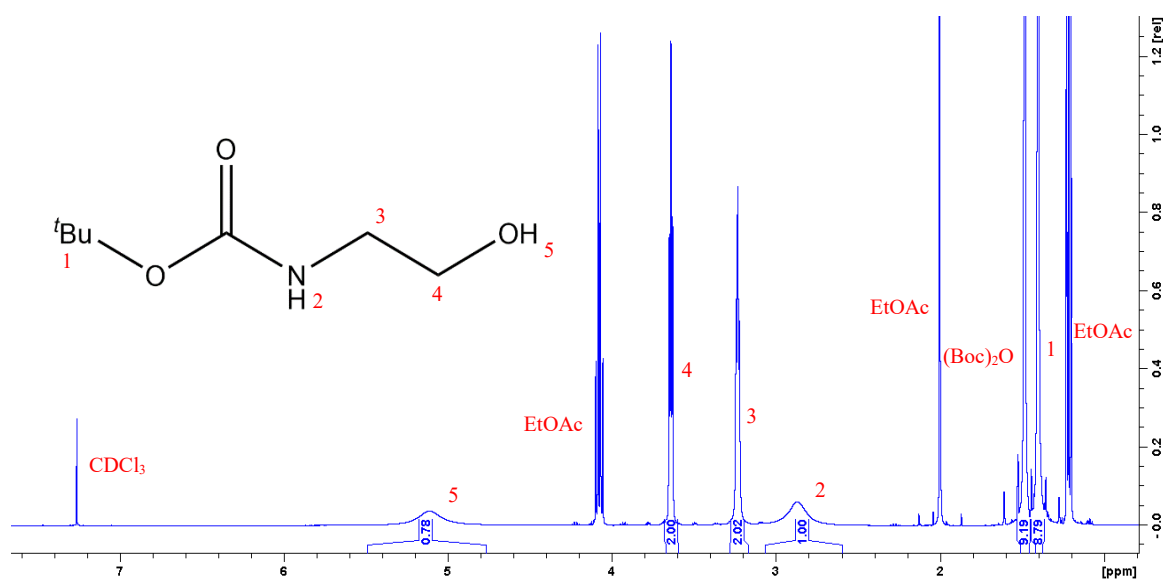
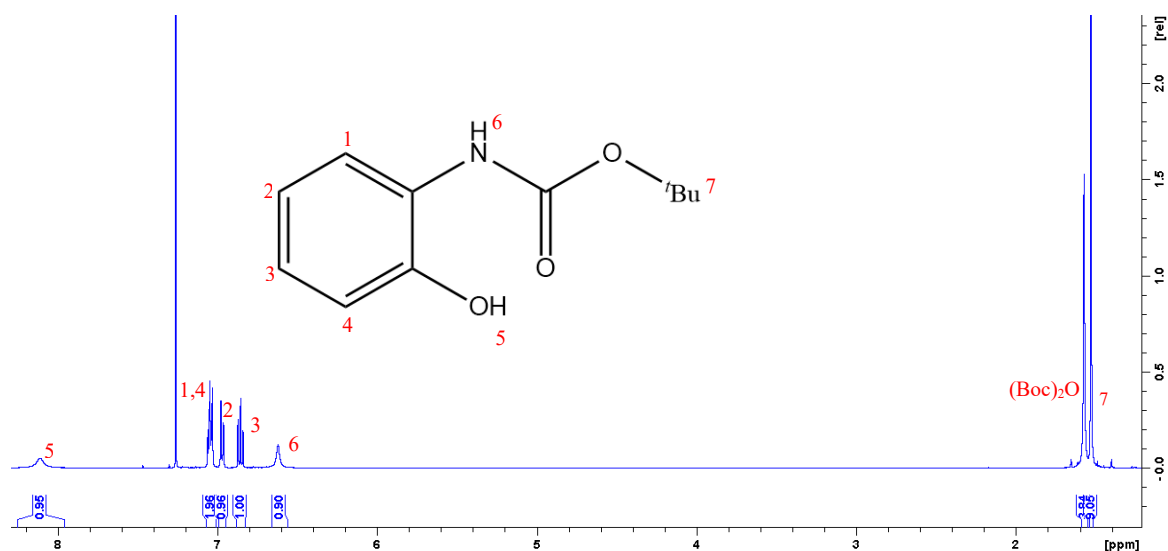


Figure A1.1. Assigned <sup>1</sup>H NMR spectra of *N*-Boc protection of 2-aminoethanol and 2-aminophenol. Top spectrum shows the <sup>1</sup>H NMR spectrum of *tert*-butyl (2-hydroxyphenyl)carbamate by of Chankeshwara *et al.* (step iv). Middle spectrum shows the <sup>1</sup>H NMR spectrum of *tert*-butyl (2-hydroxyethyl)carbamate by Chen *et al.* (step i). Bottom spectrum shows the <sup>1</sup>H NMR spectrum of *tert*-butyl (2-hydroxyethyl)carbamate by Devine *et al.* (step ii).

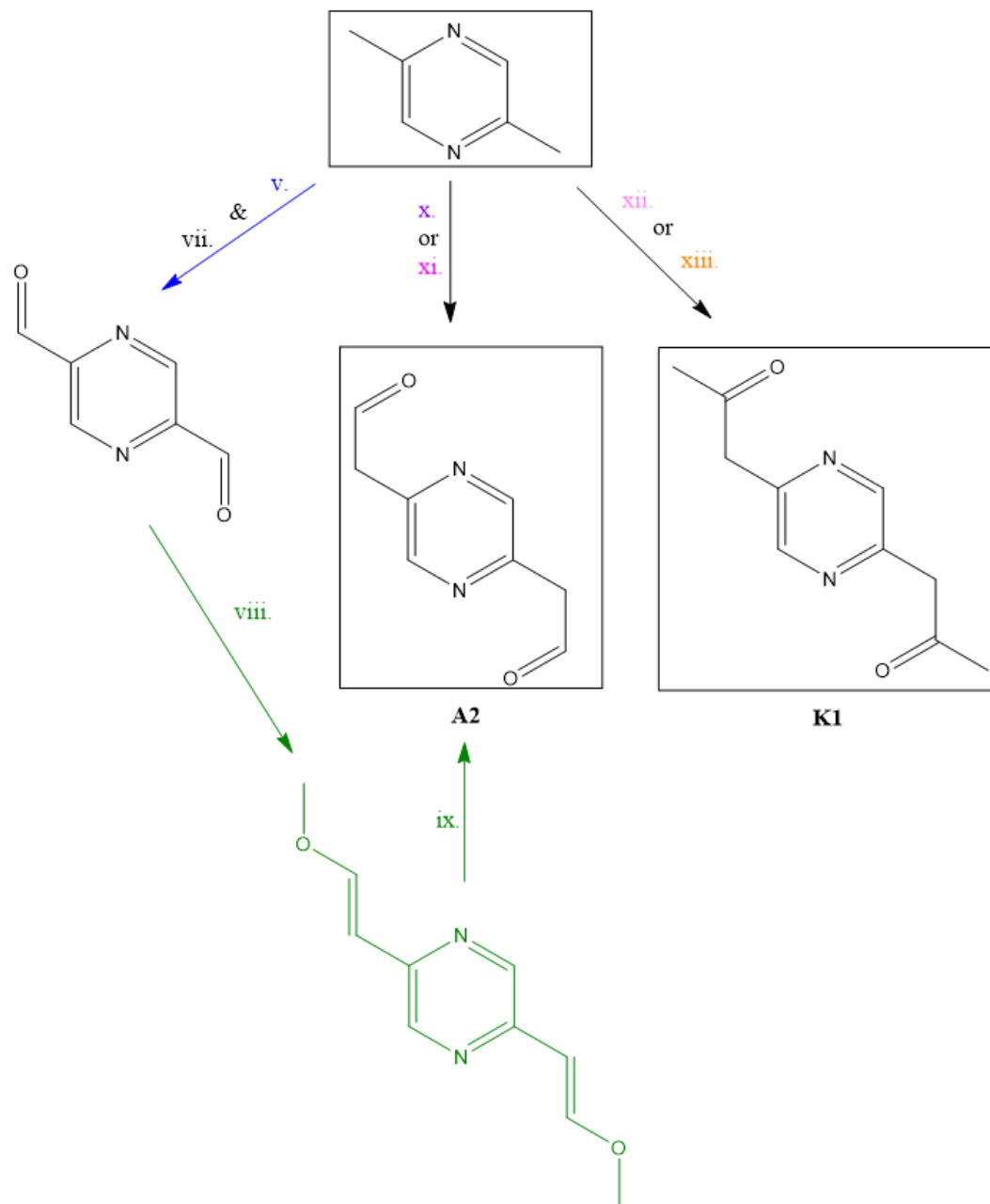


#### A1.4 Conclusion

The synthesis of **L6** and **L7** was unsuccessful, however synthetic efforts have provided a path forward. Future directions in the synthesis of these desired ligands would be to isolate the *N*-Boc-2-(2-aminoethoxy)acetic acid ethyl ester (step iii in the red method in Scheme A1.2). Following this, the acidic hydrolysis of the specified precursor as specified by Späth *et al.* (using either diethyl ether saturated in HCl or 1N aqueous HCl) will be used to produce **L6**. The synthetic approach will also be adapted to produce **L7**.

## Appendix 2                      Synthesis of Pyrazine-2,5-diacetaldehyde (A2) and 2,5-pyrazinyldiacetone (K1)

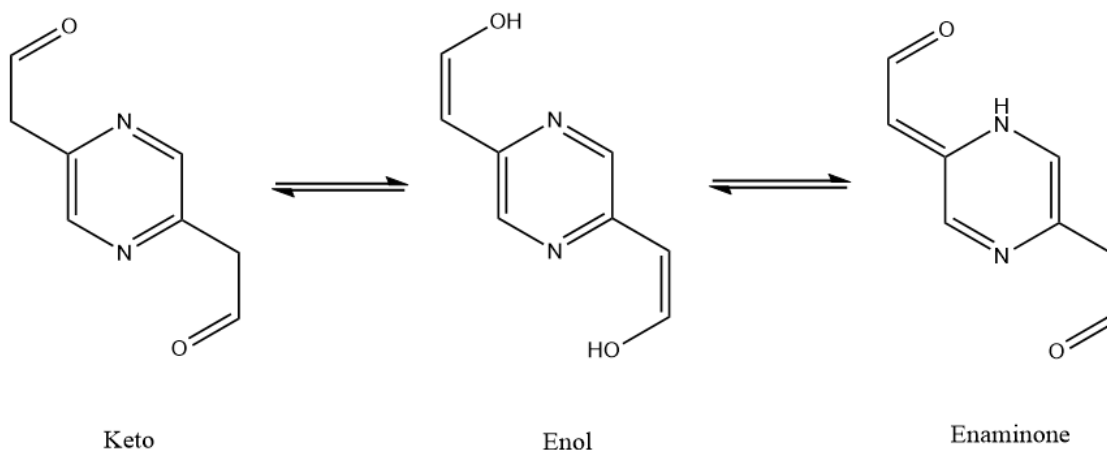
As mentioned in section 2.2, the incorporation of an additional carbon on pyrazine-2,5-diacetaldehyde provides several differences. Other than the aforementioned increase in the alkyl chain's flexibility, Schiff base condensation would result in an imine capable of forming a 6-membered chelate ring on complexation. Such a ring size favours



Scheme A2.1. Synthetic scheme for the synthesis of pyrazine-2,5-diacetaldehyde (A2) and (K1). (viii) The reaction conditions for (v) and (vii) are present in Scheme 1. (viii)  $[\text{Ph}_3\text{PCH}_2\text{OCH}_3]\text{Cl}$ , *t*-BuOK, dry THF, -78 °C, 4 hr. (ix) HCOOH (1 – 10 M), DCM, o/n. (x) *n*-BuLi (2.5 M in hexanes), dry THF, -78 °C, 1.5 hr, DMF, -78 °C – rt. (xi) LDA, dry THF, -78 °C, 1.5 hr, DMF, -78 °C – rt. (xii) LDA, dry THF, -78 °C, 1 hr, *N,N*-dimethylacetamide, -78 °C – rt. (xiii) *n*-BuLi (2.5 M in hexanes), dry THF, 0 °C – rt, 4hr, MeCN, 0 °C – rt, 6hr, H<sub>2</sub>SO<sub>4</sub> (60 % aq. solution), rt, o/n. Unfortunately, no reaction produced A2 or K1 as pure products.

coordination of smaller metal ions such as 3*d* metals.<sup>24</sup> Although there are currently no reported methods for the synthesis of pyrazine-2,5-diacetaldehyde (**A2**), previous work on similar six-membered *N*-heterocyclic systems have provided a foundation to go from (Scheme A2.1). As mentioned in Section 2.1, ketones are capable of undergoing Schiff base condensations reactions as well; therefore, if efforts to synthesise **A2** were unsuccessful, focus would also be directed towards the synthesis of 2,5-dipyrazinylacetone (**K1**).

The potential benefit of using a dialdehyde at the  $\beta$ -position might be offset by the introduction of keto/enol tautomerism.<sup>117</sup> This system may exhibit 3 tautomers: ketone, enol or enaminone (Scheme A2.2). Due to the loss of aromaticity around the pyrazine ring in the enaminone, it is unlikely that this species will be observed.<sup>118</sup>



Scheme A2.2. The keto, enol and enaminone tautomers of pyrazine-2,5-diacetaldehyde.

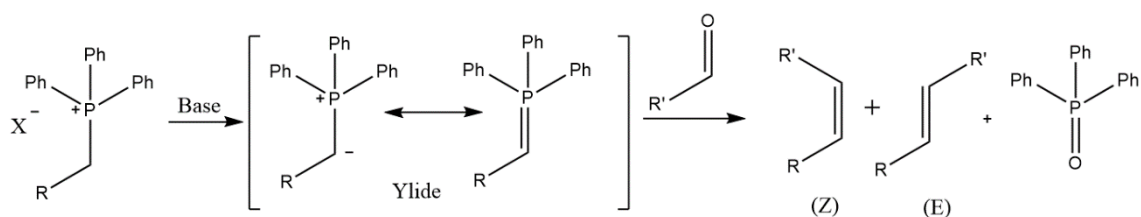
The following section discusses the attempted synthesis of both **A2** and **K1**, beginning with the initial attempts to synthesise **A2**.

### A2.1 Synthesis of pyrazine-2,5-diacetaldehyde (**A2**)

The initial approach to synthesise **A2** involved modification of existing literature describing the synthesis of benzene acetaldehyde derivatives from benzene carboxaldehyde species. The plan was to start from pyrazine-2,5-dicarbaldehyde (**A1**), which would undergo a Wittig reaction with a (methoxymethyl)triphenylphosphonium

salt (either a bromide or chloride salt) to form the dimethyl enol ether product (step viii. in Scheme A2.1). Acidic hydrolysis of the product should yield the desired pyrazine-2,5-diacetaldehyde (step ix. in Scheme A2.1). This route has not been investigated on many *N*-heterocyclic systems, where only the initial Wittig reaction between 2-pyridinecarboxaldehyde and (methoxymethyl)triphenylphosphonium chloride had been reported.<sup>119</sup> Initial attempts to synthesise **A1** followed the work by Campa *et al.* and Zaytsev *et al.* who successfully synthesised benzene-1,4-diacetaldehyde and benzacetaldehyde respectively from their carboxaldehyde counterparts.<sup>87,88</sup>

Firstly, attempts were made at replicating the reported procedure by Campa *et al.* with (methoxymethyl)triphenylphosphine chloride ( $[Ph_3PCH_2OCH_3]Cl$ ) on benzaldehyde and terephthalaldehyde as these were easily accessible compared to pyrazine-2,5-dicarbaldehyde which required initial synthesis first. The Wittig reaction required the generation of a phosphonium ylide, which was achieved by the deprotonation of the  $CH_2$  neighbouring the triphenylphosphine moiety with potassium *tert*-butoxide (*t*-BuOK) (Scheme A2.3). Phosphonium ylides are sensitive to water, therefore they are prepared under an inert atmosphere using anhydrous solvents where the successful formation of the ylide was indicated by the formation of a blood-red solution. Both the desired mono- and dimethoxyvinyl benzene products were synthesised (as indicated by  $^1H$  NMR spectroscopy), as a mixture of both the *E* and *Z* isomers were present. As the desired diacetaldehyde product will possess a flexible alkyl chain, the geometry of the stereoisomers is irrelevant. Attempts were made to purify the product by recrystallization



Scheme A2.3. General Wittig reaction scheme ( $X = \text{halogen}$ ). In this case,  $R = OCH_3$  and  $R' = \text{pz}$ .

from hexane (to remove any triphenylphosphine oxide), and ethyl acetate. These attempts had no success in separating the desired product from the crude material. It was then decided that the methoxyvinyl products did not need to be purified prior to hydrolysis as the impurities would not affect the next reaction. Attempts were made to form the pyrazine enol ether species under identical conditions, and this yielded a brown oil, with  $^1\text{H}$  NMR spectroscopy indicating the successful formation of 2,5-methoxyvinylpyrazine within the crude material (Figure A2.1). As the spectrum in Figure A2.1 is of the crude material, it is difficult to accurately assign each peak with appropriate integrations; however by comparing with literature, some assumptions were made as to where certain peaks will be found.

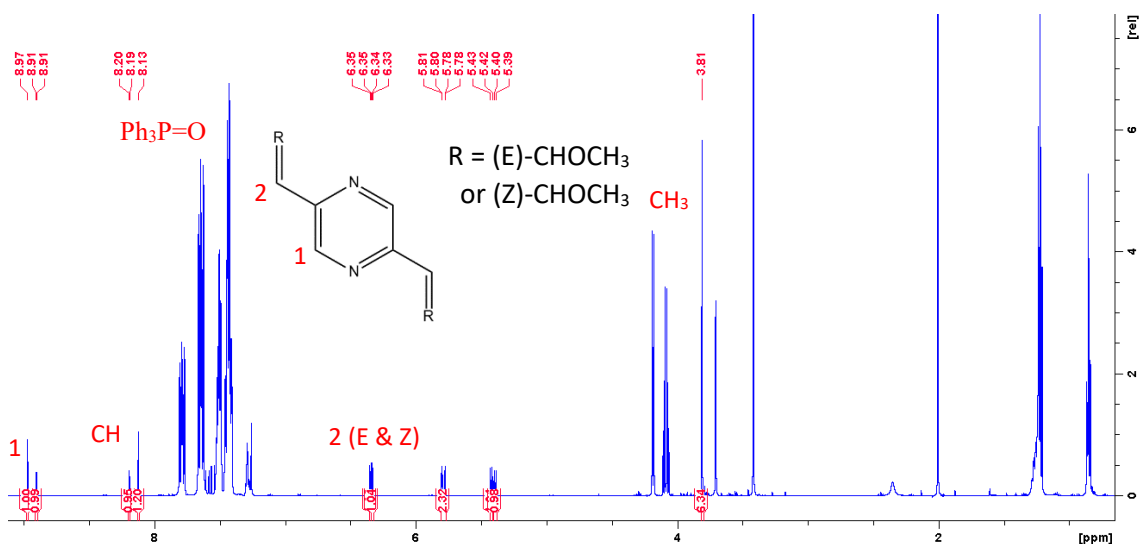
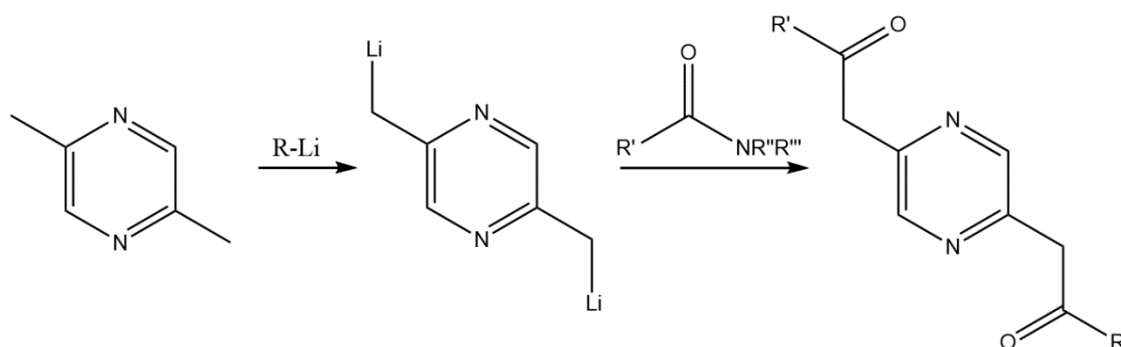


Figure A2.1.  $^1\text{H}$  NMR spectrum of pyrazine dimethoxyvinyl ether crude product ( $\text{CDCl}_3$ ).

Both the pyrazine and benzene methoxyvinyl derivatives were subjected to acidic hydrolysis with formic acid of varying concentrations in an effort to produce the respective pyrazine and benzene acetaldehyde and diacetaldehyde counterparts. Although Zaytsev *et al.* stated that this produced the benzene ethyl aldehyde species,  $^1\text{H}$  NMR spectroscopy suggested this was unsuccessful.<sup>88</sup> It was also shown by Campe *et al.* that highly energetic acidic hydrolysis conditions (perchloric acid in moist ether, perchloric acid in DME/water, sulfuric acid in acetone/water or oxalic acid in DME/water under

reflux) were not effective in hydrolysing 1,4-(dimethoxyvinyl)benzene.<sup>87</sup> Instead harsher conditions (refluxing THF/H<sub>2</sub>O with mercuric acetate) were necessary for the successful conversion. Due to the toxic nature of mercuric acetate, this step was not attempted and this synthetic route for synthesising pyrazine-2,5-diacetaldehyde was abandoned for another simpler and safer route.

An alternative approach involves the deprotonation of the  $\alpha$ -methyl group in 2,5-dimethylpyrazine (step x in Scheme A2.1).<sup>70,120,121</sup> The reaction typically involves lithiation at -78 °C with an organolithium reagent such as *n*-butyllithium (*n*-BuLi) or lithium diisopropylamide (LDA), followed by addition of a suitable electrophile such as DMF.<sup>122,123</sup> Unfortunately, this method provides a potential drawback of over-addition, which could lead to problems during the workup process. As indicated, the addition of a stoichiometric amount of an organometallic reagent (to the amide) will result in the formation of the desired carbonyl functionality. Addition of an excess of an organometallic reagent will likely further react with the carbonyl species (as opposed to the amide functionality as carbonyls are more reactive than amides), producing a tertiary alcohol in place of a carbonyl.<sup>124</sup> Assuming that the required organometallic reagent is added precisely within a carefully controlled environment; this approach, if successful, will yield the desired pyrazine-2,5-diacetaldehyde species in a two-step one-pot reaction (see Scheme A2.4).



Scheme A2.4. Reaction scheme for the lithiation and electrophilic substitution of an amide on 2,5-dimethylpyrazine.

The lithiation and addition of DMF has not been reported on a pyrazine system, but it has been achieved on 2-picoline (2-methylpyridine).<sup>119</sup> This was sufficient precedent to try it on our system.<sup>121</sup> Unfortunately the majority of literature discussing the lithiation and electrophilic substitution of amides on these systems targeted the formation of ketone species ( $R' \neq H$ )<sup>89,123,125</sup>, with only a select few papers synthesising the aldehyde counterpart ( $R' = H$ ).<sup>123</sup>

Adapting the method provided by Guimond *et al.* who successfully formed 2-(pyridin-2-yl)propanal from 2-methylpyridine should lead to the desired dialdehyde product.<sup>89</sup> Initial attempts tried to make the aldehyde by treating 2,5-dimethylpyrazine in THF at -78 °C with an organolithium reagent under an inert atmosphere. This mixture was stirred for two hours, followed by the addition of DMF. Both *n*-BuLi (step x. in Scheme A2.1) and LDA (step xi. in Scheme A2.1) were investigated, but only *n*-BuLi showed any signs of success. The crude product was characterised using <sup>1</sup>H NMR spectroscopy (Figure A2.2) and mass spectrometry (Figure AS.10), indicating that the product may have been formed in the reaction, but it required purification. As Figure A2.2 shows the <sup>1</sup>H NMR spectrum of the crude **A2** which could not be purified, it is difficult to assign each peak accurately

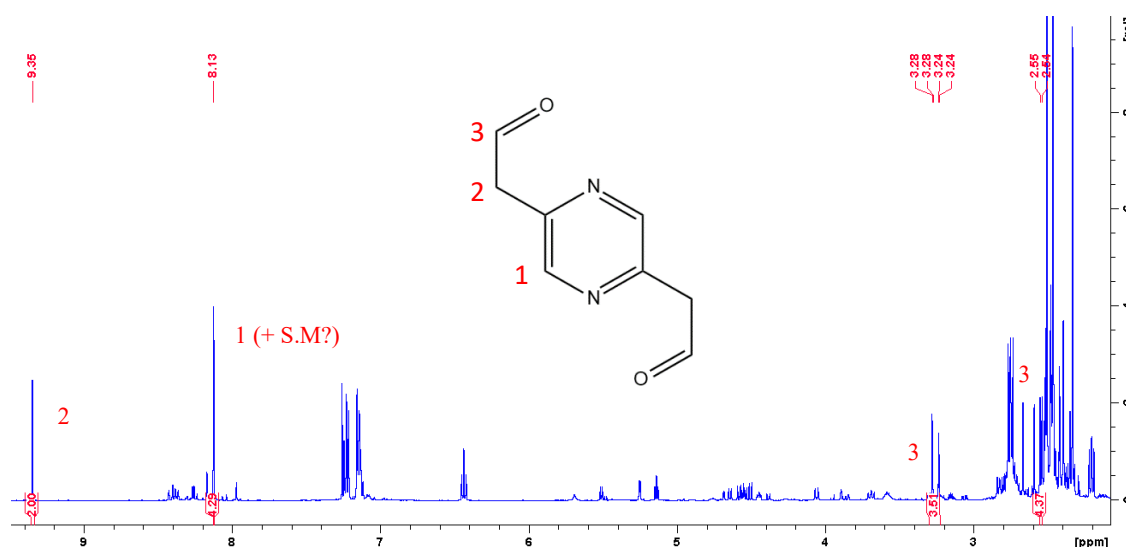
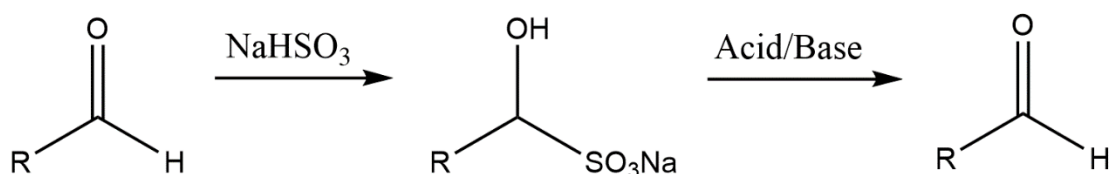


Figure A2.2. <sup>1</sup>H NMR spectrum of the crude product obtained from the lithiation with *n*-BuLi and electrophilic substitution with DMF, possibly containing 2,5-pyrazinediacetaldehyde, with assigned peaks (CDCl<sub>3</sub>). S.M = starting material (2,5-dimethylpyrazine).

with appropriate integrations, however by comparing with literature, some assumptions were made as to where certain peaks may be found.

An attempt was made to purify the aldehyde by formation of a bisulfite adduct of the aldehyde with sodium bisulfite ( $\text{NaHSO}_3$ ).<sup>126,127</sup> This should allow the organic molecule to enter the aqueous layer. the bisulfite adduct can then be hydrolysed and the aldehyde regenerated upon exposure to acidic or basic conditions (see Scheme A2.5).<sup>126</sup>



Scheme A2.5. General reaction scheme for the formation of a bisulfite adduct of an aldehyde, followed by the hydrolysis back into the desired aldehyde compound.

The procedure used is an adaptation of the method by Kjell *et al.* where the mixture of the aldehyde species and  $\text{NaHSO}_3$  was stirred in EtOAc for 2.5 hours at 40 °C.<sup>126</sup> Due to the similar chemical structure of this new dialdehyde with the previous dialdehyde (**A1**), pyrazine-2,5-diacetaldehyde (**A2**) was assumed to have the same degradation properties, so the reaction was attempted at room temperature. This attempt to purify **A2** was unsuccessful.



## A2.2 Synthesis of 2,5-pyrazinyldiacetone (**K1**)

Due to the failed isolation of the dialdehyde species, the synthesis of 2,5-pyrazinyldiacetone (**K1**) was attempted. The reaction was conducted similar to that of **A2** whereby 2,5-dimethylpyrazine in dry THF was first lithiated, by LDA then subjected to *N,N*-dimethylacetamide, according to a modification of the method of Paine *et al.*<sup>125</sup> The reaction produced a dark red mixture, which upon working up produced a brown oily product. <sup>1</sup>H NMR (Figure A2.3) spectroscopy of the crude mixture indicated that the desired product may have been formed, however attempts to purify the product were not attempted. This was due to the purification method provided by Paine *et al.* potentially being too harsh for **K1** (silica gel chromatography, followed by a distillation above 60 °C).

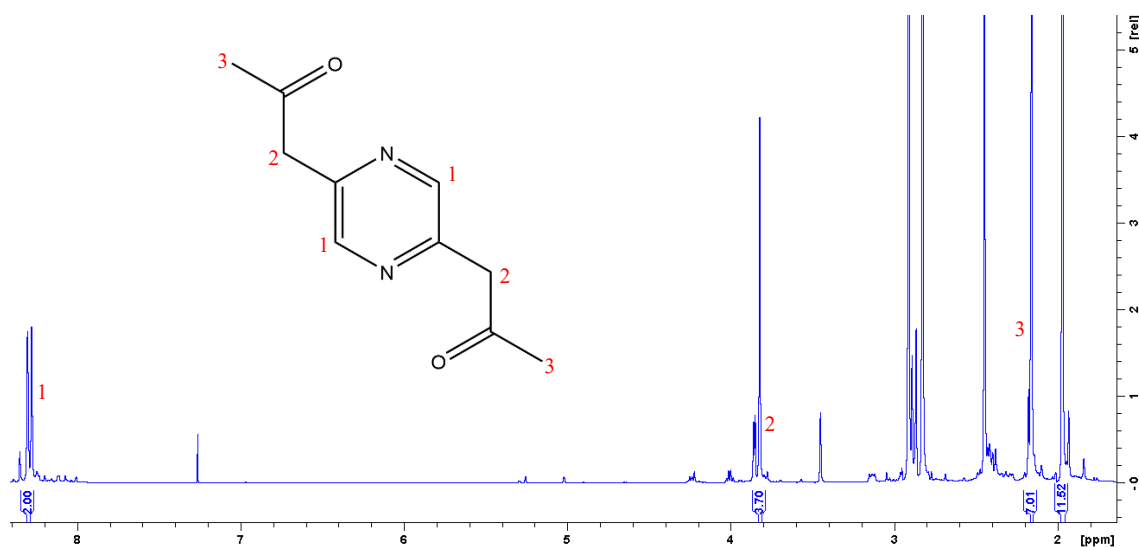
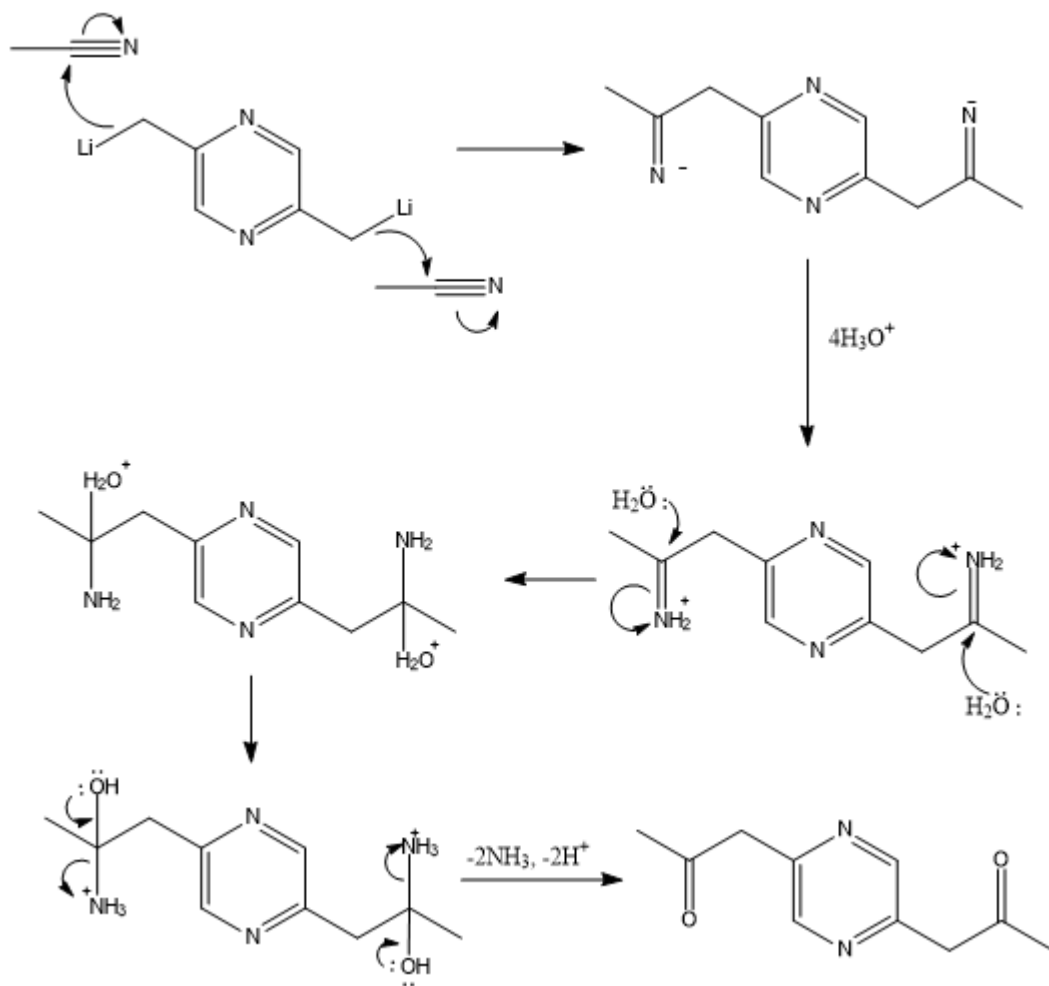


Figure A2.3. <sup>1</sup>H NMR spectrum of the crude 2,5-pyrazinyldiacetone (**K1**) obtained from the procedure by Paine *et al.* with assigned peaks (CDCl<sub>3</sub>).

Another attempt was made to synthesise the desired diketone species following the method of Bai *et al.* who successfully synthesised 1-(2-pyridinyl)-2-propanone from 2-methylpyridine.<sup>117</sup> This was achieved by the base-promoted condensation of methyl-heterocycles with a nitrile compound, followed by acidic hydrolysis (see Scheme A2.6).<sup>117</sup> In this case, the base used was *n*-BuLi, the nitrile used was acetonitrile (dry) and the acid used for the acidic hydrolysis was sulfuric acid (40 % in water). The <sup>1</sup>H NMR spectrum of the crude reaction mixture indicated the product may have been formed as it is similar to the <sup>1</sup>H NMR spectrum of the previous attempt. (Figure A2.4).<sup>117</sup> Bai *et al.* indicated that the crude 1-(2-pyridinyl)-2-propanone product was recrystallized by reduced pressure distillation. This route would not be a first choice in the purification of



Scheme A2.6. Mechanism for the base-promoted condensation of 2,5-dimethylpyrazine with MeCN.

the pyrazine derivative due to the potential degradation caused by high temperatures. Due to time constraints, no attempts were made at the purification of the crude product.

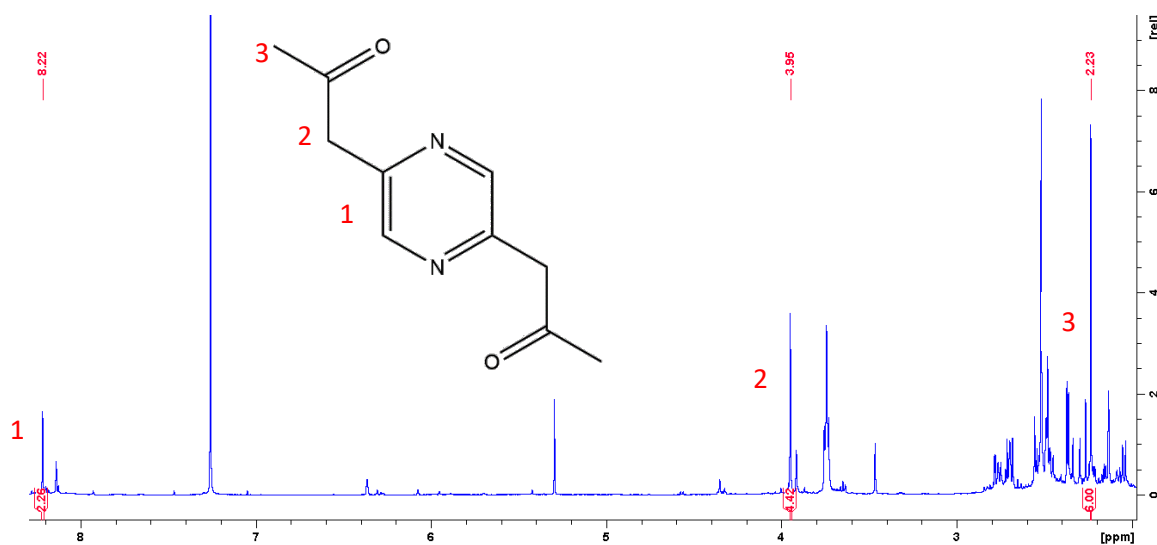
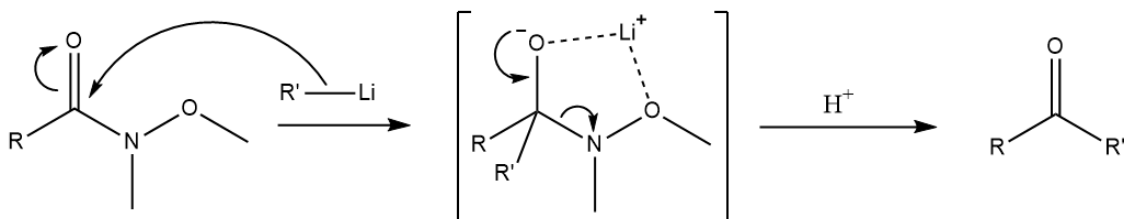


Figure A2.4.  $^1\text{H}$  NMR spectrum of 2,5-pyrazinyldiacetone from the base-promoted condensation of 2,5-dimethylpyrazine with MeCN, with assigned peaks ( $\text{CDCl}_3$ ).

### A2.3 Future work

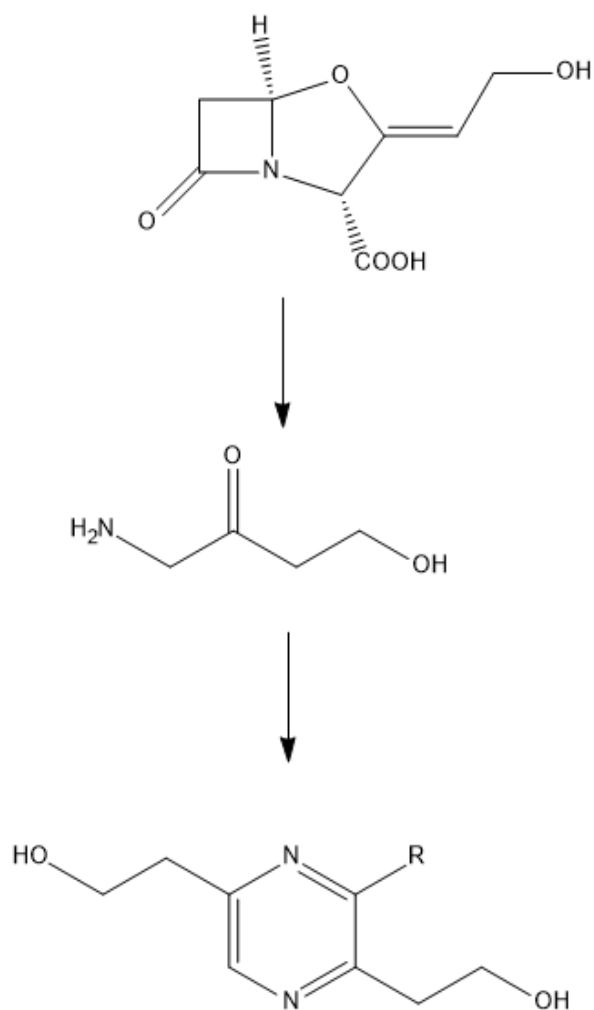
As this aspect of the project (Sections 3.3 and 3.4) wasn't investigated until the closing months, there are still plenty of alternative purification and synthetic methods to consider in regards to the synthesis of **A2** and **K1**. Another method that would have been investigated if time had allowed would have been to substitute *N,N*-dimethylacetamide with a Weinreb amide (left structure on Scheme A2.7). First reported in 1981 by Weinreb and Nahm<sup>124</sup>, *N*-methoxy-*N*-methylamides structurally resemble *N,N*-dimethylacetamide, however introduce a methoxy group in place of the methyl group. Several Weinreb amides are commercially available, whereas others can be synthesised by various routes.<sup>124,128-131</sup> Treatment of these species with organometallic reagents will result in the formation of a tetrahedral intermediate, which is stabilised by the chelation of the metal ion to the methoxy group (middle structure in Scheme A2.7). The formation of the tetrahedral intermediate prevents the issue of over-addition (as mentioned previously). Quenching with acid at low temperatures can result in the formation of the aldehyde or

ketone species (right structure in Scheme A2.7), which can then be extracted with an organic solvent.<sup>131</sup>



Scheme A2.7. Mechanism for the formation of the stable tetrahedral intermediate and the desired carbonyl product brought on by the addition of an organolithium reagent to a Weinreb amide. R is typically exhibited as an alkyl chain. R' = alkyl chain.

Another potential route that would have been pursued if time had allowed would be to start from clavulanic acid, a natural compound produced from the bacteria *Streptomyces clavuligerus*.<sup>132,133</sup> The hydrolysis (under neutral or basic conditions<sup>133</sup>) of clavulanic acid (and potassium clavulanate) causes the acid to decompose into the reactive intermediate 1-amino-2-oxo-butan-4-ol (Scheme A2.8), leading to the formation of an additional three major decomposition products (as observed by high performance liquid chromatography, HPLC).<sup>133-137</sup> Compound **CA3** closely resembles the diol species reported by Das *et al.*, indicating that by exposing 2,5-di(hydroxyethyl)pyrazine (**CA3** in Scheme A2.8) to similar oxidation conditions used to oxidise di(hydroxymethyl)pyrazine (fourth step in the red procedure in Scheme 3.1) by Das *et al.* (activated MnO<sub>2</sub> in dry 1,4-dioxane) could potentially yield the desired pyrazine-2,5-diacetaldehyde.



R = H (**CA1**), CH<sub>2</sub>CH<sub>3</sub> (**CA2**), CH<sub>2</sub>CH<sub>2</sub>COOH (**CA3**)

Scheme A2.8. Clavulanic acid (top structure) and its degradation products.

#### A2.4 Summary

Unfortunately, the synthesis of pure **A2** was unsuccessful; however, <sup>1</sup>H NMR spectroscopy and mass spectrometry both indicated that the desired product was likely present within the crude material. Several methods of purification were trialled, but proved to be fruitless. Focus was shifted towards the synthesis of **K1**, which <sup>1</sup>H NMR spectroscopy and mass spectrometry indicated the product was likely formed. Purification attempts on **K1** also yielded no significant results. There are still many paths to explore to purify both **A2** and **K1**, which would have been explored if not for time constraints.

### A3.1 Experimental generic description

#### A3.1.1 Reagents and solvents

Unless otherwise stated, all reagents were purchased from commercial sources with no further purification prior to use. Solvents used in the reactions were of high quality (typically analytical grade). If a solvent was stated as dry, they were further purified with the following procedure: THF and DCM were passed through an alumina column on an in-house solvent purification system and placed into a Schott bottle with dried 3 Å molecular sieves, MeCN was stored in an argon-flushed Schott bottle with dried 3 Å molecular sieves. The 3 Å molecular sieves were dried in a muffle furnace at 650 °C overnight.

#### A3.1.2 Synthetic methods

All reactions were carried out in water- and acetone-washed, oven dried glassware under atmosphere (unless stated otherwise) with magnetic stirring. Solvents that were removed or concentrated under reduced pressure was performed with a rotary evaporator.

Microwave synthesis was performed on the CEM Discovery monomode, model: explorer, operating at 100 Watts. Each reaction was magnetically stirred in the apparatus with no set pressure.

Ozonolysis was performed on the CD10/AD Corona Discharge Ozone Generator. The generation of ozone was set at the maximum that the apparatus can produce (1.3 g hr<sup>-1</sup>).

Column chromatography was carried out on silica gel (grade 60, mesh size 230 – 400, Scharlau).

#### A3.1.3 Characterisation methods

All new compounds were characterised by <sup>1</sup>H, <sup>13</sup>C NMR spectroscopy, mass spectrometry, ATR-IR spectroscopy, UV-visible spectroscopy, determination of melting

point, elemental analysis and SCXRD (if suitable crystals of the complex can be grown). Complexes were also further characterised by conductivity measurements to determine the quantity of electrolytes present. For complexes that produced reasonable data from SCXRD, these were further characterised by thermogravimetric analysis (TGA) and cyclic voltammetry (CV).

$^1\text{H}$  and  $^{13}\text{C}$  NMR spectroscopy work was performed on the Bruker Avance 400 and 500 MHz NMR spectrometers. The NMR spectrometer used is specified for each compound. All spectra were reported with residue solvent as the standard.

Mass spectra and high resolution mass spectrometry were performed at Massey University, using a ThermoScientific Q Exactive Focus Hybrid Quadrupole-Orbitrap Mass Spectrometer. The samples were run in positive and negative mode (the charge is specified for each compound).

The Campbell Microanalytical Laboratory, University of Otago, provided elemental analysis by CHN analysis. This characterisation technique determines the composition of a compound by converting organic compounds into gaseous molecules through high temperature decomposition. A common variation of this allows the determination of the carbon, hydrogen and nitrogen composition in a compound, referred to as CHN analysis.<sup>20</sup>

All UV-Vis spectra were collected on a Shimadzu UV-3101PC spectrophotometer using UV Probe v1.1.

Melting points were recorded on a Gallenkamp melting point apparatus and are uncorrected.

Conductivity measurements were run on a Philips PW9509 conductivity meter. The following settings were imposed on the conductivity meter: frequency (Hz) = 2,000, MTC depression, cell constant = 3, coefficient % ( $^{\circ}\text{C}^{-1}$ ) = 2.50, temperature ( $^{\circ}\text{C}$ ) = 20.0.

Samples were dissolved in A.R grade acetonitrile.  $\kappa_s$  values were recorded with A.R grade dry acetonitrile prior to analysis of the sample.

X-ray of **L3** crystals were covered in inert oil and suitable single crystals were selected under a microscope and mounted on an Agilent SuperNova diffractometer fitted with an EOS S2 detector. Data were collected at the temperature indicated using focused microsource Cu K $\alpha$  radiation at 1.54184 Å. The structure was solved with SHELXS and refined with SHELXL-97, implemented within Olex2 program.<sup>138</sup>

X-ray data for **C3A** was collected at reduced temperature (-150 °C) on a Rigaku Spider diffractometer equipped with a copper rotating anode X – ray source and a curved image plate detector. The crystals were mounted in an inert oil and transferred into the cold gas stream of the detector and irradiated with graphite monochromated Cu K $\alpha$  ( $\lambda = 1.54178$  Å) X – rays. The data was collected by the CrystalClear program (v.1.4.0) and processed with FS-PROCESS to apply the Lorentz and polarisation corrections to the diffraction spots (integrated 3 dimensionally). The structures were solved by direct methods SHELXS-13 and refined using the SHELXL-13 as implemented in the Olex2 program.<sup>138</sup>

Absorption data scalings corrections were carried out using multiscan. Hydrogens were calculated at their ideal positions unless otherwise stated. Due to the quality of the data obtained, samples of **C3A** were sent to Australian Synchrotron, Victoria, Australia for further analysis.

Crystals of both **C3A** and **C3B** were harvested with a 0.20 mm nylon loop and flash-cooled in liquid nitrogen. Diffraction data was collected at 110 K on the MX2 beamline at the Australian Synchrotron, Victoria, Australia at a wavelength of 0.7093 Å. The dataset was processed and evaluated using XDS.<sup>139</sup> The resulting reflections were scaled using AIMLESS<sup>140</sup> from the CCP4 program suite.<sup>141</sup> The structures were solved by direct methods SHELXS-13 and refined using the SHELXL-13 as implemented in the Olex2



program.<sup>138</sup> Absorption data scalings corrections were carried out using multiscan. Hydrogens were calculated at their ideal positions unless otherwise stated.

Thermogravimetric analysis (TGA) was performed on a Q50 TGA apparatus. The apparatus was operated with the TA Instruments Universal Analysis 2000 software. This technique measures the change in mass of a substance whilst exposed to varying or a set temperature.<sup>20</sup> This is achieved with the use of a temperature programmable furnace, a microbalance and a controller (collectively known as the thermobalance). The sample (which is weighed in a sample holder) is suspended in a furnace, where the temperature in the furnace can be controlled. Various modifications can also be put in place to monitor specific processes, including controlling the atmosphere within the furnace (inert or non-inert, static or flowing atmosphere).<sup>20</sup> The advantage of using a flowing atmosphere is that any volatile or corrosive species will be carried away, and it prevents the condensation of the material. This all allows TGA to be used to analyse desorption, decomposition, dehydration and oxidation processes.<sup>20</sup>

Cyclic voltammetry (CV) analysis was performed on a Autolab Potentiostat Galvanostat 30. The software used to operate this apparatus is Metrohm Autolab B.V. NOVA 2.1.2. A linear scan was chosen as the method to perform the CV scan of the compounds. The working and counter electrodes used for analysis were polished with Struers DP-Suspension, M and water prior to any analysis. The three-electrode electrochemical cell was set up, where ten scans ( $0.2 \text{ V s}^{-1}$ ) were performed on a solution of MeCN between 3 and -3 V. This was done to remove any chemically reversible species off of the electrodes. Samples were flushed with argon prior to any analysis.

### A3.2 X-Ray crystallography

**L3:** Single crystals of  $C_{20}HN_6$  were obtained by hot recrystallisation of **L3** in MeCN. A suitable crystal was selected and mounted on a SuperNova, Dual, Cu at zero, EosS2 diffractometer. The crystal was kept at 120.00(10) K during data collection. Using Olex2<sup>138</sup>, the structure was solved with the SIR2004<sup>142</sup> structure solution program using Direct Methods and refined with the ShelXL<sup>143</sup> refinement package using Least Squares minimisation.

**C3A:** Single crystals of  $C_{20}H_{20}N_6O_6Cl_{1.5}Co$  were obtained by diffusion of diethyl ether into an acetonitrile solution containing the complex. A suitable crystal was selected and mounted on a filament and analysed with the MX1 diffractometer. The crystal was kept at 100 K during data collection. Using Olex2<sup>138</sup>, the structure was solved with the ShelXS<sup>142</sup> structure solution program using Direct Methods and refined with the ShelXL<sup>143</sup> refinement package using Least Squares minimisation.

**C3B:** Single crystals of  $C_{20}H_{20}N_6O_{4.5}Cl_{1.5}Mn$  were obtained by diffusion of diethyl ether into an acetonitrile solution containing the complex. A suitable crystal was selected and mounted on a filament and analysed with the MX1 diffractometer. The crystal was kept at 100 K during data collection. Using Olex2<sup>138</sup>, the structure was solved with the Superflip<sup>142</sup> structure solution program using Charge Flipping and refined with the ShelXL<sup>143</sup> refinement package using Least Squares minimisation.

Table A3.1. X-Ray data of crystals obtained for L3, C3A and C3B

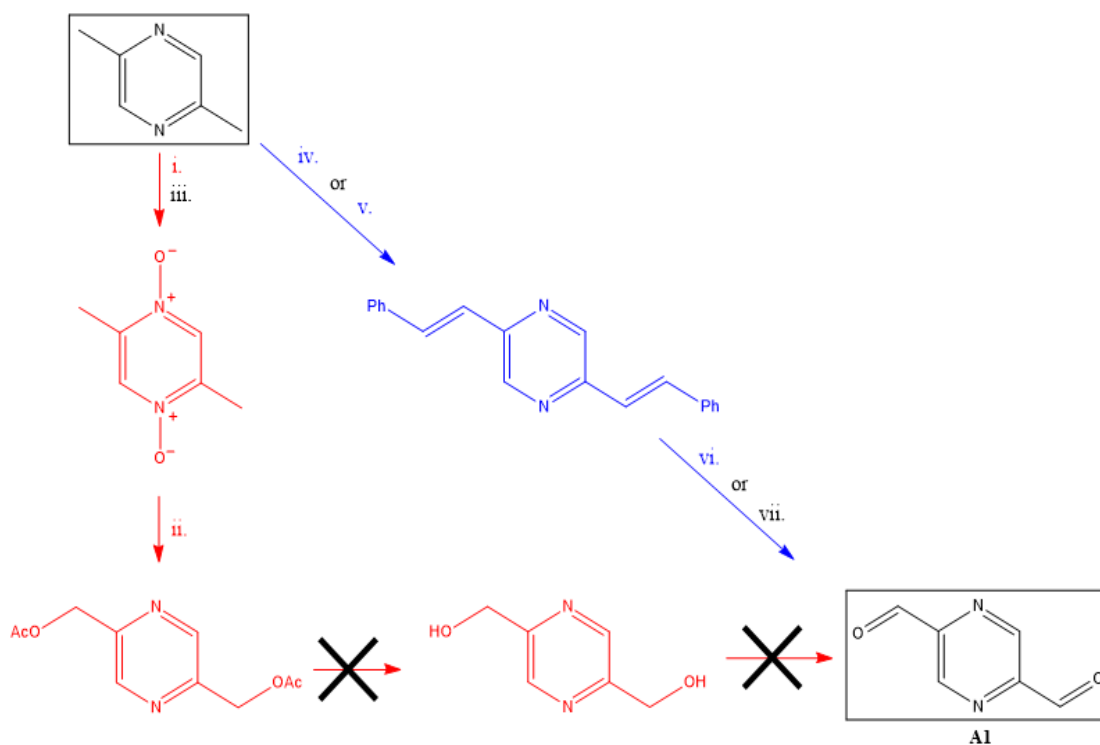
	L3	C3A	C3B
Empirical Formula	C <sub>20</sub> HN <sub>6</sub>	C <sub>20</sub> H <sub>20</sub> N <sub>6</sub> O <sub>6</sub> Cl <sub>1.5</sub> Co	C <sub>20</sub> H <sub>20</sub> N <sub>6</sub> O <sub>4.5</sub> Cl <sub>1.5</sub> Mn
Formula Weight	344.42	552.52	524.53
Temperature/K	120.00(10)	100	100
Crystal System	Monoclinic	Trigonal	Trigonal
Space Group	P2 <sub>1</sub> /c	R-3c	R-3c
a/Å	6.0968(2)	25.397(4)	25.397(4)
b/Å	4.60769(17)	25.397(4)	25.397(4)
c/Å	31.7665(12)	45.748(9)	45.748(9)
α/°	90	90	90
β/°	93.622(3)	90	90
γ/°	90	120	120
Volume/Å <sup>3</sup>	890.61(6)	25554(9)	25554(9)
Z	2	12	12
ρ <sub>calc</sub> /cm <sup>3</sup>	1.2843	0.431	0.409
μ/mm <sup>-1</sup>	0.640	0.262	0.213
F(000)	365.1	3390.0	3222.0
Crystal size/mm <sup>3</sup>	0.149 × 0.136 × 0.046	0.02 × 0.005 × 0.003	0.15 × 0.12 × 0.1
Radiation	Cu Kα (λ = 1.54184)	MoKα (λ = 0.71073)	MoKα (λ = 0.71073)
2θ range for data collection/°	11.16 to 130.14	5.342 to 52.598	5.342 to 52.734
Index Ranges	-4 ≤ h ≤ 7, - 5 ≤ k ≤ 5, - 39 ≤ l ≤ 39	-31 ≤ h ≤ 31, -31 ≤ k ≤ 31, -55 ≤ l ≤ 55	-33 ≤ h ≤ 33, -33 ≤ k ≤ 33, -60 ≤ l ≤ 60
Reflections Collected	4609	56618	136144
Independent Reflections	1511 [R <sub>int</sub> = 0.0280, R <sub>sigma</sub> = 0.0293]	5526 [R <sub>int</sub> = 0.0694, R <sub>sigma</sub> = 0.0385]	5674 [R <sub>int</sub> = 0.0720, R <sub>sigma</sub> = 0.0236]
Data/restraints/parameters	1511/0/118	5526/214/427	5674/198/428
Goodness-of-fit on F <sup>2</sup>	2.933	1.071	1.079
Final R indexes [I ≥ 2σ (I)]	R <sub>1</sub> = 0.1467, wR <sub>2</sub> = 0.5493	R <sub>1</sub> = 0.0495, wR <sub>2</sub> = 0.1426	R <sub>1</sub> = 0.0379, wR <sub>2</sub> = 0.1071
Final R indexes [all data]	R <sub>1</sub> = 0.1525, wR <sub>2</sub> = 0.5507	R <sub>1</sub> = 0.0585, wR <sub>2</sub> = 0.1503	R <sub>1</sub> = 0.0400, wR <sub>2</sub> = 0.1092
Largest diff. peak/hole / e Å <sup>-3</sup>	0.70/-0.83	0.45/-0.34	0.40/-0.45

## Appendix 4 Synthetic Methods

The following section describes the synthetic methods used to make certain compounds.

Compounds that were deemed as significantly pure by  $^1\text{H}$  NMR spectroscopy are discussed in this section. These compounds include the synthesis of the precursors to synthesising **A1**, **A1**, ligands **H<sub>2</sub>L1**, **L2** and **L3** and the *N*-Boc protection of 2-aminoethanol and 2-aminophenol (steps i, ii and iv in Scheme A1.1). Compounds that were not chemically pure (as determined by  $^1\text{H}$  NMR spectroscopy) are not mentioned in this section. Compounds included here include **A2**, **K1** and ligands **L4** – **7**, as well as any precursors or reagents to synthesising these compounds not previously mentioned. Complexations that were attempted with **H<sub>2</sub>L1**, **L2** or **L3** are discussed in this chapter. This will include both the characterised and non-characterised complexations attempted with ligands **H<sub>2</sub>L1**, **L2** and **L3**.

### A4.1 Synthesis of **A1** and precursors to **A1**

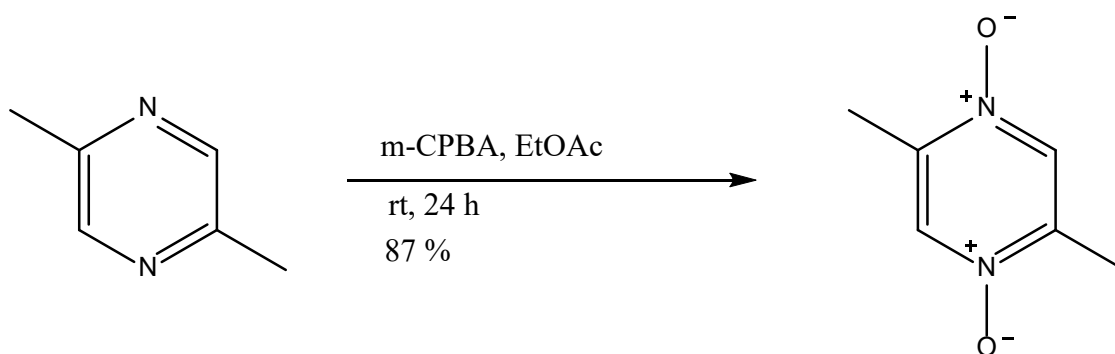


Scheme 3.1. Synthetic scheme for the synthesis of pyrazine-2,5-dicarbaldehyde (**A1**): (i) *m*-CPBA, rt, 24 h, 87 %. (ii)  $\text{Ac}_2\text{O}$ , 158 °C, 7 h, rt, 12 o/n, 15 %. (iii) glacial  $\text{CH}_3\text{COOH}$ , 30%  $\text{H}_2\text{O}_2$ , 95 °C, 24 hr, 20 %. (iv) Benzaldehyde, benzoic anhydride, reflux, 175 °C, 4 d, 54 %. (v) Benzaldehyde, benzoic anhydride, M.W., 175 °C, 6 h, 62 %. (vi)  $\text{OsO}_4$ ,  $\text{NaIO}_4$ , rt, 2-3 d, 25 %. (vii)  $\text{O}_3$ , -50 °C, 3 – 4 h, 30 %. The red scheme indicates the method by Das *et al.*, the blue scheme shows the method by Coufal *et al.*, and the black roman numerals indicate alternative reaction routes.

#### A4.1.1 2,5-dimethyl-1,4-dioxidepyrazine

##### Route 1

Prepared as per the method of Das *et al.* (step i in Scheme 3.1).<sup>85</sup>



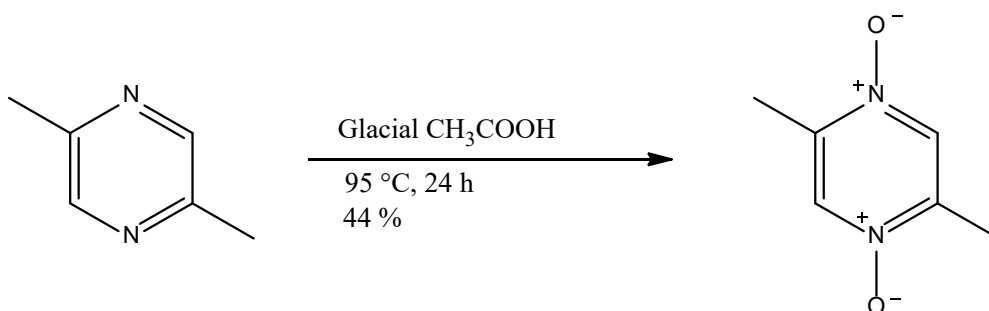
m-CPBA ( $\leq 77$  % in H<sub>2</sub>O; 50.02 g, 289.8 mmol, 3.1 eq) was suspended in EtOAc (75 mL) and washed with brine (1 x 75 mL) prior to the reaction. The organic layer was separated, dried (MgSO<sub>4</sub>) and filtered. The filtrate was added to 2,5-dimethylpyrazine (10.00 g, 10.10 mL, 46.2 mmol, 1.0 eq) in EtOAc (25 mL). The solution was stirred at room temperature for 24 hours. The resulting white precipitate was filtered and washed with EtOAc (3 x 100 mL), yielding 2,5-dimethyl-1,4-dioxidepyrazine as a white solid (11.22 g, 80.1 mmol, 87 %).  $\delta$ H (500 MHz; D<sub>2</sub>O; solvent):  $\delta$  8.50 (2H, s, pz), 2.45 (6H, s, CH<sub>3</sub>).

Data is comparable to that reported in the literature.<sup>85</sup>

The assigned <sup>1</sup>H NMR spectrum can be found in section 3.2.1 (Figure 3.1 – the top spectrum).

## Route 2

Prepared as per the method by Klein *et al.* (step iii in Scheme 3.1).<sup>90</sup>



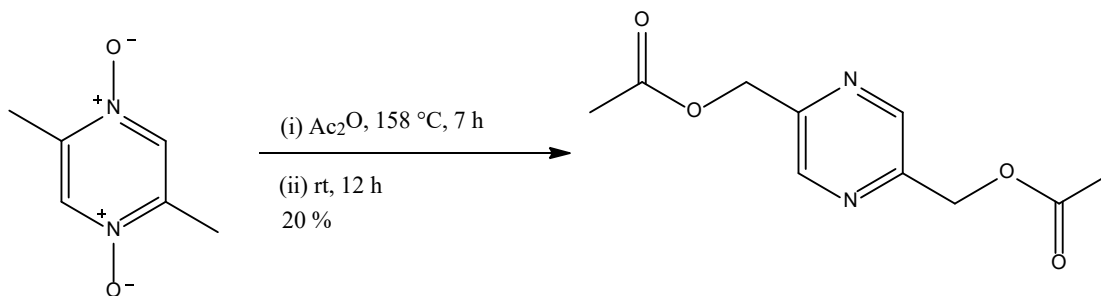
Glacial acetic acid (10.47 mL, 183.10 mmol, 10.0 eq) was added to 2,5-dimethylpyrazine (1.98 g, 2.00 mL, 18.3 mmol, 1.0 eq). Hydrogen peroxide (30 % in H<sub>2</sub>O, 1.72 mL, 73.2 mmol, 4.0 eq) was added to the reaction mixture in two portions (0.86 mL each portion) over 24 hours. The mixture was stirred and heated at 95 °C for 24 hours. The solution was then concentrated under reduced pressure to roughly one-third the original volume (~5 mL) and diluted with an equal volume of cold water. The solution was basified with NaOH (1 M) and extracted with CHCl<sub>3</sub> (3 x 20 mL). The organic layers were combined, dried (MgSO<sub>4</sub>), and filtered. The solvent was removed under reduced pressure to give a white solid, 2,5-dimethyl-1,4-dioxopyrazine (1.12 g, 8.0 mmol, 43.6 %). As the obtained product was sufficiently pure for the following reaction, further purification of this product was not performed.  $\delta$ H (500 MHz; D<sub>2</sub>O; solvent):  $\delta$  8.50 (2H, s, pz), 2.44 (6H, s, CH<sub>3</sub>).

Data is comparable to that reported in the literature.<sup>90</sup>

The assigned <sup>1</sup>H NMR spectrum can be found in section 3.2.1 (Figure 3.1 – the bottom spectrum).

#### A4.1.2 2,5-di(acetoxymethyl)pyrazine

Prepared as per the method of Das *et al.* (step ii in Scheme 3.1).<sup>85</sup>



A suspension of 2,5-dimethyl-1,4-dioxopyrazine (11.22 g, 80.1 mmol, 1.0 eq) in acetic anhydride (60 mL) was refluxed at 158 °C for 7 hours. The heating was reduced and the mixture was stirred at RT for a further 12 hours. Acetic anhydride was then removed under reduced pressure, giving a black residue. Et<sub>2</sub>O (12.5 mL) was added to the residue and stirred vigorously at room temperature for 2 hrs. The mixture was filtered and washed with Et<sub>2</sub>O (60mL). The filtrate was concentrated under reduced pressure, yielding a crude yellow solid (3.50 g, 15.6 mmol, 19.5 %). Silica gel column chromatography (40 % EtOAc in *n*-hexane) of the crude product gave a yellow solid, which was recrystallized from 40 % EtOAc in *n*-hexane to give 2,5-di(acetoxymethyl)pyrazine as a white crystalline solid (3.50 g, 15.6 mmol, 19.5 %).  $\delta$ H (500 MHz; CDCl<sub>3</sub>; solvent):  $\delta$  8.62 (2H, s, pz), 5.26 (4 H, s, CH<sub>2</sub>), 2.16 (6H, s, CH<sub>3</sub>).

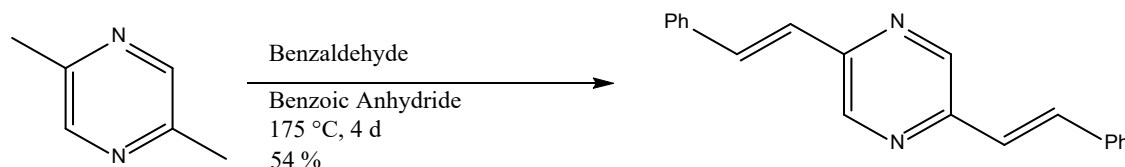
Data is comparable to that reported in the literature.<sup>85</sup>

The assigned <sup>1</sup>H NMR spectrum can be found in section 3.2.1 (Figure 3.2).

### A4.1.3 2,5-distyrylpyrazine

#### Route 1

Prepared as per the method by Coufal *et al.* (step iv in Scheme 3.1).<sup>5</sup>



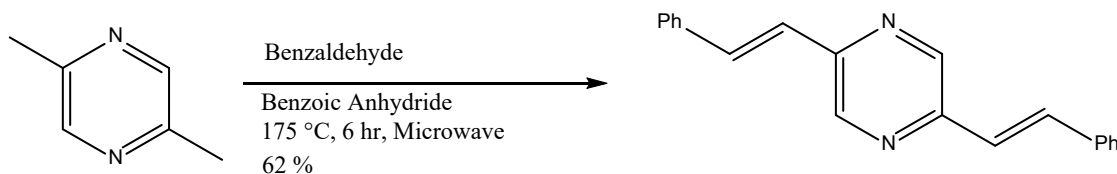
Benzaldehyde (60 mL) was washed with NaOH (1 M in H<sub>2</sub>O, 1 x 60 mL), then sat. Na<sub>2</sub>SO<sub>3</sub> (1 x 60 mL). The organic layer was collected, dried (MgSO<sub>4</sub>) and filtered. The filtrate was then vacuum distilled at 50 °C. A mixture of 2,5-dimethylpyrazine (5.00 g, 5.05 mL, 46.2 mmol, 1.0 eq), distilled benzaldehyde (21.10 g, 20.21 mL, 198.8 mmol, 4.3 eq) and benzoic anhydride (25.10 g, 111.0 mmol, 2.4 eq) was refluxed under argon at 175 °C for four days, whilst wrapped in tinfoil. The resulting brown mixture was left to cool to RT and suspended in ethanol (50 mL). The product was filtered and washed with EtOH (8 x 50 mL), yielding a yellow solid (7.08 g, 24.9 mmol, 53.8 %) The product obtained was sufficiently pure (by <sup>1</sup>H NMR) to proceed to the following reaction, therefore no further purification was performed.  $\delta$ H (500 MHz; CDCl<sub>3</sub>; solvent):  $\delta$  8.60 (2H, s, pz), 7.74 (2H, d, J = 16 Hz, CH), 7.63 - 7.59 (4H, m, ArH), 7.43 - 7.31 (6H, m, ArH), 7.19 (2H, d, J = 16 Hz, CH).

Data is comparable to that reported in the literature.<sup>5</sup>



## Route 2

Adapted from the method of Coufal *et al.* (step v in Scheme 3.1).<sup>5</sup>



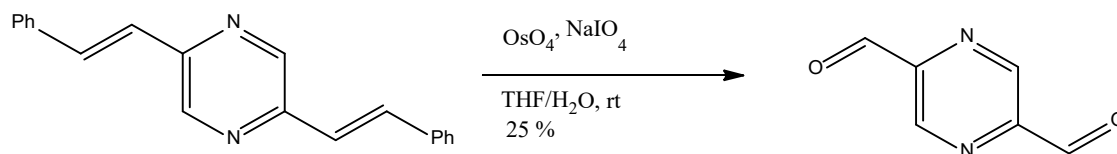
2,5-Dimethylpyrazine (0.99 g, 9.15 mmol, 1.0 eq), benzaldehyde (4.18 g, 4.00 mL, 39.4 mmol, 4.3 eq) and benzoic anhydride (4.97 g, 22.0 mmol, 2.4 eq) were placed in a 35 mL microwave tube. The mixture was stirred until all the benzoic anhydride dissolved. Argon was bubbled through the mixture for two minutes, then quickly sealed with the microwave tube lid. The yellow mixture was placed in the microwave and the temperature was maintained at 175 °C for 5 hrs, with high stirring and no set pressure. After this reaction time had passed, the dark brown solidified mixture was cooled to room temperature. The mixture was then suspended in ice cold EtOH (10 mL). The mixture was filtered and washed with ice cold EtOH (10 x 10 mL), yielding a yellow crystalline solid (1.61 g, 5.7 mmol, 62.0 %). The product obtained was sufficiently pure to proceed to the following reaction; therefore, no further purification was performed.  $\delta$ H (500 MHz; CDCl<sub>3</sub>; solvent):  $\delta$  8.60 (2H, s, pz), 7.74 (2H, d, J = 16 Hz, CH), 7.63 - 7.59 (4H, m, ArH), 7.43 - 7.31 (6H, m, ArH), 7.19 (2H, d, J = 16Hz, CH).

The assigned <sup>1</sup>H NMR spectrum can be found in the additional spectra section (Figure AS.1).

#### A4.1.4 Pyrazine-2,5-dicarbaldehyde (A1)

##### Route 1

Prepared as per the method by Coufal *et al.* (step vi in Scheme 3.1).<sup>5</sup>



2,5-(*E,E*)-Distyrylpyrazine (2.00 g, 7.0 mmol, 1.0 eq) and sodium periodate (15.04 g, 70.3 mmol, 10.0 eq) were suspended in a 2 : 1 THF : H<sub>2</sub>O (120 mL) mixture under argon. Osmium tetroxide (0.11 g, 0.4 mmol, 0.06 eq) in THF (0.50 mL) was added and stirred at room temperature until the fluorescence of 2,5-(*E,E*)-distyrylpyrazine disappeared by thin-layer chromatography (roughly two days). The orange/yellow mixture was filtered and washed with 2 : 1 THF : H<sub>2</sub>O (3 x 30 mL), yielding a white solid and a dark red filtrate. The filtrate was concentrated under reduced pressure, whilst maintaining the temperature below 40 °C. Once all the THF had been removed, the aqueous solution was then washed with Et<sub>2</sub>O (2 x 30 mL), removing any benzaldehyde and osmium tetroxide present. The aqueous layer was extracted with CHCl<sub>3</sub> (7 x 30 mL), CH<sub>2</sub>Cl<sub>2</sub> (4 x 30 mL) and EtOAc (1 x 30 mL). The organic layers were dried (MgSO<sub>4</sub>), filtered and evaporated under reduced pressure (whilst keeping temperatures below 40 °C); yielding the light brown pyrazine-2,5-dicarbaldehyde (0.24 g, 1.7 mmol, 24.8 %). The product was purified by a silica-gel chromatography (CH<sub>2</sub>Cl<sub>2</sub>) where the product was found at  $R_f = 0.27$ . The pure product was stored under nitrogen in a freezer.  $\delta$ H (500 MHz; CDCl<sub>3</sub>; solvent):  $\delta$  10.24 (2H, s, CHO), 9.31 (2H, s, pz).

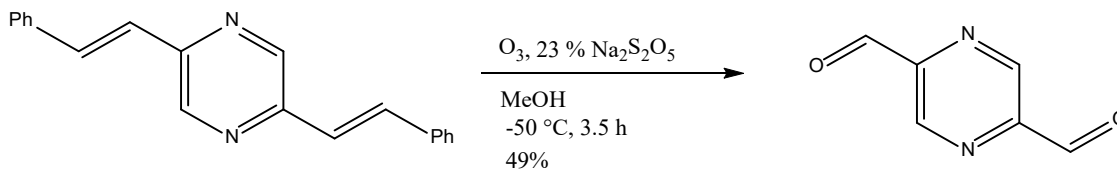
Data is comparable to that of literature.<sup>5</sup>

**Warning:** Osmium tetroxide is a toxic solid that sublimes at room temperature.

Appropriate care must be taken with use and storage of this compound.

## Route 2

Adapted from the method of Brooker *et al.*<sup>95</sup> and Hogue *et al.*<sup>1</sup> (step vii in Scheme 3.1).



2,5-Distyrylpyrazine (1.00 g, 3.5 mmol, 1.0 eq) was suspended in MeOH (200 mL) and the mixture cooled to - 50 °C in an diethylene glycol diethyl ether – dry ice bath. This temperature was maintained while ozone was bubbled through the mixture until the solution presented a pale blue colour of dissolved ozone (3.5 hrs). The excess of ozone was displaced by bubbling nitrogen through the solution until it became pale yellow. A solution of 23 % sodium meta-bisulfite in H<sub>2</sub>O (12 mL) was added dropwise. The mixture was warmed to room temperature whilst still under an argon atmosphere. The mixture was filtered and washed with MeOH (3 x 30 mL). The yellow filtrate was concentrated under reduced pressure at rt until an oily residue remained. Brine (45 mL) was added to the yellow oil and extracted with Et<sub>2</sub>O (3 x 150 mL) to remove the benzaldehyde by-product and the remaining MeOH. The aqueous layer was then extracted with CHCl<sub>3</sub> (4 x 30 mL). The organic extracts were combined, dried (MgSO<sub>4</sub>) and evaporated under reduced pressure at rt, yielding pyrazine-2,5-dicarbaldehyde (**A1**) as a yellow solid (0.24 g, 1.7 mmol, 49.0 %). No further purification was necessary.  $\delta$ H (500 MHz, CDCl<sub>3</sub>; solvent):  $\delta$  10.24 (2H, s, CHO),  $\delta$  9.31 (2H, s, pz).

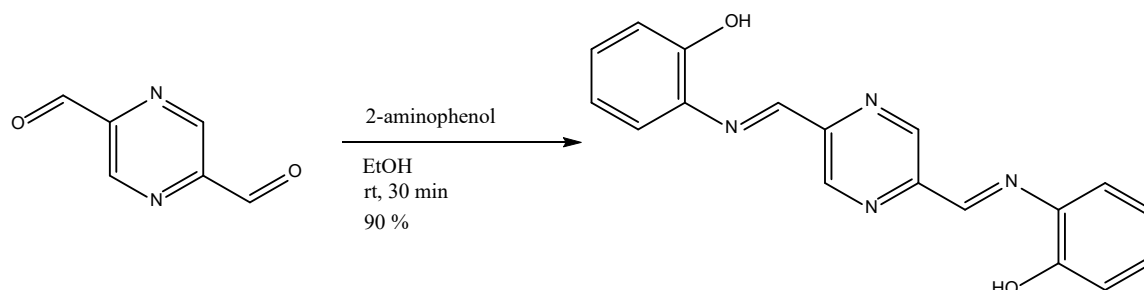
Data is comparable to that of literature.<sup>1</sup>

The assigned <sup>1</sup>H NMR spectrum can be found in section 3.2.3(Figure 3.3).

## A4.2 Synthesis of H<sub>2</sub>L1, L2 and L3

### A4.2.1 2,2'-[2,5-pyrazinediylbis(methyldynenitrilo)]bis(phenol) (H<sub>2</sub>L1)

Adapted from the method of Brooker *et al.*<sup>96</sup>



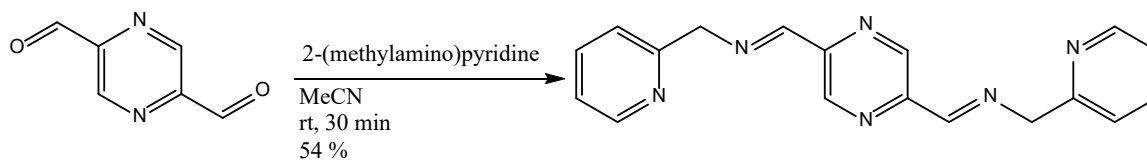
A solution of 2-aminophenol (140.4 mg, 1.3 mmol, 2.0 eq) was added to a stirred solution of pyrazine-2,5-dicarbaldehyde (86.3 mg, 0.6 mmol, 1.0 eq) in EtOH (10 mL) at room temperature. After 30 minutes, the mixture was left to stand for 3 hours at -5 °C. The precipitated solid was filtered and washed with ice cold EtOH, affording H<sub>2</sub>L1 as a yellow/orange solid (182.5 mg, 0.6 mmol, 90 %). mp 280 °C (from EtOH)<sup>d</sup>. Found C, 67.8; H, 4.4; N, 17.9 %. Calc. for C<sub>18</sub>H<sub>14</sub>N<sub>4</sub>O<sub>2</sub>: C, 67.9; H, 4.4; N, 17.6 %.  $\nu_{\max}/\text{cm}^{-1}$  3407 (w), 3073 (w), 1621 (m), 1596 (w), 1585 (w), 1494 (m), 1470 (m), 1351 (m), 1253 (m), 1244 (m), 1173 (m), 1151 (s), 1022 (m).  $\delta\text{H}$  (500 MHz; DMSO – d<sub>6</sub>; solvent) 9.70 (2H, s, imH), 9.38 (2H, brs, OH), 8.92 (2H, s pzH), 7.46 (2H, dd, J = 1.5, 7.9 Hz, ArH), 7.20 (2H, td, J = 1.6, 7.7 Hz, ArH), 6.96 (2H, dd, J = 1.3, 8.2 Hz, ArH), 6.89 (2H, td, J = 1.3, 7.6 Hz, ArH).  $\delta\text{C}$  (125.7 MHz; DMSO – d<sub>6</sub>; solvent) 156.6 (pzC), 152.5 (pzC), 149.9 (ArC), 143.2 (imC), 136.0 (ArC), 129.6 (ArC), 119.8 (ArC), 119.7 (ArC), 116.8 (ArC). m/z 319.1 (M<sup>+</sup>, 100%).

<sup>d</sup>: The sample decomposed at this temperature.

The assigned <sup>1</sup>H NMR spectrum can be found in section 4.4 (Figure 4.1 – the top spectrum). The assigned <sup>13</sup>C spectrum can be found in the additional spectra section (Figure AS.2).

#### A4.2.2 *N,N'*-(2,5-pyrazinediyl)dimethylidene)bis(2-pyridinemethanamine) (**L2**)

Adapted from the method of Brooker *et al.*<sup>96</sup>



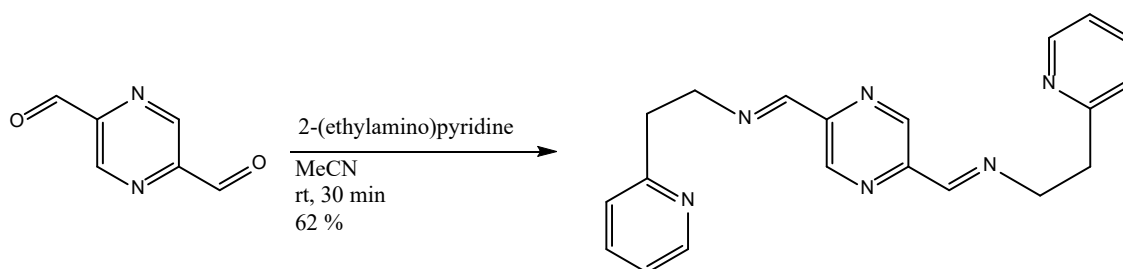
A solution of 2-(2-aminomethyl)pyridine (162.6 mg, 1.5 mmol, 2.1 eq) was added to a stirred solution of pyrazine-2,5-dicarbaldehyde (96.8 mg, 0.7 mmol, 1.0 eq) in CH<sub>3</sub>CN (5 mL) at room temperature. After 30 minutes, the mixture was left to stand for 3 hours at -5 °C. The precipitated solid was filtered and washed with ice cold MeCN affording **L2** as a purple/brown solid (122.4 mg, 54 %). mp 114 °C (from CH<sub>3</sub>CN)<sup>d</sup>. Found: C, 63.1; H, 5.2; N, 24.4. Calc. for C<sub>18</sub>H<sub>16</sub>N<sub>6</sub>·1.5 H<sub>2</sub>O: C, 63.0; H, 5.6; N, 24.5%.  $\lambda_{\text{max}}$ (MeCN)/nm 250 ( $\epsilon/\text{dm}^3 \text{ mol}^{-1} \text{ cm}^{-1}$  13750), 245 (13694) and 286 (16634).  $\nu_{\text{max}}/\text{cm}^{-1}$  1642 (m), 1590 (m), 1571 (m), 1477 (w), 1437 (m), 1379 (w), 1348 (w), 1327 (w), 1121 (s), 1086 (s), 1035 (s).  $\delta\text{H}$  (500 MHz; CDCl<sub>3</sub>; solvent) 9.31 (2 H, s, imH), 8.62 (2 H, t, J = 1.6 Hz, pzH), 8.60 (2 H, dq, J = 0.6, 1.0, 4.8 Hz, pyH), 7.71 (2 H, td, J = 1.6, 7.9 Hz, pyH), 7.45 (2 H, d, J = 7.9 Hz, pyH), 7.22 (2 H, qd J = 1.3, 4.7, pyH), 5.06 (4 H, d, J = 1.3 Hz, CH<sub>2</sub>).  $\delta\text{C}$  (125.7 MHz; CDCl<sub>3</sub>; solvent) 161.7 (pzC), 158.1 (pzC), 149.6 (pyC), 149.5 (pyC), 142.6 (imC), 136.8 (pyC), 122.6 (pyC), 122.4 (pyC), 67.0 (CH<sub>2</sub>), m/z 317.1 (M<sup>+</sup>, 100%).

<sup>d</sup>: The sample decomposed at this temperature

The assigned <sup>1</sup>H NMR spectrum can be found in section 4.4 (Figure 4.1 – the middle spectrum). The assigned <sup>13</sup>C spectrum can be found in the additional spectra section (Figure AS.4).

### A4.2.3 *N,N'*-(3,6-pyrazinediyl)dimethylidyne)bis(2-pyridineethanamine) (**L3**)

Adapted from the method of Brooker *et al.*<sup>96</sup>



2-(2-aminoethyl)pyridine (1.02 g, 3.0 mmol, 2.1 eq) was added to a stirred solution of pyrazine-2,5-dicarbaldehyde (485.5 mg, 1.4 mmol, 1.0 eq) in MeCN (10 mL) at rt. After 30 minutes, the mixture was left to stand for 3 hours at -5 °C. The precipitated solid was filtered and washed with ice cold CH<sub>3</sub>CN affording **L3** as white crystalline solid (301.0 mg, 61.5%). mp 138 °C (from CH<sub>3</sub>CN)<sup>d</sup>. Found: C, 66.4; H, 5.9; N, 23.6. Calc. for C<sub>20</sub>H<sub>20</sub>N<sub>6</sub>·H<sub>2</sub>O: C, 66.3; H, 6.1; N, 23.2%.  $\lambda_{\text{max}}$ (MeCN)/nm 257 ( $\epsilon/\text{dm}^3 \text{ mol}^{-1} \text{ cm}^{-1}$  21000), 291 (22019).  $\nu_{\text{max}}/\text{cm}^{-1}$  2959 (w), 1644 (m), 1589 (m), 1569 (m), 1473 (m), 1438 (m), 1333 (w), 1287 (w), 1262 (w), 1170 (w), 1158 (w), 1043 (m), 1024 (s).  $\delta\text{H}$  (500 MHz; CDCl<sub>3</sub>; solvent) 9.14 (2 H, s, imH), 8.55 (2 H, d, *J* = 4.10 Hz, pyH), 8.35 (2 H, t, *J* = 1.27 Hz, pzH), 7.58 (2 H, td, *J* = 1.57, 7.6 Hz, pyH), 7.18 (2 H, d, *J* = 7.87 Hz, pyH), 7.12 (2 H, qd, *J* = , pyH), 4.13 (4 H, td, *J* = 1.26, 7.26 Hz, CH<sub>2</sub>), 3.24 (4 H, t, *J* = 7.1 Hz, CH<sub>2</sub>).  $\delta\text{C}$  (125.7 MHz; CDCl<sub>3</sub>; solvent) 160.37 (pzH), 159.47 (pz), 149.6 (pyN), 149.53 (pyCN), 142.69 (CHN), 136.43 (py), 123.81 (py), 121.58 (py), 61.39 (CH<sub>2</sub>N), 39.3 (CH<sub>2</sub>py). *m/z* 345 (M<sup>+</sup>, 100%).

<sup>d</sup>: The sample decomposed at this temperature

The assigned <sup>1</sup>H NMR spectrum can be found in section 4.4 (Figure 4.1 – the bottom spectrum). The assigned <sup>13</sup>C spectrum can be found in the additional spectra section (Figure AS.6).

#### A4.2.4 Crystallisation attempts of H<sub>2</sub>L1, L2 and L3

Table A4.1. Crystallisation attempts of H<sub>2</sub>L1, L2 and L3 (√ indicates successful crystal growth, X indicates unsuccessful crystal growth, / indicates no attempts were made for the method of crystallisation, (i) indicates the ligand was insoluble in the solvent, (n/a) indicates the crystals grown were not of sufficient quality for SCXRD).

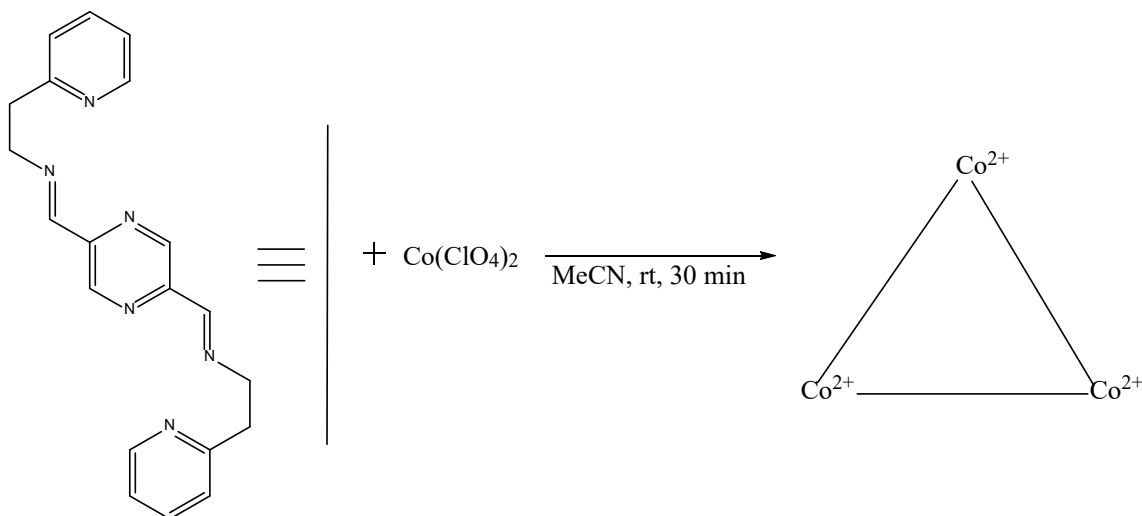
	Solvent	Vapour diffusion of Et <sub>2</sub> O	Vapour diffusion of <i>n</i> -pentane	Hot recrystallisation	Slow evaporation
H <sub>2</sub> L1	MeCN	X	/	√ (n/a)	X
	CHCl <sub>3</sub>	X	/	/	X
	THF	X	/	/	/
	MeOH	X	/	/	X
	EtOH	X	/	/	X
	DMSO	√ (n/a)	/	/	/
	DCM	/	/	X	X
	Et <sub>2</sub> O	/	/	X	√ (n/a)
L2	CHCl <sub>3</sub>	X	X	X	/
	DCM	/	X	/	/
	MeCN	/	/	X	/
	THF	/	/	X	/
	<i>n</i> -pentane	/	/	X (i)	/
	<i>n</i> -hexane	/	/	X (i)	/
	MeOH	/	/	X	/
	EtOH	/	/	X	/
	1:1 <i>n</i> -hexane: CHCl <sub>3</sub>	/	/	X	/
L3	MeCN	/	/	√	/

### A4.3 Synthesis of complexes

The general protocol used for complexations with ligands **L1**, **L2** and **L3** is briefly mentioned in section 5.2. The following section will discuss the synthetic procedures used for each complexation and the respective characterisation data. All complexations were adapted from the method by Klingele *et al.*<sup>144</sup>

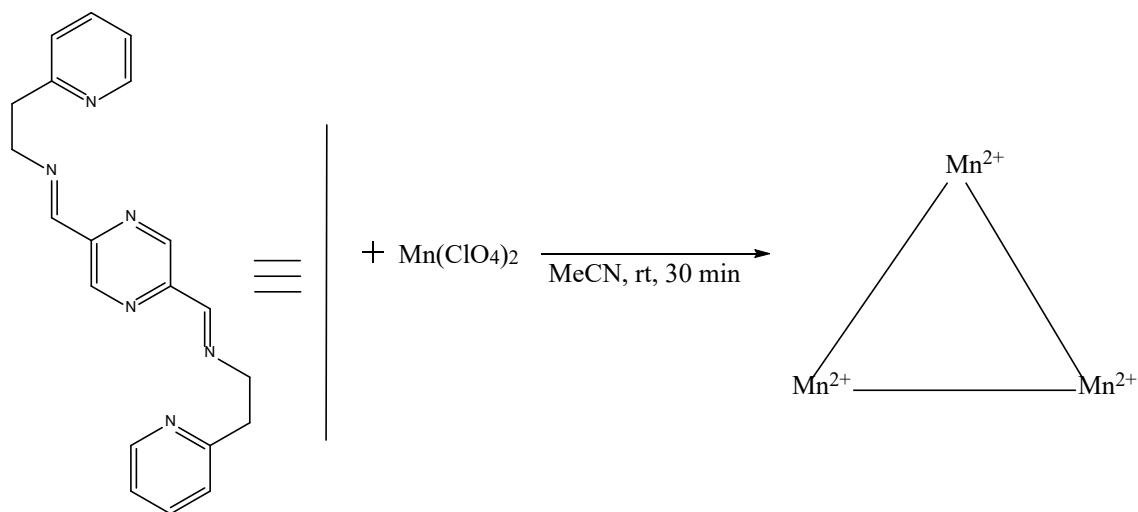


A4.3.1      Complexation with **L3**  
**C3A**



To a stirred solution of **L3** (134.1 mg, 389  $\mu\text{mol}$ , 1.0 eq) in  $\text{CH}_3\text{CN}$  (30 mL) a solution of  $\text{Co}(\text{ClO}_4)_2 \cdot 6\text{H}_2\text{O}$  (143.7 mg, 392  $\mu\text{mol}$ , 1.0 eq) in  $\text{CH}_3\text{CN}$  (3 mL) was added, giving a dark green colour. The mixture was stirred for 30 minutes. The mixture was concentrated under reduced pressure, yielding dark green crystals, which were filtered with  $\text{Et}_2\text{O}$  (3 x 10 mL). Vapour diffusion of  $\text{Et}_2\text{O}$  in the solution over 7 days yielded more dark green crystals in a brown solution. The product was filtered with  $\text{Et}_2\text{O}$  to give  $[\text{Co}_3\text{L3}](\text{ClO}_4)_6$  as a dark green solid. The product was dissolved in MeCN and recrystallized by vapour diffusion of  $\text{Et}_2\text{O}$  over 5 days, yielding more of the product as dark green crystals (95.4 mg, 130  $\mu\text{mol}$ , 39 %). Elemental analysis. Found: C, 37.70; H, 3.42; N, 13.06%. Calculated for  $\text{C}_{60}\text{H}_{60}\text{N}_{18}\text{Co}_3\text{Cl}_6\text{O}_{24} \cdot 5\text{H}_2\text{O}$ : C, 37.99; H, 3.72; N, 13.29%.  $\nu_{\text{max}}/\text{cm}^{-1}$  1631 (w) 1608 (m) 1571 (w) 1484 (w) 1446 (m) 1402 (w) 16363 (w) 1317 (m) 1307 (m) 1251 (w) 1191 (m) 1165 (w) 1019 (m) 985 (w) 952 (m) 882 (w) 864 (w) 840 (w) 831 (w) 825 (w) 813 (w) 784 (w) 768 (m) 755 (m) 741 (m) 724 (m) 717 (m) 699 (w) 684 (w). UV/Vis ( $\text{CH}_3\text{CN}$ ):  $\lambda_{\text{max}}(\text{MeCN})/\text{nm}$  240 ( $\epsilon/\text{dm}^3 \text{ mol}^{-1} \text{ cm}^{-1}$  50195), 326 (33512), 406 (8,305). Conductivity: 0.0179 g of  $[\text{Co}_3\text{L3}](\text{ClO}_4)_6$  was dissolved in  $\text{CH}_3\text{CN}$  (A.R). Conductivity of  $\text{CH}_3\text{CN}$  (A.R) =  $0.87 \mu\text{S cm}^{-1}$ ; Conductivity of  $[\text{Co}_3\text{L3}](\text{ClO}_4)_6$  in  $\text{CH}_3\text{CN}$  (A.R) =  $0.416 \text{ mS cm}^{-1}$ . Leading to a molar conductivity of  $419.01 \text{ S cm}^2 \text{ mol}^{-1}$ .

### C3B



To a stirred solution of **L3** (119.4 mg, 347  $\mu\text{mol}$ , 1.0 eq) in  $\text{CH}_3\text{CN}$  (20 mL) a solution of  $\text{Mn}(\text{ClO}_4)_2 \cdot 6\text{H}_2\text{O}$  (125.5 mg, 347  $\mu\text{mol}$ , 1.0 eq) in  $\text{CH}_3\text{CN}$  (10 mL) was added, giving a dark red colour. The mixture was stirred for 30 minutes and then concentrated under reduced pressure. Vapour diffusion of  $\text{Et}_2\text{O}$  in the solution over 7 days yielded dark red crystals in a red solution. The product was filtered with  $\text{Et}_2\text{O}$  to give  $[\text{Mn}_3\text{L}_3](\text{ClO}_4)_6$  as a dark red solid (33.5 mg, 116  $\mu\text{mol}$ , 15 %).  $\nu_{\text{max}}/\text{cm}^{-1}$  1641 (w) 1608 (m) 1486 (w) 1443 (m) 1403 (w) 1311 (m) 1183 (m) 1017 (m) 959 (m) 844 (m) 768 (m). UV/Vis ( $\text{CH}_3\text{CN}$ ):  $\lambda_{\text{max}}(\text{MeCN})/\text{nm}$  248 ( $\epsilon/\text{dm}^3 \text{ mol}^{-1} \text{ cm}^{-1}$  41565), 306 (38730). Conductivity: 0.0258 g of  $[\text{Mn}_3\text{L}_3](\text{ClO}_4)_6$  was dissolved in  $\text{CH}_3\text{CN}$  (A.R). Conductivity of  $\text{CH}_3\text{CN}$  (A.R) = 1.01  $\mu\text{S cm}^{-1}$ ; Conductivity of  $[\text{Mn}_3\text{L}_3](\text{ClO}_4)_6$  in  $\text{CH}_3\text{CN}$  (A.R) = 0.320  $\text{mS cm}^{-1}$ . Leading to a molar conductivity of 554.76  $\text{S cm}^2 \text{ mol}^{-1}$ .

### A4.3.2 Complexation with **L2**

#### **C2A**

To a stirred solution of **L2** (90.2 mg, 285.1  $\mu\text{mol}$ , 1.0 eq) in  $\text{CH}_3\text{CN}$  (15 mL) was added a solution of  $\text{Co}(\text{ClO}_4)_2 \cdot 6\text{H}_2\text{O}$  (104.8 mg, 286.4  $\mu\text{mol}$ , 1.0 eq) in  $\text{CH}_3\text{CN}$  (5 mL) resulting in the formation of a dark blue solution. The mixture was stirred for 30 minutes. The mixture was concentrated under reduced pressure. Vapour diffusion of  $\text{Et}_2\text{O}$  in the solution produced a dark blue precipitate.  $\nu_{\text{max}}/\text{cm}^{-1}$  1614 (w), 1587 (m), 1567 (w), 1502 (w), 1432 (m), 1394 (m), 1342 (m), 1237 (m), 1154 (m), 1083 (s), 894 (m), 762 (m), 626 (s).  $m/z$  1424 [**L2** $_2\text{Co}_4(\text{ClO}_4)_4(\text{MeCN})_3(\text{OH})_2$ ], 810 [**L2** $\text{Co}_2(\text{ClO}_4)_2(\text{MeCN})_3(\text{H}_2\text{O}_3)$ ], 763 [**L2** $(\text{ClO}_4)_2(\text{MeCN})_6$ ]. Conductivity of **C2A** in  $\text{CH}_3\text{CN}$  (A.R) = 0.527  $\text{mS cm}^{-1}$ .

#### **C2B**

To a stirred solution of **L2** (7.2 mg, 22.8  $\mu\text{mol}$ , 1.0 eq) in  $\text{CH}_3\text{CN}$  (5 mL) was added a solution of  $\text{Mn}(\text{ClO}_4)_2 \cdot 6\text{H}_2\text{O}$  (9.0 mg, 24.9  $\mu\text{mol}$ , 1.1 eq) in  $\text{CH}_3\text{CN}$  (1 mL) resulting in a dark red coloured solution. The mixture was stirred for 30 minutes. The mixture was concentrated under reduced pressure. Vapour diffusion of  $\text{Et}_2\text{O}$  in the solution produced a dark red precipitate. Evaporation in air led to a dark green colour change.  $\nu_{\text{max}}/\text{cm}^{-1}$  1655 (m), 1627 (m), 1595 (w), 1398 (m), 1385 (m), 1083 (m), 930 (w), 757 (m).  $m/z$  1200 [**L2** $_2\text{Mn}_4(\text{ClO}_4)_3$ ], 710 [**L2** $\text{Mn}_2(\text{MeCN})_4$ ], 584 [**L2** $\text{Mn}(\text{ClO}_4)_2(\text{OH})$ ]. Conductivity of **C2B** in  $\text{CH}_3\text{CN}$  (A.R) = 0.661  $\text{mS cm}^{-1}$ .

### A4.3.3 Complexation with L1

#### C1A

To a stirred solution of H<sub>2</sub>L1 (63.5 mg, 199.5 μmol, 1.0 eq) in CH<sub>3</sub>CN (10 mL) was added a solution of Co(ClO<sub>4</sub>)<sub>2</sub>·6H<sub>2</sub>O (73.5 mg, 200.9 μmol, 1.0 eq) in CH<sub>3</sub>CN (5 mL) resulting in the development of a dark brown solution. The mixture was stirred for 30 minutes. The mixture was concentrated under reduced pressure. Vapour diffusion of Et<sub>2</sub>O in the solution produced a dark brown precipitate.  $\nu_{\max}/\text{cm}^{-1}$  3519 (br, m), 3263 (br, s), 2958 (w), 2923 (m), 2853 (w), 1626 (m), 1505 (m), 1467 (m), 1394 (m), 1321 (m), 1288 (m), 1079 (s), 930 (w), 756 (m), 627 (s). m/z 1490 [L1<sub>2</sub>Co<sub>4</sub>(H<sub>2</sub>O)<sub>3</sub>(ClO<sub>4</sub>)<sub>5</sub>MeCN], 810 [L1K<sub>2</sub>(C<sub>6</sub>H<sub>4</sub>OH<sub>2</sub>)<sub>2</sub>(ClO<sub>4</sub>)<sub>2</sub>], 763 [L1(ClO<sub>4</sub>)<sub>2</sub>(MeCN)<sub>6</sub>]. Conductivity of C1A in CH<sub>3</sub>CN (A.R) = 0.207 mS cm<sup>-1</sup>.

#### C1B

To a stirred solution of H<sub>2</sub>L1 (98.2 mg, 309 μmol, 1.0 eq) in CH<sub>3</sub>CN (15 mL) was added a solution of Mn(ClO<sub>4</sub>)<sub>2</sub>·6H<sub>2</sub>O (105 mg, 325 μmol, 1.0 eq) in CH<sub>3</sub>CN (2 mL) resulting in the formation of a red solution. The mixture was stirred for 30 minutes. The mixture was concentrated under reduced pressure. Vapour diffusion of Et<sub>2</sub>O in the solution produced crystals not suitable for SCXRD. Attempts to recrystallise in same conditions resulted in the precipitation of the complex.  $\nu_{\max}/\text{cm}^{-1}$  3521 (br, m), 2924 (m), 1620 (m), 1465 (w), 1322 (w), 1299 (w), 10074 (s), 930 (w), 757 (w), 627 (s). m/z 1424 [L1<sub>2</sub>Co<sub>4</sub>(ClO<sub>4</sub>)<sub>4</sub>(MeCN)<sub>3</sub>(OH)<sub>2</sub>], 910 [L1Co<sub>2</sub>(ClO<sub>4</sub>)<sub>3</sub>(MeCN)<sub>4</sub>H<sub>2</sub>O], 810 [L1K<sub>2</sub>(C<sub>6</sub>H<sub>4</sub>OH<sub>2</sub>)<sub>2</sub>(ClO<sub>4</sub>)<sub>2</sub>], 763 [L1(ClO<sub>4</sub>)<sub>2</sub>(MeCN)<sub>6</sub>]. Conductivity of C1B in CH<sub>3</sub>CN (A.R) = 0.253 mS cm<sup>-1</sup>.

## **C1C**

### NMR Tube Route

Within an NMR tube, a solution of  $\text{Zn}(\text{CH}_3\text{COO})_2 \cdot 2\text{H}_2\text{O}$  (6.6 mg, 30.1  $\mu\text{mol}$ , 1.3 eq) in  $\text{MeOH} - d_4$  was added to a solution of  $\text{H}_2\text{L1}$  (7.2 mg, 22.6  $\mu\text{mol}$ , 1.0 eq) in  $\text{MeOH} - d_4$  (1mL), resulting in an immediate solution colour change to dark blue.

### Round Bottom Flask Route

To a solution of  $\text{H}_2\text{L1}$  (9.9 mg, 31.1  $\mu\text{mol}$ , 1.0 eq) in  $\text{CHCl}_3$  (25 mL), a solution of  $\text{Zn}(\text{CH}_3\text{COO})_2 \cdot 2\text{H}_2\text{O}$  (7.0 mg, 31.8  $\mu\text{mol}$ , 1.0 eq) in EtOH (1mL) was added, where an instant solution colour change to dark blue was observed. The mixture was stirred at 61 °C for 30 minutes. The solvent was reduced under reduced pressure. Vapour diffusion of  $\text{Et}_2\text{O}$  in a solution of the complex in  $\text{CHCl}_3$  led to the precipitation of the complex.  $\nu_{\text{max}}/\text{cm}^{-1}$  3374 (br, w), 1585 (m), 1535 (m), 1494 (w), 1447 (m), 1311 (m), 1266 (s), 1213 (m), 1174 (m), 1147 (s), 1113 (m), 1025 (w), 942 (w), 864 (m), 790 (m), 753 (m).  $m/z$  755 [ $\text{L1Zn}_2(\text{CH}_3\text{COO})_4(\text{H}_2\text{O})_4$ ]. Conductivity of **C1C** in  $\text{CH}_3\text{CN}$  (A.R) = 6.40  $\mu\text{S cm}^{-1}$ .

## **C1D**

To a stirred solution of  $\text{H}_2\text{L1}$  (102.0 mg, 320.4  $\mu\text{mol}$ , 1.0 eq) in EtOH (7 mL) was added a solution of  $\text{Co}(\text{CH}_3\text{COO})_2 \cdot 4\text{H}_2\text{O}$  (82.1 mg, 329.6  $\mu\text{mol}$ , 1.0 eq) in EtOH (3 mL) leading to a dark brown solution colour change. The mixture was stirred for 30 minutes. The solvent was removed under reduced pressure. Vapour diffusion of  $\text{Et}_2\text{O}$  in a solution of the complex in EtOH resulted in the formation of a dark brown precipitate.

## **C1E**

To a stirred solution of  $\text{H}_2\text{L1}$  (37.9 mg, 119.1  $\mu\text{mol}$ , 1.0 eq) in EtOH (12 mL) was added a solution of  $\text{Fe}(\text{ClO}_4)_3 \cdot \text{H}_2\text{O}$  (43.2 mg, 122.0  $\mu\text{mol}$ , 1.0 eq) in EtOH (1.5 mL) resulting in

the formation of a dark brown colour solution. The mixture was stirred for 30 minutes. The mixture was concentrated under reduced pressure. Vapour diffusion of Et<sub>2</sub>O in the solution yielded a dark brown precipitate.

### **C1F**

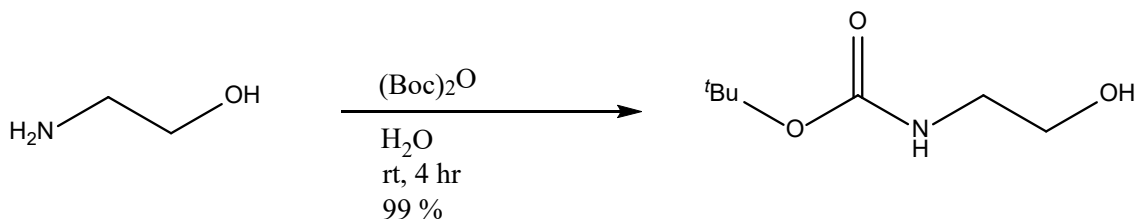
To a stirred solution of H<sub>2</sub>L1 (10.5 mg, 32.98 μmol, 1.0 eq) in MeCN (15 mL), a solution of Mn(NO<sub>3</sub>)<sub>2</sub>·4H<sub>2</sub>O (8.6 mg, 34.26 μmol, 1.0 eq) in EtOH (1 mL) was added, giving a dark brown colour. The mixture was stirred for 30 minutes. The solvent was removed under reduced pressure. Vapour diffusion of Et<sub>2</sub>O into solutions of **C1F** resulted in the formation of a precipitate. The solvents used to prepare the various crystallisation attempts are presented below.

- EtOH
- *n*-BuOH
- CHCl<sub>3</sub>
- DCM
- DMF
- DMSO
- Pyridine
- Benzene
- Nitromethane
- EtOAc
- THF
- MeCN
- Toluene
- Diisopropyl ether
- 2-propanol
- IPA

## A4.4 Synthesis of N-Boc protected 2-aminoethanol

### Route A

Prepared by the method of Chen *et al.*<sup>115</sup>



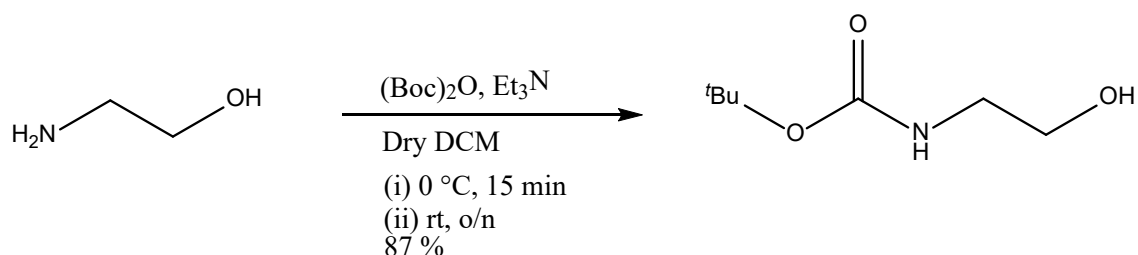
To 2-aminoethanol (4.20 g, 69 mmol, 1.0 eq) in deionized water (50 mL) was added di-*tert*-butyl carbonate (15.0 g, 69 mmol, 1.0 eq). The reaction mixture was stirred at room temperature for 2 hours until the solution became transparent and was reacted for a further 2 hours. The reaction mixture was extracted with EtOAc (3 x 100 mL), then was washed with deionized water (1 x 100 mL). The organic layer was dried (MgSO<sub>4</sub>), filtered and the solvent was removed under reduced pressure, yielding Boc-2-aminoethanol as a transparent oil (11.0 g, 68 mmol, 99.0 %).  $\delta$ H (500 MHz; CDCl<sub>3</sub>; solvent) 5.11 (brs, 1H, OH), 3.64 (t, J = 5.0, CH<sub>2</sub>), 3.23 (t, J = 4.9, CH<sub>2</sub>), 2.87 (brs, 1H, NH), 1.40 (s, 9H, <sup>t</sup>Bu).

Data is comparable to that of literature.<sup>115</sup>

The assigned <sup>1</sup>H NMR spectrum can be found in section A1.3. (Figure A1.1 – the middle spectrum).

## Route B

Prepared by the method of Devine *et al.*<sup>116</sup>



To a solution of 2-ethanolamine (2.03 g, 2.01 mL, 33.3 mmol, 1.0 eq) in dry DCM (100 mL) at  $0\text{ }^\circ\text{C}$ ,  $\text{Et}_3\text{N}$  (5.56 g, 7.67 mL, 55.0 mmol, 1.5 eq) and di-*tert*-butyl carbonate (8.00 g, 8.43 mL, 36.7 mmol, 1.1 eq) was added. The mixture was allowed to warm up to room temperature, where it was then stirred overnight. Saturated  $\text{NH}_4\text{Cl}$  (200 mL) was added to the colourless mixture and was extracted with EtOAc (3 x 200 mL). The combined organic layers were washed with brine (300 mL), dried over anhydrous  $\text{Na}_2\text{SO}_4$  and concentrated to give Boc-2-aminoethanol as a colourless oil (4.65 g, 28.9 mmol, 86.7 %).  $\delta\text{H}$  (500 MHz;  $\text{CDCl}_3$ ; solvent) 4.97 (brs, 1H, OH), 3.69 (t,  $J = 4.9$ ,  $\text{CH}_2$ ), 3.28 (q,  $J = 4.0$ ,  $\text{CH}_2$ ), 2.29 (brs, 1H, NH), 1.44 (s, 9H,  $\text{tBu}$ ).

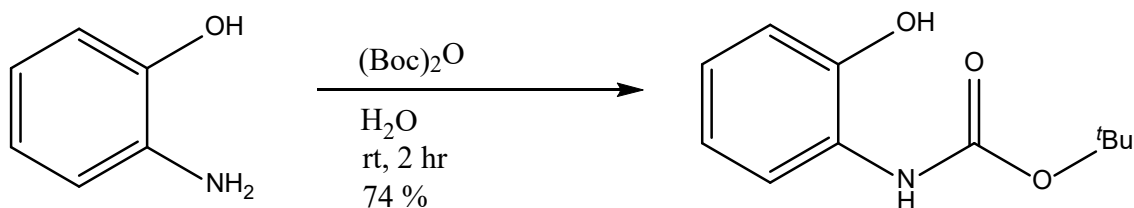
Data is comparable to that of literature.<sup>116</sup>

The assigned  $^1\text{H}$  NMR spectrum can be found in section A1.3. (Figure A1.1 – the bottom spectrum).



#### A4.5 Synthesis of N-Boc protected 2-aminophenol

Prepared by the method of Chankeshwara *et al.*<sup>114</sup>



To 2-aminophenol (3.75 g, 34.4 mmol, 1.0 eq) in deionized water (50 mL) was added di-*tert*-butyl carbonate (8.26 g, 37.9 mmol, 1.1 eq). The reaction mixture was stirred at room temperature for 2 hours, producing a white precipitate. The supernatant water was decanted off. Deionized water (50 mL) was added to the solid residue and stirred for roughly 2 minutes. The supernatant water was decanted again. The addition of water, stirring and decantation was repeated three times. The residue was dried under vacuum to yield Boc-2-aminophenol as a white solid (5.35 g, 25.6 mmol, 74.3 %).  $\delta$ H (500 MHz; CDCl<sub>3</sub>; solvent) 8.11 (brs, 1H, OH), 7.05 (m, 2H, ArH), 6.97 (dd, J = 1.3, 8.2, ArH), 6.86 (td, J = 1.6, 7.6, ArH), 6.62 (brs, 1H, NH), 1.53 (s, 9H, <sup>t</sup>Bu).

Data is comparable to that of literature.<sup>114</sup>

The assigned <sup>1</sup>H NMR spectrum can be found in section A1.3. (Figure A1.1 – the top spectrum).

## References

- (1) Hogue, R. W.; Dhers, S.; Hellyer, R. M.; Luo, J.; Hanan, G. S.; Larsen, D. S.; Garden, A. L.; Brooker, S. *Chemistry - A European Journal* **2017**, *23*, 14100.
- (2) Steed, J. W.; Atwood, J. L. *Supramolecular Chemistry*; John Wiley & Sons, 2013, 2nd ed, pp 304.
- (3) Bark, T.; Düggele, M.; Stoeckli-Evans, H.; Zelewsky, A. v. *Angewandte Chemie International Edition* **2001**, *40*, 2848.
- (4) Orchard, A. F. *Magnetochemistry*; Oxford University Press, 2003, pp 172.
- (5) Coufal, R.; Prusková, M.; Císařová, I.; Drahoňovský, D.; Vohlídal, J. *Synthetic Communications* **2016**, *46*, 348.
- (6) Shen, F.; Huang, W.; Wu, D.; Zheng, Z.; Huang, X.-C.; Sato, O. *Inorganic Chemistry* **2016**, *55*, 902.
- (7) Späth, A.; Gonschor, J.; König, B. *Monatshefte für Chemie - Chemical Monthly* **2011**, *142*, 1289.
- (8) Hausmann, J.; Brooker, S. *Chemical Communications* **2004**, 1530.
- (9) Greig, L. M.; Philp, D. *Chemical Society Reviews* **2001**, *30*, 287.
- (10) Hanan, G. S.; Volkmer, D.; Lehn, J.-M. *Canadian Journal of Chemistry* **2004**, *82*, 1428.
- (11) Holliday, B. J.; Mirkin, C. A. *Angewandte Chemie International Edition* **2001**, *40*, 2022.
- (12) Leininger, S.; Olenyuk, B.; Stang, P. J. *Chemical Reviews* **2000**, *100*, 853.
- (13) Chakrabarty, R.; Mukherjee, P. S.; Stang, P. J. *Chemical Reviews* **2011**, *111*, 6810.
- (14) Roy, S.; Mandal, T. N.; Barik, A. K.; Gupta, S.; Fallah, M. S. E.; Tercero, J.; Butcher, R. J.; Kar, S. K. *Dalton Transactions* **2009**, 8215.
- (15) Calzado, C. J.; Evangelisti, S. *Dalton Transactions* **2014**, *43*, 2988.

- (16) Anwar, M. U.; Al-Harrasi, A.; Gavey, E. L.; Pilkington, M.; Rawson, J. M.; Thompson, L. K. *Dalton Transactions* **2018**, 47, 2511.
- (17) Zhao, L.; Matthews, C. J.; Xu, Z.; Thompson, L. K.; Miller, D. O. *Molecular Crystals & Liquid Crystals Science & Technology, Section A: Molecular Crystals & Liquid Crystals* **2002**, 376, 389.
- (18) Thompson, L. K. *Coordination Chemistry Reviews* **2002**, 233-234, 193.
- (19) Thompson, L. K.; Zhao, L.; Xu, Z.; Miller, D. O.; Reiff, W. M. *Inorganic Chemistry* **2003**, 42, 128.
- (20) Shriver, D. F.; Atkins, P. W.; Overton, T. L.; Rourke, J. P.; Weller, M. T.; Armstrong, F. A. *Shriver & Atkins' Inorganic Chemistry*; Oxford University Press, 2006, pp 822.
- (21) Anderson, P. W. *Physical Review* **1950**, 79, 350.
- (22) Anderson, P. W. *Physical Review* **1959**, 115, 2.
- (23) El Ghachtouli, S.; Cadiou, C.; Dechamps-Olivier, I.; Chuburu, F.; Aplincourt, M.; Roisnel, T.; Turcry, V.; Patinec, V.; Le Baccon, M.; Handel, H. *European Journal of Inorganic Chemistry* **2008**, 4735.
- (24) Housecroft, C. E.; Sharpe, A. G. *Inorganic Chemistry*; Harlow, England ; New York : Pearson, 2012, 4th ed, pp 1098.
- (25) Lalena, J. N.; Cleary, D. A. *Principles of Inorganic Materials Design*; Hoboken, N.J. : Wiley-Interscience, 2005, pp 419.
- (26) Spaldin, N. A. *Magnetic materials : Fundamentals and Applications*; Cambridge ; New York : Cambridge University Press, 2011, 2nd ed, pp 290.
- (27) Fagaly, R. *Review of Scientific Instruments*, **2006**, 77.
- (28) Granata, C.; Vettoliere, A. *Physics Reports* **2016**, 614, 1.

- (29) Kleiner, R.; Koelle, D.; Ludwig, F.; Clarke, J. *Proceedings of the Institute of Electrical and Electronics Engineers* **2004**, *92*, 1534.
- (30) Kettle, S. F. A. *Physical Inorganic Chemistry : A Coordination Chemistry Approach*; Sausalito, Calif. : University Science Books, 1996, pp 1415.
- (31) O'Connor, C. J. *Progress in Inorganic Chemistry* **1982**, *29*, 203.
- (32) Milway, V. A.; Dawe, L. N.; Thompson, L. K. *Canadian Journal of Chemistry* **2014**, *92*, 966.
- (33) Ward, M. D. *Chemical Society Reviews* **1995**, *24*, 121.
- (34) Broere, D. L. J.; Modder, D. K.; Blokker, E.; Siegler, M. A.; van der Vlugt, J. I. *Angewandte Chemie International Edition* **2016**, *55*, 2406.
- (35) Gusev, D. G.; Peris, E. *Dalton Transactions* **2013**, *42*, 7359.
- (36) Zhao, Y.; Guo, D.; Liu, Y.; He, C.; Duan, C. *Chemical Communications* **2008**, 5725.
- (37) Creutz, C.; Taube, H. *Journal of the American Chemical Society* **1973**, *95*, 1086.
- (38) Mayoh, B.; Day, P. *Journal of the American Chemical Society* **1972**, *94*, 2885.
- (39) Vilà, N.; Zhong, Y.-W.; Henderson, J. C.; Abruña, H. D. *Inorganic Chemistry* **2010**, *49*, 796.
- (40) Robin, M. B.; Day, P. In *Advances in Inorganic Chemistry and Radiochemistry*; Emeléus, H. J., Sharpe, A. G., Eds.; Academic Press: 1968; Vol. Volume 10, p 247.
- (41) Day, P.; Hush, N. S.; Clark, R. J. H. *Philosophical Transactions: Mathematical, Physical and Engineering Sciences* **2008**, 366, 5.
- (42) Glover, S. D.; Lear, B. J.; Salsman, J. C.; Londergan, C. H.; Kubiak, C. P. *Philosophical Transactions: Mathematical, Physical and Engineering Sciences* **2008**, 366, 177.

- (43) Parthey, M.; Gluyas, J. B. G.; Fox, M. A.; Low, P. J.; Kaupp, M. *Chemistry - A European Journal* **2014**, *20*, 6895.
- (44) Parthey, M.; Kaupp, M. *Chemical Society Reviews* **2014**, *43*, 5067.
- (45) Bersuker, I. B. *Electronic Structure and Properties of Transition Metal Compounds : Introduction to the Theory*; Hoboken, N.J. : Wiley, 2010, 2nd ed, pp 759.
- (46) Demadis, K. D.; Hartshorn, C. M.; Meyer, T. J. *Chemical Reviews* **2001**, *101*, 2655.
- (47) D'Alessandro, D. M.; Topley, A. C.; Davies, M. S.; Keene, F. R. *Chemistry – A European Journal* **2006**, *12*, 4873.
- (48) Yang, J.; Zhang, W.; Si, Y.; Zhao, Y. *The Journal of Physical Chemistry B* **2012**, *116*, 14126.
- (49) Nelsen, S. F.; Schultz, K. P.; Telo, J. P. *The Journal of Physical Chemistry A* **2008**, *112*, 12622.
- (50) Yip, J. H. K.; Wu, J.; Wong, K.-Y.; Ho, K. P.; Pun, C. S.-N.; Vittal, J. J. *Journal of the Chinese Chemical Society* **2004**, *51*, 1245.
- (51) Elgrishi, N.; Rountree, K. J.; McCarthy, B. D.; Rountree, E. S.; Eisenhart, T. T.; Dempsey, J. L. *Journal of Chemical Education* **2018**, *95*, 197.
- (52) Thompson, L. K.; Kelly, T. L.; Dawe, L. N.; Grove, H.; Lemaire, M. T.; Howard, J. A. K.; Spencer, E. C.; Matthews, C. J.; Onions, S. T.; Coles, S. J.; Horton, P. N.; Hursthouse, M. B.; Light, M. E. *Inorganic Chemistry* **2004**, *43*, 7605.
- (53) Nirmaier, H. P.; Henze, G. *Electroanalysis* **1997**, *9*, 619.
- (54) Creutz, C.; Taube, H. *Journal of the American Chemical Society* **1969**, *91*, 3988.

- (55) Concepcion, J. J.; Dattelbaum, D. M.; Meyer, T. J.; Rocha, R. C. *Philosophical Transactions: Mathematical, Physical and Engineering Sciences* **2008**, *366*, 163.
- (56) Crutchley, R. J. In *Advances in Inorganic Chemistry*; Sykes, A. G., Ed.; Academic Press: 1994; Vol. 41, pp 273.
- (57) Zhang, L. T.; Ko, J.; Ondrechen, M. J. *Journal of the American Chemical Society* **1987**, *109*, 1666.
- (58) Cotton, F. A.; Dalal, N. S.; Liu, C. Y.; Murillo, C. A.; North, J. M.; Wang, X. *Journal of the American Chemical Society* **2003**, *125*, 12945.
- (59) Herrmann, C.; Elmisz, J. *Chemical Communications* **2013**, *49*, 10456.
- (60) Warzajtis, B.; Glišić, B. Đ.; Radulović, N. S.; Rychlewska, U.; Djuran, M. I. *Polyhedron* **2014**, *79*, 221.
- (61) Ramírez, J.; Stadler, A.-M.; Rogez, G.; Drillon, M.; Lehn, J.-M. *Inorganic Chemistry* **2009**, *48*, 2456.
- (62) Rochon, F. D.; Fakhfakh, M. *Inorganica Chimica Acta* **2009**, *362*, 1455.
- (63) Pal, A. K.; Hanan, G. S. *Chemical Society Reviews* **2014**, *43*, 6184.
- (64) Ferretti, A.; Improta, R.; Lami, A.; Villani, G. *Physical Chemistry Chemical Physics* **2001**, *3*, 2576.
- (65) Oshio, H.; Nagashima, U. *Inorganic Chemistry* **1990**, *29*, 3321.
- (66) Kang, D.-B. *Bulletin of the Korean Chemical Society* **2010**, *31*, 1704.
- (67) Hay, P. J.; Thibeault, J. C.; Hoffmann, R. *J. Am. Chem. Soc.* **1975**, *97*, 4884.
- (68) Hausmann, J. Transition Metal Complexes of Pyrazine-Based Bis-Terdentate Diamide Ligands. Ph.D. Thesis, University of Otago, New Zealand, 2004.
- (69) Otieno, T.; Thompson, R. C. *Canadian Journal of Chemistry* **1995**, *73*, 275.

- (70) Joule, J. A.; Mills, K. *Heterocyclic Chemistry*; Chichester, U.K. : Wiley, 2010, 5th ed, pp 718.
- (71) Ašanin, D. P.; Živković, M. D.; Rajković, S.; Warzajtis, B.; Rychlewska, U.; Djuran, M. I. *Polyhedron* **2013**, *51*, 255.
- (72) Silberberg, M. *Chemistry: The Molecular Nature of Matter and Change*; McGraw-Hill, 2006, pp 1088.
- (73) Uppadine, L. H.; Gisselbrecht, J. P.; Kyritsakas, N.; Nättinen, K.; Rissanen, K.; Lehn, J. M. *Chemistry - A European Journal* **2005**, *11*, 2549.
- (74) Carmona-Vargas, C. C.; Váquiro, I. Y.; Jaramillo-Gómez, L. M.; Lehn, J.-M.; Chaur, M. N. *Inorganica Chimica Acta* **2017**, *468*, 131.
- (75) Dawe, L. N.; Shuvaev, K. V.; Thompson, L. K. *Chemical Society Reviews* **2009**, *38*, 2334.
- (76) Wałęsa-Chorab, M.; Gorczyński, A.; Kubicki, M.; Hnatejko, Z.; Patroniak, V. *Polyhedron* **2012**, *31*, 51.
- (77) Han, F.; Teng, Q.; Zhang, Y.; Wang, Y.; Shen, Q. *Inorganic Chemistry* **2011**, *50*, 2634.
- (78) Benelli, C.; Gatteschi, D. *Introduction to Molecular Magnetism : From Transition Metals to Lanthanides*; Weinheim, Germany : Wiley-VCH, 2015, pp 450.
- (79) Brown, W. H.; Poon, T. *Introduction to Organic Chemistry*; Hoboken, NJ : John Wiley & Sons, 2014, 5th ed, pp 792.
- (80) Stuart, B. *Infrared Spectroscopy : Fundamentals and Applications*; Chichester, West Sussex, England ; Hoboken, NJ : J. Wiley, 2004, pp 203.
- (81) Frischmann, P. D.; Jiang, J.; Hui, J. K. H.; Grzybowski, J. J.; MacLachlan, M. J. *Organic Letters* **2008**, *10*, 1255.

- (82) Pearson, R. G. *Journal of the American Chemical Society* **1963**, *85*, 3533.
- (83) LoPachin, R. M.; Gavin, T.; DeCaprio, A.; Barber, D. S. *Chemical Research in Toxicology* **2012**, *25*, 239.
- (84) Farrow, Z.; Rowlands, G. *Private Communication*, **2018**.
- (85) Das, S. K.; Frey, J. *Tetrahedron Letters* **2012**, *53*, 3869.
- (86) Iovel', I. G.; Yansone, I. Y.; Gol'dberg, Y. S.; Shimanskaya, M. V. *Chemistry of Heterocyclic Compounds* **1990**, *26*, 456.
- (87) Campa, C.; Sanchez-Ferrando, F.; Tristan-Polo, M. *Nouveau Journal de Chimie* **1985**, *9*, 493.
- (88) Zaytsev, A.; Dodd, B.; Magnani, M.; Ghiron, C.; Golding, B. T.; Griffin, R. J.; Liu, J.; Lu, X.; Micco, I.; Newell, D. R.; Padova, A.; Robertson, G.; Lunec, J.; Hardcastle, I. R. *Chemical Biological & Drug Design* **2015**, *86*, 180.
- (89) Guimond, N.; MacDonald, M. J.; Lemieux, V.; Beauchemin, A. M. *Journal of the American Chemical Society* **2012**, *134*, 16571.
- (90) Klein, B.; Berkowitz, J. *Journal of the American Chemical Society* **1959**, *81*, 5160.
- (91) Harjani, J. R.; Nara, S. J.; Salunkhe, M. M. *Tetrahedron Letters* **2002**, *43*, 1127.
- (92) Zhang, W.; Liang, J.; Liu, Y.; Sun, S.; Ren, X.; Jiang, M. *Chinese Journal of Catalysis* **2013**, *34*, 559.
- (93) Carey, F. A.; Giuliano, R. M. *Organic Chemistry*; New York : McGraw-Hill, 2011, 8th ed, pp 802.
- (94) Stadler, A.-M.; Puntoriero, F.; Campagna, S.; Kyritsakas, N.; Welter, R.; Lehn, J.-M. *Chemistry - A European Journal* **2005**, *11*, 3997.
- (95) Brooker, S.; Kelly, R. J. *Journal of the Chemical Society, Dalton Transactions* **1996**, 2117.



- (96) Brooker, S.; Iremonger, S. S.; Plieger, P. G. *Polyhedron* **2003**, *22*, 665.
- (97) Wickenden, A. E.; Krause, R. A. *Inorganic Chemistry* **1965**, *4*, 404.
- (98) Lewis, D. L.; Estes, E. D.; Hodgson, D. J. *Journal of Crystal and Molecular Structure* **1975**, *5*, 67.
- (99) Manura, J. J.; Manura, D. J. Scientific Instrument Services. Retrieved from <http://www.sisweb.com/mstools/spectrum.htm>.
- (100) Geary, W. J. *Coordination Chemistry Reviews* **1971**, *7*, 81.
- (101) E., S. K. *Angewandte Chemie International Edition in English* **1970**, *9*, 946.
- (102) Tycko, R. *Accounts of Chemical Research* **2013**, *46*, 1923.
- (103) Plieger, P. G.; Downard, A. J.; Moubaraki, B.; Murray, K. S.; Brooker, S. *Dalton Transactions* **2004**, 2157.
- (104) Yoshitomo, K.; Yumiko, T.; Kentaro, Y.; Tetsuya, O. *Electroanalysis* **2013**, *25*, 2575.
- (105) Thirumoorthi, A.; Elango, K. P. *Journal of Chemical Sciences* **2007**, *119*, 289.
- (106) Yaman Şeniz, Ö.; Esentürk, E.; Kayran, C.; Önal Ahmet, M. In *Zeitschrift für Naturforschung B* 2002; Vol. 57, p 92.
- (107) Hellyer, R. M.; Larsen, D. S.; Brooker, S. *European Journal of Inorganic Chemistry* **2009**, *2009*, 1162.
- (108) Nakamoto, K. *Infrared and Raman Spectra of Inorganic and Coordination Compounds*; New York : Wiley, 1997, 5th ed, pp 400.
- (109) Needham, T. E., Jr, The Solubility of Amino Acids in Various Solvent Systems. Ph.D. Thesis, University of Rhode Island, 1970.
- (110) Şakıyan, İ. *Transition Metal Chemistry* **2007**, *32*, 131.
- (111) Sari, N.; Gürkan, P. *Verlag der Zeitschrift für Naturforschung* **2004**, *59b*, 628.

- (112) Alghool, S.; Zoromba, M. S.; El-Halim, H. F. A. *Journal of Rare Earths* **2013**, *31*, 715.
- (113) Alsahme, A.; Laeeq, S.; Dwivedi, S.; Khan, M. S.; Al Farhan, K.; Musarrat, J.; Khan, R. A. *Spectrochimica Acta Part A: Molecular and Biomolecular Spectroscopy* **2016**, *163*, 1.
- (114) Chankeshwara, S. V.; Chakraborti, A. K. *Organic Letters* **2006**, *8*, 3259.
- (115) Sheng-Qi, C.; Lulu, X.; Chen, H.; Peng-Yun, L.; Xiao-Xia, L.; Jia-Min, L.; Hui-Juan, L.; Wei-Dong, H.; Lihua, Y. *Journal of Polymer Science Part A: Polymer Chemistry* **2016**, *54*, 3462.
- (116) Devine, W. G.; Diaz-Gonzalez, R.; Ceballos-Perez, G.; Rojas, D.; Satoh, T.; Tear, W.; Ranade, R. M.; Barros-Álvarez, X.; Hol, W. G. J.; Buckner, F. S.; Navarro, M.; Pollastri, M. P. *American Chemical Society Infectious Diseases* **2017**, *3*, 225.
- (117) Bai, J.; Wang, P.; Cao, W.; Chen, X. *Journal of Molecular Structure* **2017**, *1128*, 645.
- (118) Carey, A. R. E.; O'Ferrall, R. A. M.; Murphy, M. G.; Murray, B. A. *Journal of the Chemical Society, Perkin Transactions 2* **1994**, 2471.
- (119) Baxter, A.; Brough, S.; Faull, A.; Johnstone, C.; McNally, T.; AstraZeneca AB, Heteroaromatic Carboxamide Derivatives and their Use as Inhibitors of the Enzyme IKK-2. Swed. Patent. Appl. 2001000248, 2001.
- (120) Joule, J. A.; Mills, K. *Heterocyclic Chemistry at a Glance*; John Wiley & Sons, 2012, pp 230.
- (121) Davies, D. T.; Davies, D. T. *Aromatic Heterocyclic Chemistry*; Oxford University Press Oxford, 1992, pp 96.

- (122) Clayden, J.; Clayden, L. O. C. J. *Organolithiums: Selectivity for Synthesis*; Elsevier Science & Technology Books, 2002, pp 400.
- (123) Jusseau, X.; Yin, H.; Lindhardt, A. T.; Skrydstrup, T. *Chemistry - A European Journal* **2014**, *20*, 15785.
- (124) Nahm, S.; Weinreb, S. M. *Tetrahedron Letters* **1981**, *22*, 3815.
- (125) Paine, J. B., III *Journal of Heterocyclic Chemistry* **1991**, *28*, 1463.
- (126) Kjell, D. P.; Slattery, B. J.; Semo, M. J. *The Journal of Organic Chemistry* **1999**, *64*, 5722.
- (127) Boucher, M. M.; Furigay, M. H.; Quach, P. K.; Brindle, C. S. *Organic Process Research & Development* **2017**, *21*, 1394.
- (128) Shimizu, T.; Osako, K.; Nakata, T.-i. *Tetrahedron Letters* **1997**, *38*, 2685.
- (129) Niu, T.; Zhang, W.; Huang, D.; Xu, C.; Wang, H.; Hu, Y. *Organic Letters* **2009**, *11*, 4474.
- (130) Martinelli, J. R.; Freckmann, D. M. M.; Buchwald, S. L. *Organic Letters* **2006**, *8*, 4843.
- (131) Mentzel, M.; Hoffmann, H. M. R. *Journal für Praktische Chemie/Chemiker-Zeitung* **1997**, *339*, 517.
- (132) Qin, R.; Zhong, C.; Zong, G.; Fu, J.; Pang, X.; Cao, G. *Electronic Journal of Biotechnology* **2017**, *28*, 41.
- (133) Brethauer, S.; Held, M.; Panke, S. *Journal of Pharmaceutical Sciences* **2008**, *97*, 3451.
- (134) Brethauer, S.; Held, M.; Panke, S. *Biotechnology and Bioengineering* **2008**, *100*, 439.
- (135) Finn, M. J.; Harris, M. A.; Hunt, E.; Zomaya, I. I. *Journal of the Chemical Society, Perkin Transactions I* **1984**, 1345.

- (136) Haginaka, J. U. N.; Yasuda, H.; Uno, T.; Nakagawa, T. *Chemical and Pharmaceutical Bulletin* **1985**, *33*, 218.
- (137) Bellur Atici, E.; Yazar, Y.; Ağtaş, Ç.; Ridvanoğlu, N.; Karlığa, B. *Journal of Pharmaceutical and Biomedical Analysis* **2017**, *136*, 1.
- (138) Dolomanov, O. V.; Bourhis, L. J.; Gildea, R. J.; Howard, J. A. K.; Puschmann, H. *Journal of Applied Crystallography* **2009**, *42*, 339.
- (139) Kabsch, W. *Acta Crystallographica Section D: Biological Crystallography* **2010**, *66*, 125.
- (140) Evans, P. *Acta Crystallographica Section D* **2006**, *62*, 72.
- (141) Winn, M. D.; Ballard, C. C.; Cowtan, K. D.; Dodson, E. J.; Emsley, P.; Evans, P. R.; Keegan, R. M.; Krissinel, E. B.; Leslie, A. G. W.; McCoy, A.; McNicholas, S. J.; Murshudov, G. N.; Pannu, N. S.; Potterton, E. A.; Powell, H. R.; Read, R. J.; Vagin, A.; Wilson, K. S. *Acta Crystallographica Section D* **2011**, *67*, 235.
- (142) Palatinus, L.; van der Lee, A. *Journal of Applied Crystallography* **2008**, *41*, 975.
- (143) Sheldrick, G. M. *Acta Crystallographica. Section C, Structural Chemistry* **2015**, *71*, 3.
- (144) Klingele, J.; Boas, J. F.; Pilbrow, J. R.; Moubaraki, B.; Murray, K. S.; Berry, K. J.; Hunter, K. A.; Jameson, G. B.; Boyd, P. D. W.; Brooker, S. *Dalton Transactions* **2007**, 633.

## Additional Spectra

The following section contains previously unreported  $^1\text{H}$ ,  $^{13}\text{C}$  NMR and mass spectra of compounds.

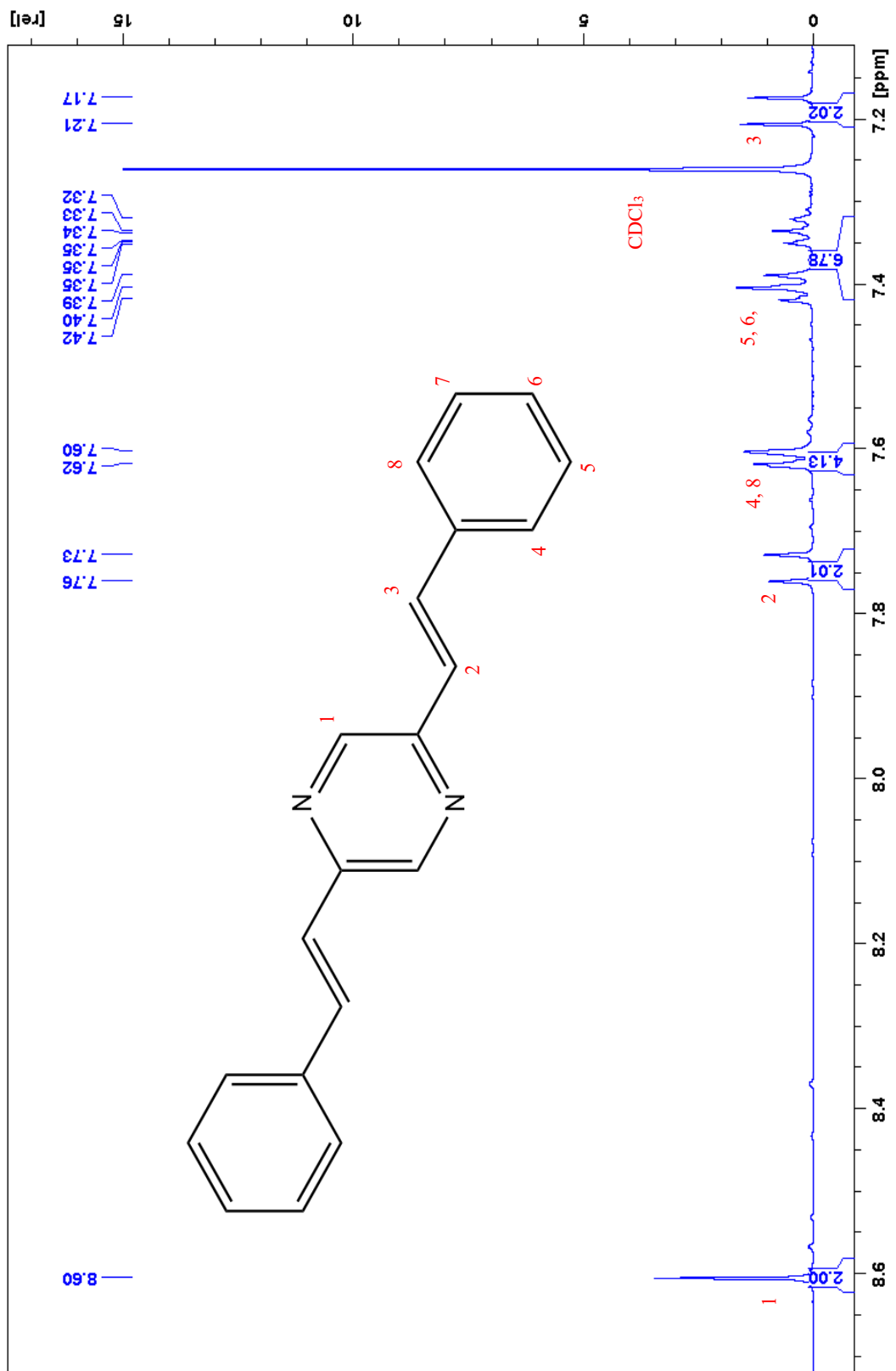


Figure AS1. Assigned <sup>1</sup>H NMR spectrum of 2,5-E,E-distyrylpyrazine. Microwave synthesis adaptation from the method of Coufal *et al.*<sup>5</sup> (CDCl<sub>3</sub>). <sup>1</sup>H NMR spectrum of 2,5-E,E-distyrylpyrazine obtained from using the method by Coufal *et al.* produced an almost identical spectrum.

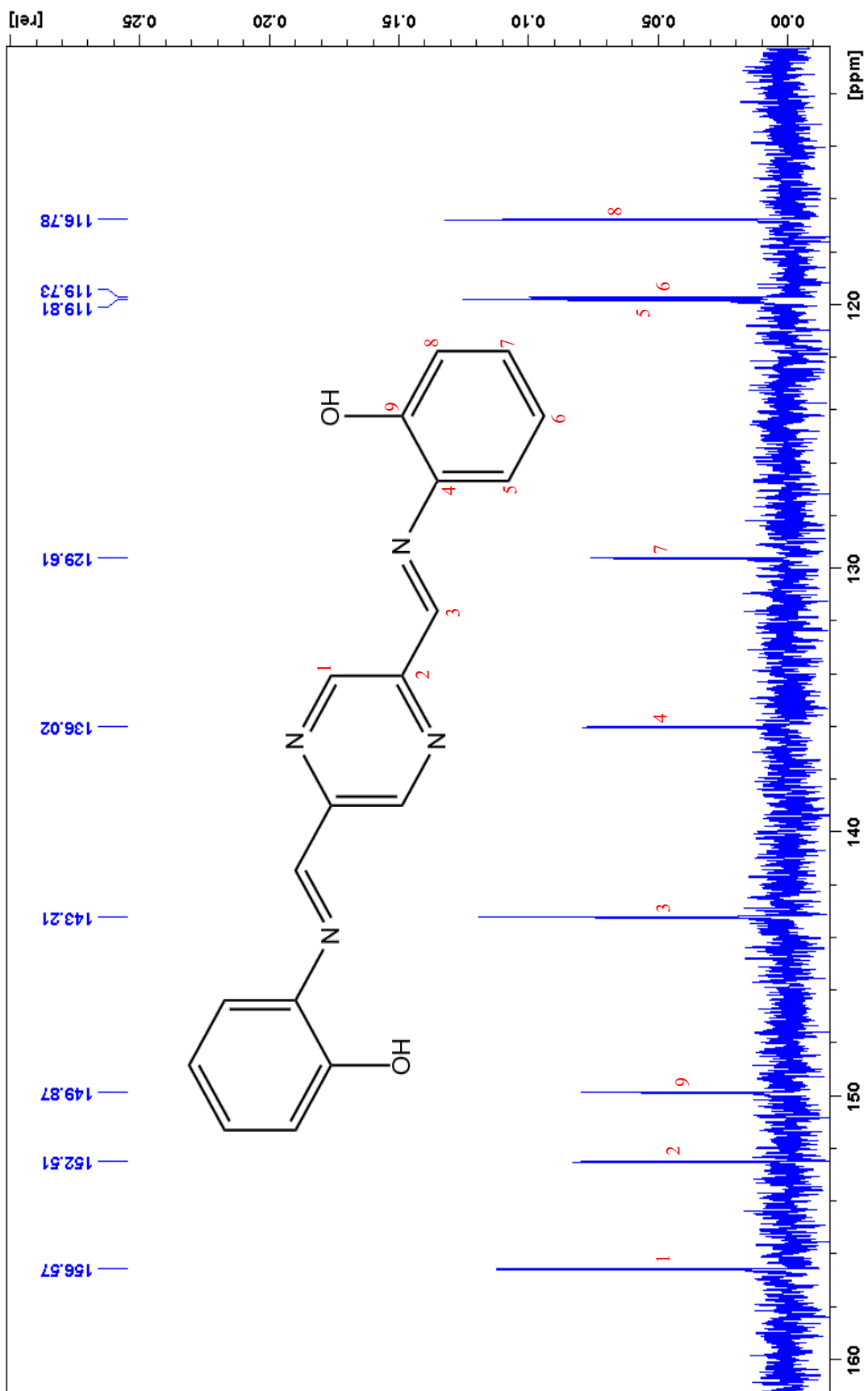


Figure AS2. Assigned  $^{13}\text{C}$  NMR spectrum of L1 (DMSO -  $d_6$ ).

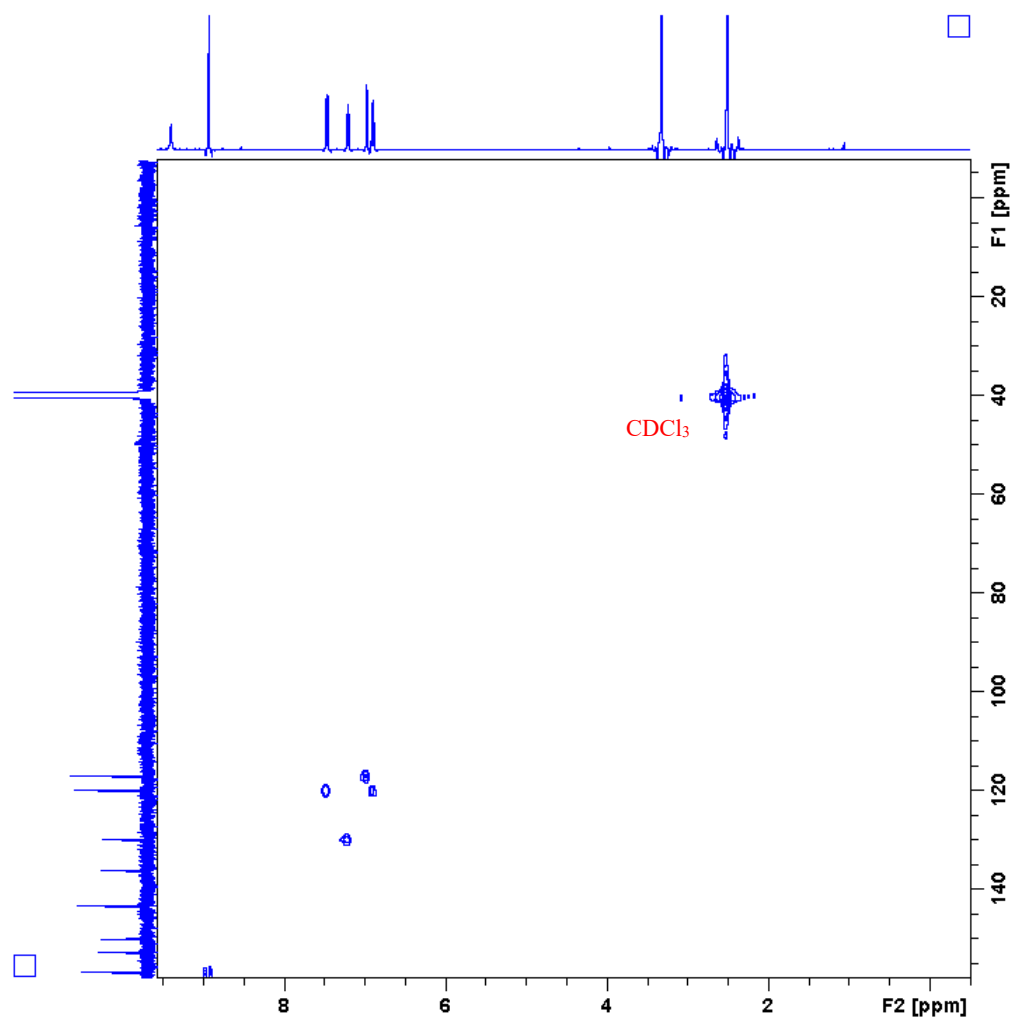


Figure AS3. HMQC spectrum of **L1** with solvent peak assigned (DMSO – d<sub>6</sub>). Left axis = <sup>13</sup>C NMR spectrum of **L1**. Top axis = <sup>1</sup>H NMR spectrum of **L1**.



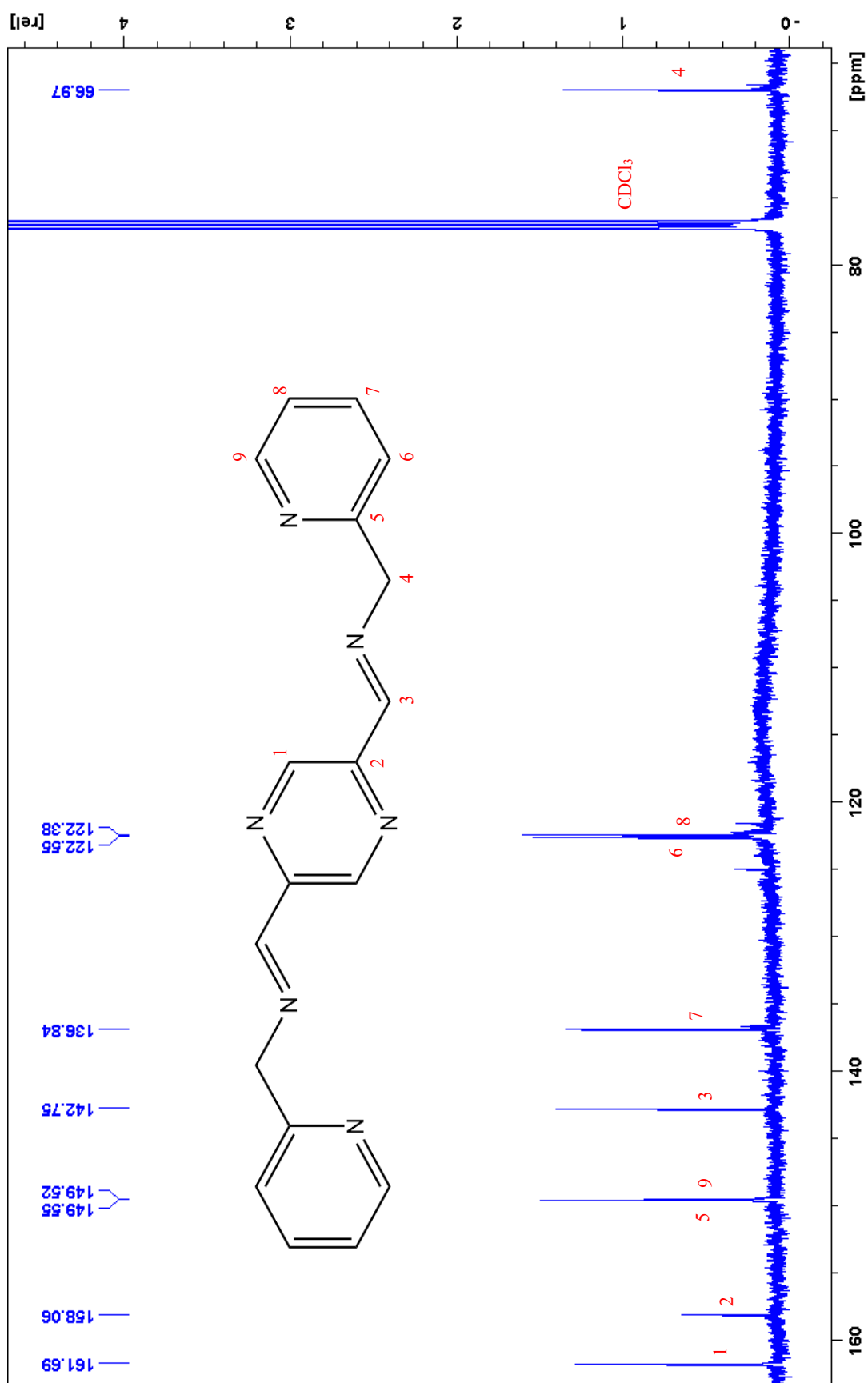


Figure AS4. Assigned  $^{13}\text{C}$  NMR spectrum of L2 ( $\text{CDCl}_3$ ).

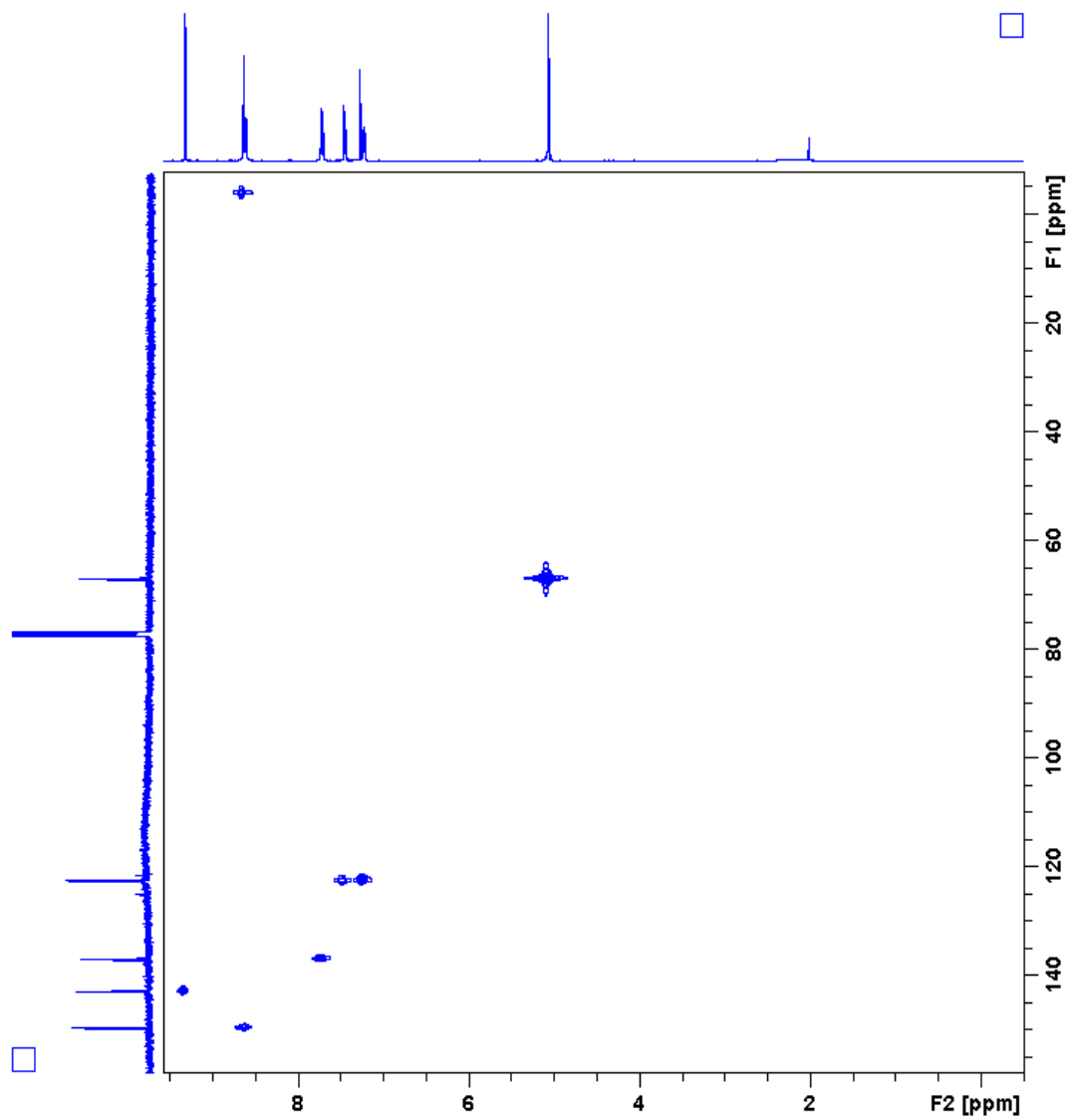


Figure AS5. HMQC spectrum of L2 (CDCl<sub>3</sub>). Left axis = <sup>13</sup>C NMR spectrum of L2. Top axis = <sup>1</sup>H NMR spectrum of L2.

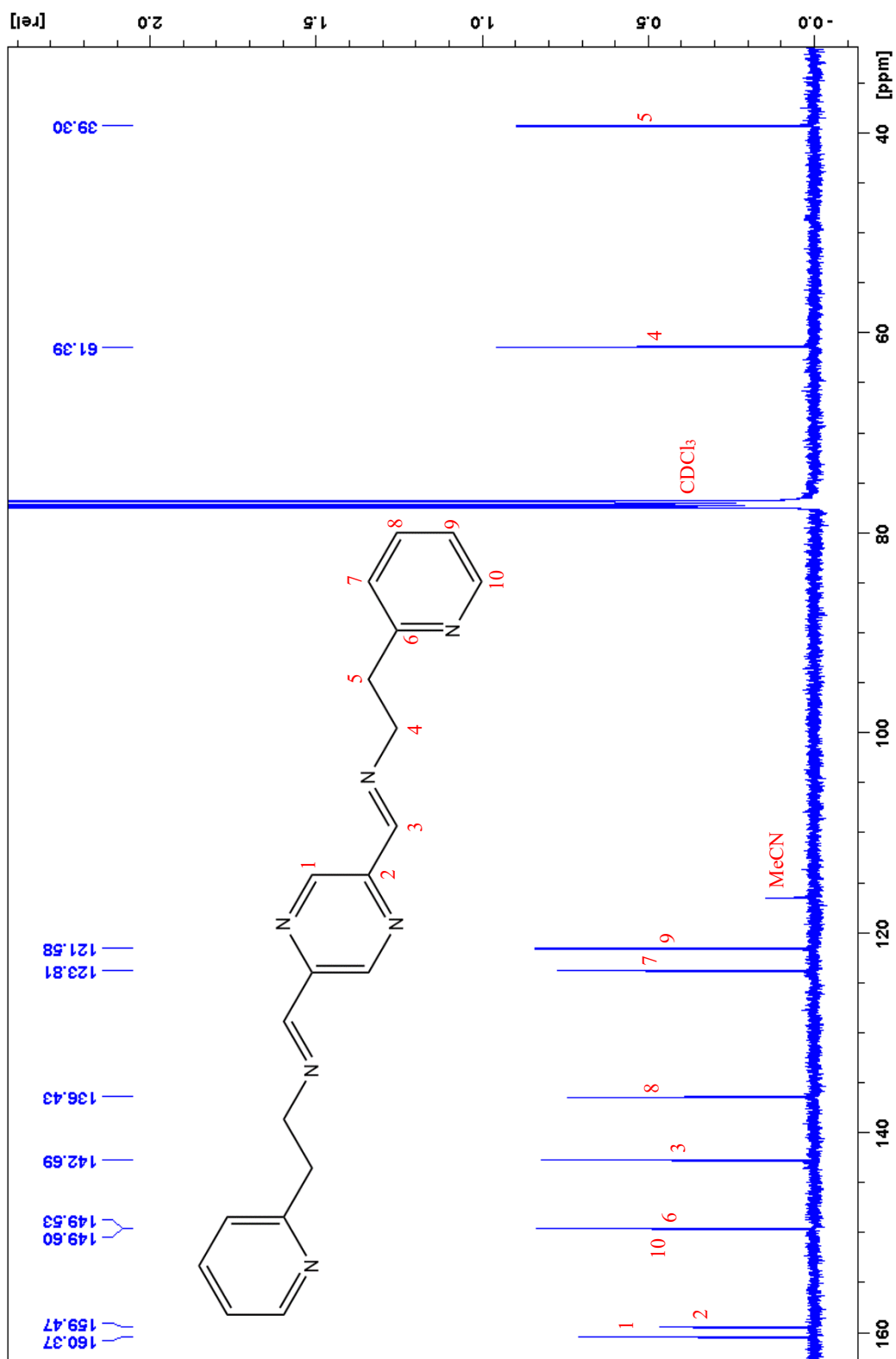


Figure AS6. Assigned  $^{13}\text{C}$  NMR spectrum of L3 ( $\text{CDCl}_3$ ).

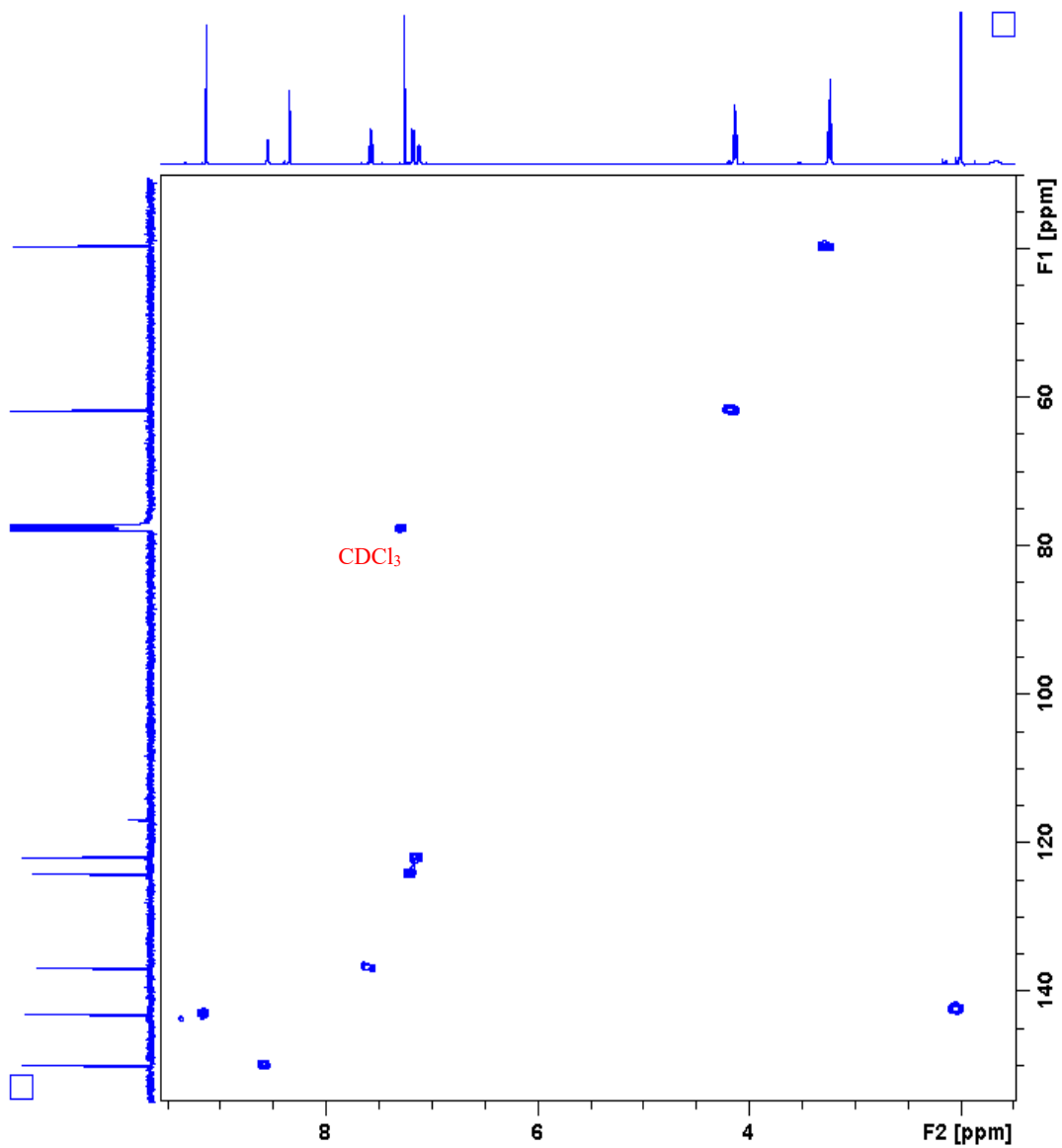


Figure AS7. HMQC spectrum of L3 (CDCl<sub>3</sub>). Left axis = <sup>13</sup>C NMR spectrum of L3. Top axis = <sup>1</sup>H NMR spectrum of L3.

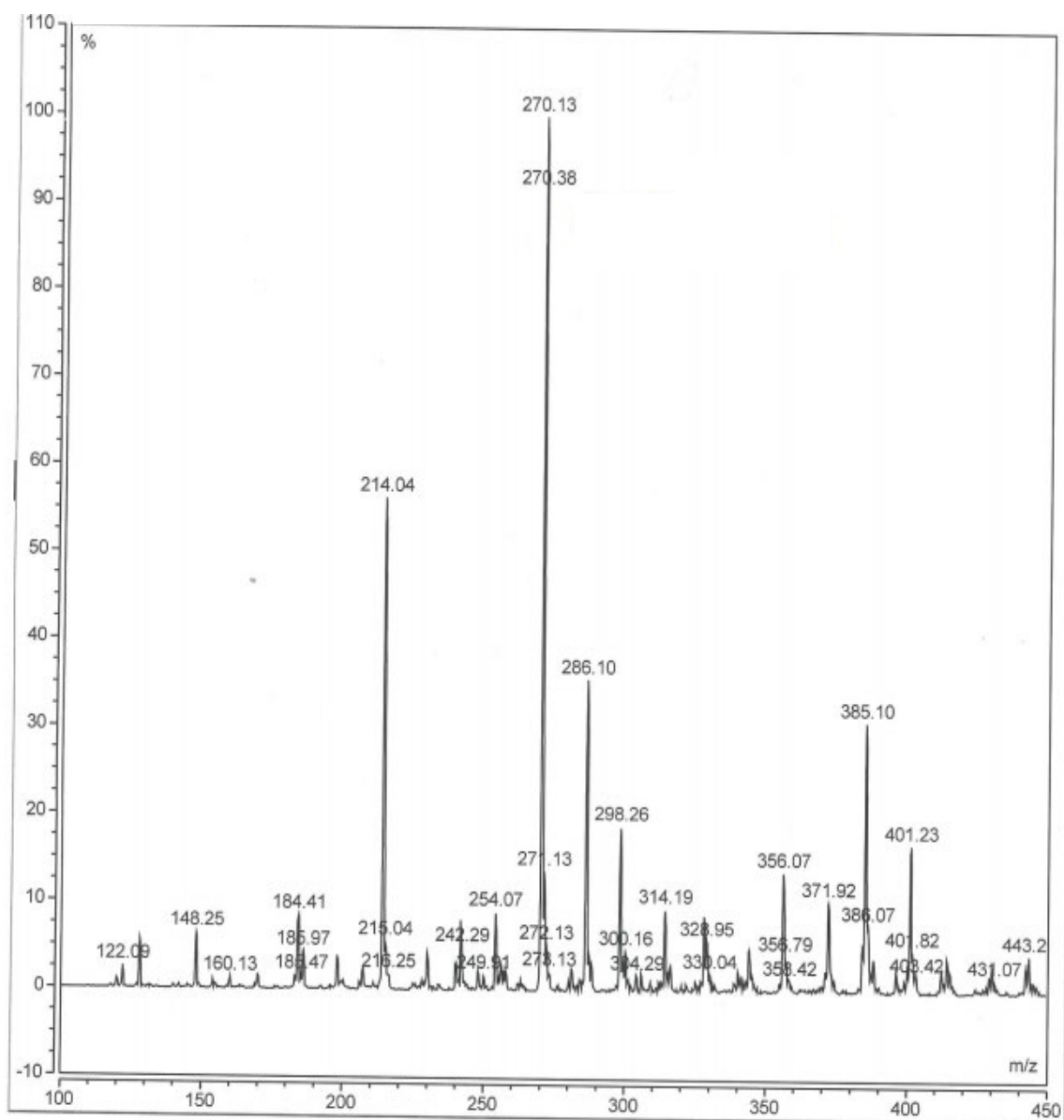


Figure AS8. Mass spectrum of impure 2-[2-(*tert*-butoxycarbonylamino)ethoxy]acetic acid ethyl ester (step iii in Scheme A1.1).  $M^+$  = 270.13 (100 %).

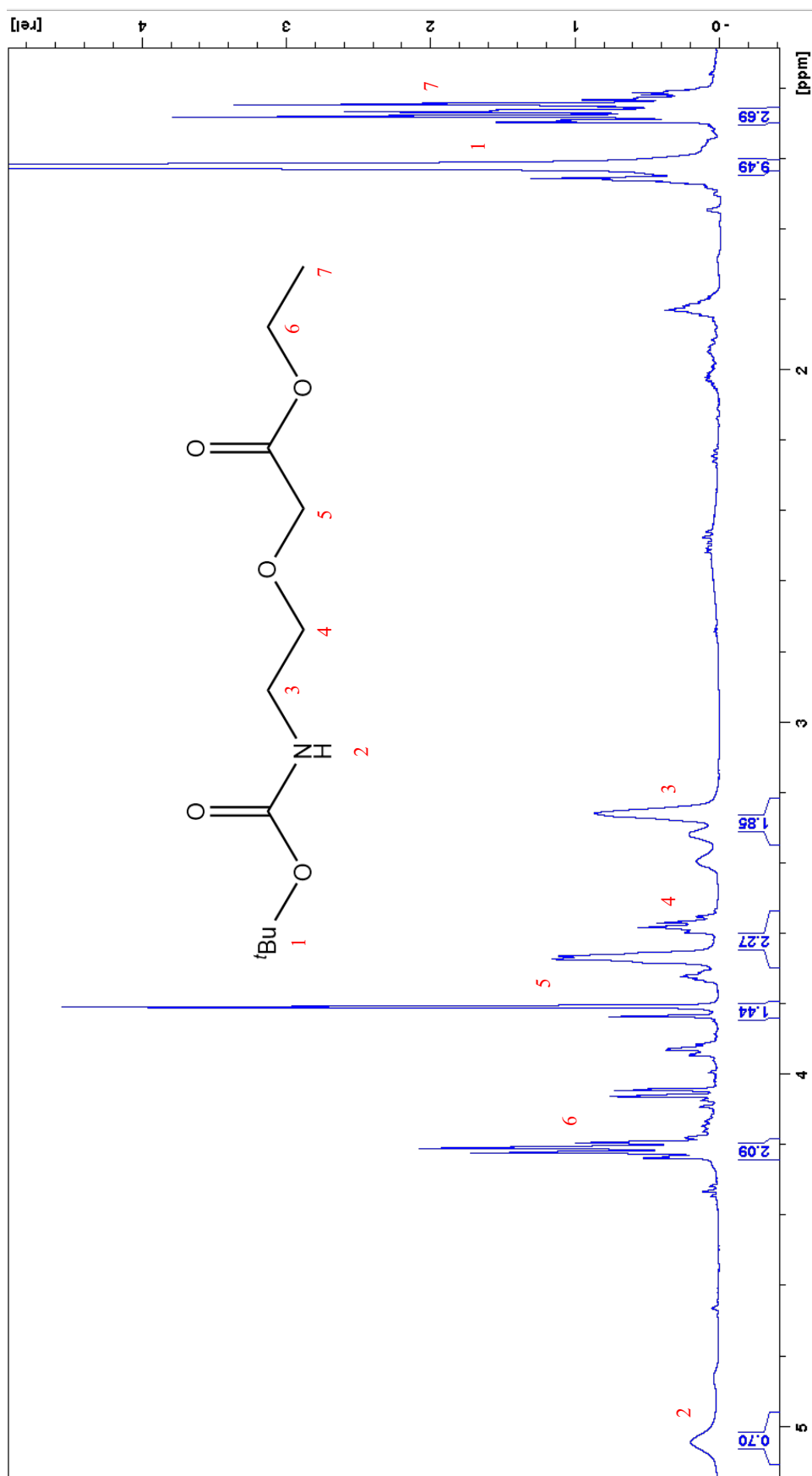


Figure AS9. Assigned <sup>1</sup>H NMR spectrum of 2-[2-(tert-butoxycarbonylamino)ethoxy]acetic acid ethyl ester (step iii in Scheme A1.1). As spectrum obtained is of the crude product, assignments are compared to that of the literature with only the compound peaks assigned.<sup>7</sup>

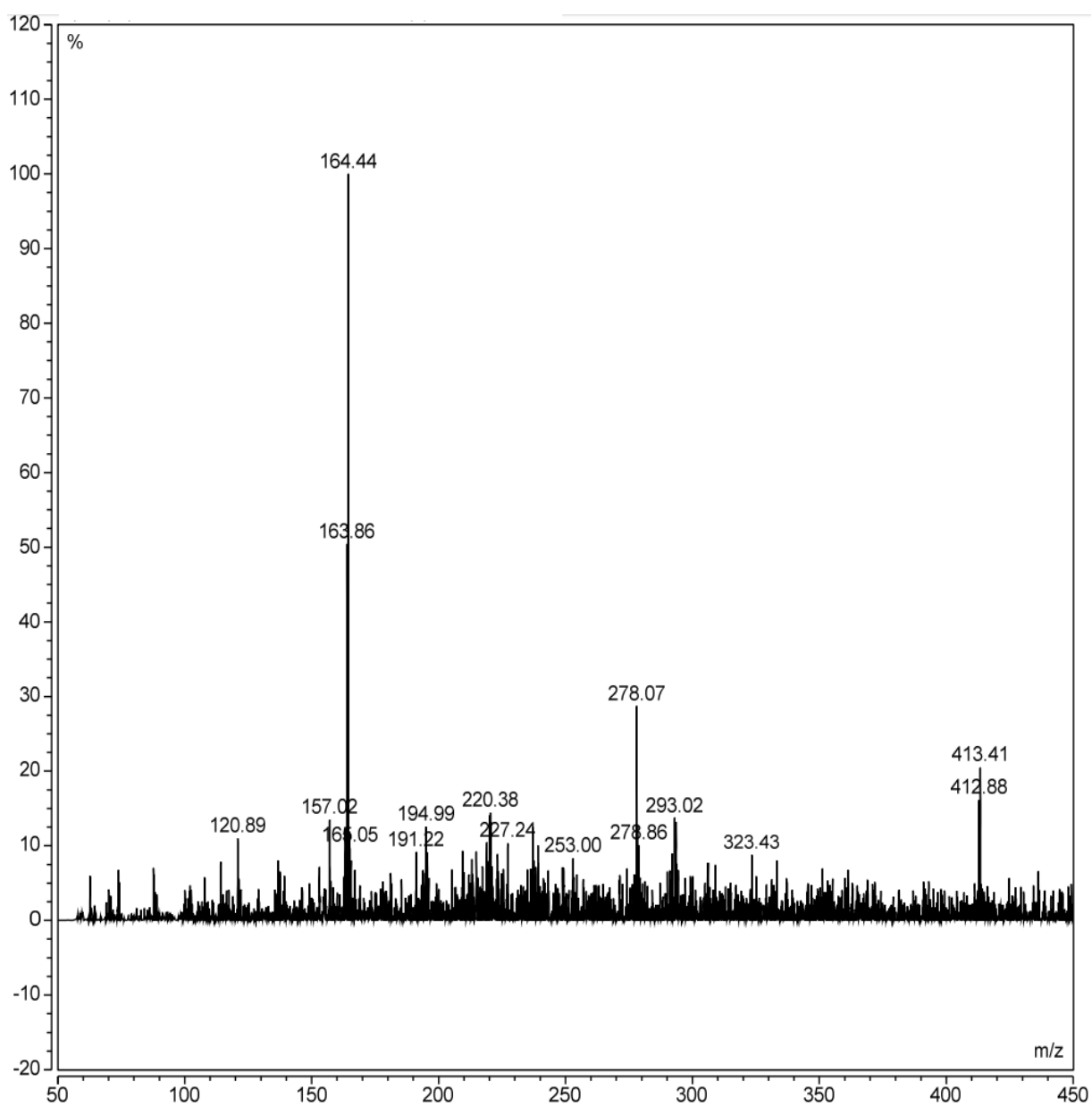


Figure AS10. Mass spectrum of impure **A2**.  $M^+ = 164.44$  (100 %).



**Title:** Supramolecular Coordination: Self-Assembly of Finite Two- and Three-Dimensional Ensembles

**Author:** Rajesh Chakrabarty, Partha Sarathi Mukherjee, Peter J. Stang

**Publication:** Chemical Reviews

**Publisher:** American Chemical Society

**Date:** Nov 1, 2011

Copyright © 2011, American Chemical Society

[LOGIN](#)

If you're a [copyright.com](#) user, you can login to RightsLink using your [copyright.com](#) credentials. Already a [RightsLink](#) user or want to [learn more?](#)

## PERMISSION/LICENSE IS GRANTED FOR YOUR ORDER AT NO CHARGE

This type of permission/license, instead of the standard Terms & Conditions, is sent to you because no fee is being charged for your order. Please note the following:

- Permission is granted for your request in both print and electronic formats, and translations.
- If figures and/or tables were requested, they may be adapted or used in part.
- Please print this page for your records and send a copy of it to your publisher/graduate school.
- Appropriate credit for the requested material should be given as follows: "Reprinted (adapted) with permission from (COMPLETE REFERENCE CITATION). Copyright (YEAR) American Chemical Society." Insert appropriate information in place of the capitalized words.
- One-time permission is granted only for the use specified in your request. No additional uses are granted (such as derivative works or other editions). For any other uses, please submit a new request.

If credit is given to another source for the material you requested, permission must be obtained from that source.

[BACK](#)[CLOSE WINDOW](#)

Copyright © 2018 [Copyright Clearance Center, Inc.](#) All Rights Reserved. [Privacy statement.](#) [Terms and Conditions.](#) Comments? We would like to hear from you. E-mail us at [customer care@copyright.com](mailto:customer care@copyright.com)

Figure AS11. Permission to use Figures 1.2 and 1.14 in this thesis from Chakrabarty, R.; Mukherjee, P. S.; Stang, P. J. *Chemical Reviews* **2011**, 111, 6810.





**Title:** Redox Modulation of Spin Crossover within a Cobalt Metallogrid  
**Author:** Fuxing Shen, Wei Huang, Dayu Wu, et al  
**Publication:** Inorganic Chemistry  
**Publisher:** American Chemical Society  
**Date:** Jan 1, 2016

Copyright © 2016, American Chemical Society

LOGIN

If you're a [copyright.com](#) user, you can login to RightsLink using your [copyright.com](#) credentials. Already a [RightsLink](#) user or want to [learn more?](#)

**PERMISSION/LICENSE IS GRANTED FOR YOUR ORDER AT NO CHARGE**

This type of permission/license, instead of the standard Terms & Conditions, is sent to you because no fee is being charged for your order. Please note the following:

- Permission is granted for your request in both print and electronic formats, and translations.
- If figures and/or tables were requested, they may be adapted or used in part.
- Please print this page for your records and send a copy of it to your publisher/graduate school.
- Appropriate credit for the requested material should be given as follows: "Reprinted (adapted) with permission from (COMPLETE REFERENCE CITATION). Copyright (YEAR) American Chemical Society." Insert appropriate information in place of the capitalized words.
- One-time permission is granted only for the use specified in your request. No additional uses are granted (such as derivative works or other editions). For any other uses, please submit a new request.

If credit is given to another source for the material you requested, permission must be obtained from that source.

BACK

CLOSE WINDOW

Copyright © 2018 [Copyright Clearance Center, Inc.](#) All Rights Reserved. [Privacy statement](#). [Terms and Conditions](#). Comments? We would like to hear from you. E-mail us at [customercare@copyright.com](mailto:customercare@copyright.com)

Figure AS12. Permission to use Figure 1.11 in this thesis from Shen, F.; Huang, W.; Wu, D.; Zheng, Z.; Huang, X.-C.; Sato, O. *Inorganic Chemistry* **2016**, 55, 902.